Observations of CH_4 and N_2O from ground-based Fourier Transform Infrared Spectrometer at Addis Ababa: Retrieval, source identification and characterization of retrieval errors.

A thesis submitted to the School of Graduate Studies
Addis Ababa University

In partial fulfillment of the Requirements for the degree of
Doctor of philosophy in Atmospheric Physics

By

Temesgen Yirdaw Berhe

Addis Ababa, Ethiopia

September 2020

The undersigned hereby certify that they have read and recommended to the Faculty of Science School of Graduate Studies acceptance of a thesis entitled **"Observations of CH_4 and N_2O from ground-based Fourier Transform Infrared Spectrometer at Addis Ababa: Retrieval, source identification and characterization of retrieval errors"** by **Temesgen Yirdaw Berhe** in partial fulfillment of the requirements for the degree of **Doctor of Philosophy**.

Dated: September 2020

Prof. Gizaw Mengistu, Supervisor .....

Professor, Department of Physics
Addis Ababa University, Ethiopia

Prof. Leonard K. Amekudzi, External Examiner .....

Dr. Gemechu Fanta, Internal Examiner .....

Dr. Teshome Debela, Examining Chair .....

This dissertation is dedicated to my family

Acknowledgements

I have a very high gratitude to my academic supervisor, Prof. Gizaw Mengistu for his many suggestions, his scientific encouragements and for his constructive advice and criticisms throughout the process of this study.
I would also like to express my appreciation to Addis Ababa University and Mekelle University for offering me the chance to pursue my PhD study at Addis Ababa University. I reserve my deepest gratitude for my friends Kinfe Gebremedhin, Solomon Weldegerima and Mokennen Abreha for their financial and moral support. Special thanks go to Dr. Samuel takele for his contribution to preparing the spectra measured by the FTIR for analysis, Dr. Teshome Senbeta (chairman of physics Department) and W/r Tsilat Adnew the secretary of the physics department, whose support made progress through a painful time possible.
I am grateful to the Goddard Space Flight Center for providing temperature and pressure profiles via auto mailer system. I greatly acknowledge the FTIR team (Jungfraujoch, Ny-Ålesund), MLS, MIPAS and WACCM science teams for the provision of data used in this study.
I would also like to express my deepest appreciation to my beloved Father Yirdaw Berhe, my mother Zafu Tassew, my brothers Mengisteab Yirdaw, Dr. Micheal Yirdaw and my sisters Senait Yiradw and Selam Yirdaw for their support to complete my study. At last but certainly not the least I want to thank my **God** for giving me the strength and courage to complete this task.

Addis Ababa University — Temesgen Yirdaw
September 2020

Publications

Chapters of this work described in this thesis have been reported in the following publications:

- Yirdaw Berhe, T. and Mengistu Tsidu, G., Blumen stock, T., Hase, F. and Stiller, G. P.: Methane (CH_4) and nitrous oxide (N_2O) from Ground-based FTIR at Addis Ababa: observations, error analysis and validation, Atmos. Meas. Tech., 13, 4079–4096, doi.org/10.5194/amt-13-4079-2020.

- Yirdaw Berhe, T. and Mengistu Tsidu, G., Blumen stock, T., Hase, F. and von Clarmann, T., Notholt, J., Mahieu, E.: Impacts of H_2O Variability on accuracy of CH_4 observations from MIPAS satellite over tropics, Atmos. Meas. Tech. Discuss., https://dio.org/10.5194/amt-2019-209, 2019.

Abstract

A ground-based high spectral resolution Fourier-transform infrared (FTIR) solar absorption spectrometer has been operational at the Addis Ababa University (9.01° N, 38.76° E, 2443 m a.s.l) since May 2009 to obtain information on the total column abundances and vertical distribution of various constituents in the atmosphere. Retrieval strategy and results on information content and corresponding full error budget evaluation of methane and nitrous oxide are presented. Optimal estimation retrieval technique is used to analyses the observed spectra and provide regular vertical profiles, total and partial column measurements of trace gases. The volume mixing ratio profiles of CH_4 and N_2O are simultaneously retrieved from ground-based FTIR solar absorption spectra measured between May 2009 and March 2013. The ground-based FTIR CH_4 and N_2O at Addis Ababa, Ethiopia were compared with Michelson Interferometer for Passive Atmospheric Sounding (MIPAS) (version V5R_CH4_220, V5R_CH4_224, V5R_N2O_220 and V5R_N2O_224), the Microwave Limb Sounder on board of the Aura satellite (Aura/MLS) (MLS v3.3 of N_2O and CH_4 derived from MLS v3.3 products of CO, N_2O and H_2O) and the Atmospheric Infrared Sounder (AIRS) (CH_4) to validate the instrument performance. Relative differences range in vertical profiles of CH_4 and N_2O from the measurements between MIPAS (version V5R_CH4_220, V5R_CH4_224, V5R_N2O_220 and V5R_N2O_224) and FTIR in altitude ranges of 15-27 km are -15 % to -3.8 %, -4.8 % to 4.6 %, 2 % to 10 %, -7 % to 15 % respectively. Moreover, the mean differences in partial column of CH_4 and N_2O within altitude ranges of 15 to 27 km are -11 % , -5.5 %, 2.39 % and 0.5 % respectively. Relative differences in vertical profiles of CH_4 and N_2O from the measurements between MLS v3.3 and FTIR in altitude ranges of 17-27 km are less than 9 % and 15 % respectively. Relative differences range in vertical profiles of CH_4 from the measurements between AIRS and FTIR in altitude ranges of 11-27 km is -4.8 % to 9 %. The bias obtained between FTIR and the new data version of MIPAS_CH4_224 has been reduced in the altitude range of 15-27 km when the interfering gas H_2O is fitted jointly with the target gas, CH_4. Therefore, the ground-based FTIR spectrometer can be recommended for CH_4 and N_2O satellite data (MIPAS, MLS and AIRS) validation.

Uncertainties of tropical methane concentrations, retrieved from spectra recorded by the MIPAS, MIPAS_CH4_220 are large at upper troposphere and lower stratosphere. The relation of these uncertainties with water vapour variability is explored and the uncertainties have been reduced in MIPAS_CH4_224. Coincident measurements of CH_4 by MIPAS, ground based FTIR and EOS MLS CH_4 are used to estimate the standard uncertainty of MI-

PAS_CH4_220, MIPAS_CH4_224 and natural variability of H_2O. Different methods such as bias evaluation, differential method and correlation coefficient are employed to explore the latitudinal variations of standard uncertainty of MIPAS_CH4_220 and natural variability of water vapour as well as its reduction in MIPAS_CH4_224. The averaged bias between MIPAS_CH4_220 and ground-based FTIR measurements in the altitude range 15-22 km are 12.3 %, 8.9 % and -1.2 % for the tropics, mid-latitudes and high latitudes, respectively. Whereas the averaged bias for MIPAS_CH4_224 is 3.4 %, -2.8 % and -2.4 %. The average estimated uncertainties of MIPAS_CH4_220 methane are 5.9 %, 4.8 % and 4.7 % at altitude ranges of 15 to 27 km in the tropics, mid-latitudes and high latitudes, respectively. On the other hand, the average estimated uncertainties of MIPAS_CH4_224 methane were obtained 2.4 %, 1.4 % and 5.1 %. Moreover, the correlation coefficient between MIPAS_CH4_220 and MIPAS_N2O_220 are found to be 0.30, 0.98 and 0.96 in the lower stratosphere of the tropics, mid and high latitudes respectively. However, the correlation coefficient between MIPAS_CH4_224 and MIPAS_N2O_224 are 0.62, 0.80 and 0.66. The correlation coefficient between the uncertainty of MIPAS_CH4_220, MIPAS_CH4_224 and the variability of water vapour in the lower stratosphere are 0.70 and 0.51 on monthly temporal scales. It was found that the relation between the uncertainty in methane and the variability of water vapor has been reduced in the new data version. Therefore, the natural variability of water vapour was a cause for high uncertainties in the MIPAS_CH4_220 measurements over tropics.

In summary, this study has derived column abundances and profiles of CH_4 and N_2O from solar absorption measurements taken by FTIR at tropical high altitude site of Addis Ababa, Ethiopia for a period that covers May 2009 to March 2013. The quality of the data is assessed through comparison with data from MIPAS, MLS and AIRS sensors onboard satellites. Moreover, the different retrieval errors and their sources are fully characterized to allow the use of the data in further scientific studies as it represents unique environment of tropical Africa, a region poorly investigated in the past.

Table of contents

List of figures

List of tables

Chapter 1

Introduction

Half of the global human population resides in the tropical region, about one third of the global land mass, about 60-80 % of the global bio-diversity and half of the global wetlands are found in tropical region [1]. Moreover, strong tropical convection that covers approximately 10 % of the tropics is characterized by inflow at low levels, rapid vertical transport and outflow near altitudes of 12–14 km [2]. Two of the primary greenhouse gases, namely methane (CH_4) and nitrous oxide (N_2O) are tracer species as they are useful indicators of the dynamical and the photochemical history of an air mass. Besides, CH_4 and N_2O have tropospheric originated and therefore considered as source gases to the chemical families NO_x, HO_x. The reaction of CH_4 with hydroxyl radicals in the troposphere creates a reduction of ozone products in the troposphere and it influences the lifetime or production of other atmospheric constituents such as stratospheric water vapour and CO_2 [3, 4]. Methane and nitrous oxide are the most important anthropogenic greenhouse gases (GHGs) after carbon dioxide (CO_2) [5] and their long atmospheric lifetimes of approximately 9 and 131 years allow them to get well mixed in the troposphere and influence atmospheric chemistry directly and indirectly [6].

For several decades, tropical environment has been changing as a result of rapidly growing demand for energy (predominantly fossil fuel derived), rapid land-use changes, rapid population growth, industrial development and deforestation. The tropical atmosphere, specifically the equatorial region of the globe is one of the least studied, even though the composition of the tropical atmosphere and its change are of significant importance for global climate changes. Moreover, emissions within the tropics contribute substantially to the global budgets of many important trace gases [7, 8]. Tropics is the location where two important exchange processes in the atmosphere are taking place, the interhemispheric exchange and

the entry of tropospheric air mass into the stratosphere [9–11]. The composition of the tropical atmosphere also plays a critical role for stratospheric chemistry [12, 13]. Measurements and interpretation of atmospheric trace gas composition of tropics are vital for a better understanding of the budgets, sources and sinks of trace gases in the atmosphere and their effects on atmospheric chemistry, greenhouse effect and climate changes globally.

Methane retrievals from near-infrared spectra recorded by the SCIAMACHY instrument on board ENVISAT suggested unexpectedly large tropical CH_4 emissions and the impact of water spectroscopy on methane retrievals [8]. The slowdown of concentration growth of methane started in the late 80s starting from 14 ppb/year to almost close to zero in between 1999 and 2005 [7]. However, the recent increasing impact of CH_4 and N_2O of the global warming has also been assessed by the last AR4 IPCC report [5, 7] and the persistent increase of methane observed during mid 2006 to Sep 2011 using FTIR, also suggests various possibilities: an increase in emissions from natural wetlands, an increase in fossil fuel related emissions or a decrease in OH concentrations [14]. Nitrous oxide (N_2O) becomes the dominant ozone depleting substance emitted in the 21^{st} century [15]. In 2007 and 2008, IASI shows an increase of mid-tropospheric methane in the tropical region of 9.5 $\pm$2.8 and 6.3 ± 1.7ppbv yr^{-1} respectively [16]. Two atmospheric inversion models and ORCHIDEE wetland ecosystem model show increment at tropical regions for the 2006-2008 period [17]. According to the World Meteorological Organization (WMO), 2010 report [18], 96 % of the increase in radiative forcing is due to the five long-lived greenhouse gases: carbon dioxide, methane, nitrous oxide, CFC$-$12 and CFC$-$11. The sources and sinks of atmospheric methane (CH_4) and its budget in the tropics are not yet well quantified, particularly in the tropics a large uncertainty of CH_4 budget exists due to the scarcity of measurements [19]. As part of global effort to alleviate this problem, ground-based FTIR measurement at the Addis Ababa site has been launched since 2009 in collaboration with the Institute of Meteorology and Climate Research of the Karlsruhe Institute of Technology, Germany to measure concentrations of various trace gases in the lower and middle atmosphere over Addis Ababa. The quality of ground-based FTIR measurements of atmospheric trace gases and their used to understand various lower and middle atmospheric processes have been reported in a number of previous studies [20–24]. H_2O VMR profiles and integrated column amounts of ground-based FTIR measurements of the Addis Ababa site were also compared with the coincident satellite observations of Tropospheric Emission Spectrometer (TES), Atmospheric Infrared Sounding (AIRS) and Modular Earth Sub model System (MESSy) model and the result confirmed reasonably good agreement [25].

A ground-based FTIR solar absorption spectrometry is a well-established remote sensing

technique for the measurement of atmospheric trace gases by retrieving the Column densities of different trace gas species from the infrared spectral region. In particular for the tropical atmospheric condition this measurement technique is significant as there is a lack of continuous atmospheric observations exists and the uncertainty of satellite measurements of atmospheric trace gases over the tropics is high [8, 19]. The extensive analysis of FTIR CH_4 and N_2O have been reported in the region of subtropics and mid latitudes (e.g.[26–29, 31]). The intercomparison of CH_4 mole fraction of FTIR near Saint Petersburg, Russia (59.9° N, 29.8° E, 20 m a.s.l.) with GOSAT (Greenhouse gases Observing SATel-lite) has been reported by Gavrilov et al. [30] and found the bias is -15 ppb and standard deviation of the bias is 13 ppb. However, this is the first ground-based FTIR CH_4 and N_2O at equatorial region. Therefore, the focus of this thesis is on retrieval of methane and nitrous oxide from ground-based FTIR operated in Addis Ababa and intercomparison of CH_4 and N_2O measurements from ground-based FTIR in Addis Ababa with those of satellite observations (MIPAS, MLS and AIRS) to assess the quality of retrieval results. The observed differences between ground-based FTIR and satellite observation of CH_4 and N_2O are analyzed using the statistical tools detailed in von Clarmann [38].

Accurate measurement and prediction of atmospheric composition is therefore a critical component in the effort to understand the atmospheric dynamical process, chemistry, radiation budget, which are linked to climate change, ozone depletion, global warming and also provide the data that are required for the modeling of atmospheric processes of the region [39, 40]. Ground-based high resolution Fourier Transform Infrared (FTIR) instrument and space based sensors such as, Michelson Interferometer for Passive Atmospheric Sounding (MIPAS), Microwave Limb Sounder (MLS), Atmospheric Infrared Sounding (AIRS), Atmospheric Chemistry Experiment (ACE), Infrared Atmospheric Sounding Interferometer (IASI) and Japanese Greenhouse Gases Observing SATellite (GOSAT) are some instruments dedicated to monitoring of CH_4 and N_2O profiles at a global scale.

Satellite measurements of atmospheric trace gases has become useful to understand the spatiotemporal distribution and trends of various global trace, but at the cost of lower precision. However, thermal structure and other dynamic parameters of the atmospheric constituents are only available at a discrete geographic locations and times. The later problems can be addressed using the ground-based FTIR spectrometer, which is a powerful technique to make continuous observations with high temporal resolution and offers a good opportunity for investigation of the variability of the trace gas species with different temporal scales. Therefore, satellite or space based data may contribute to better understanding of the spatial and temporal pattern of atmospheric constituents in particular if they are complemented by

the ground-based FTIR data.

In the upper troposphere and lower stratosphere (56 hPa to 146 hPa) the radiative and chemical effects of water vapour are large and the concentration of H_2O varies considerably with the temperature and relative humidity [25]. Tropical Tropopause Layer (TTL) (121 to 68 hPa) is a transition layer sharing Upper Tropospheric (UT) and Lower Stratospheric (LS) characteristics and as a result, it is an important gateway for Troposphere to Stratosphere Transport (TST) and plays a vital role in the global composition and circulation of the stratosphere [17, 41–43]. Water vapour is a strong absorber in the infrared with high spatiotemporal variability as compared to other greenhouse gases [44]. Much of the stratospheric variability of water vapour in the tropics is a result of oxidation of methane [45]. Furthermore, H_2O is one of the interfering gases that affected the retrieval CH_4 profiles from remote sensing measurements. However, the impacts of atmospheric H_2O variability on the measurements of other greenhouse gases have not yet been studied. Although, the impacts of water spectroscopy in the overestimation of methane observations over tropics were reported in Frankenberg et al. [8] and a related water vapour, methane interference problem had been described for satellite retrievals [8]. Hence, the influence of water vapor variability of methane retrievals from spectra recorded with the Michelson Interferometer for Passive Atmospheric Sounding (MIPAS, Fischer et al. [43]) performed at the institute of Meteorology and Climate Research (IMK) in cooperation with the instito de Astrofía (IAA) is investigated.

The data sets used are MIPAS_CH4_220 [39], water vapor profiles that has been described by von Clarmann [46], Milz et al. [47] and data version V5R_CH4_224 [48]. Despite uncertainties in the latter data product have been largely reduced, measurements of methane at tropical sites are still difficult. This is because in the tropics the upper troposphere and lower stratosphere (UT/LS) is very humid and strong vertical gradients are prevailing [49]. Evidence of substantial diurnal variations of atmospheric water vapour has been exhibited as reported in Wang et al. [50] and the spatiotemporal variability of water vapour in the upper troposphere has already been examined in detail [44, 51].

Methane and nitrous oxide are produced at the surface, and they are not directly coupled chemically. In the UT/LS, the mixing ratios of these long-lived trace gases are largely controlled by dynamical processes, generally resulting in compact tracer-tracer correlations. These correlations are usually more compact in high and mid-latitudes, while in the tropics a somewhat larger scatter is observed in Payan et al. [27], Plumb et al. [52]. In this paper, we inquire into the bias and random error of the MIPAS methane products.

In the lower stratosphere (below 25 km) MIPAS methane has long been known to be biased high (see e.g., [53]). However, the retrieval setup has been improved, leading to a smaller bias in MIPAS V5R_CH4_224 [48]. In the new set up, H_2O concentrations are included in the list of species fitted along with the target species, reducing the propagation H_2O a priori assumption onto the CH_4 profile. A high bias and large random uncertainties in the tropical UT/LS are not a feature of the IMK methane only. Moreover, in the operational ESA data product, a high bias and random uncertainty of MIPAS ESA CH_4 product in the tropical upper troposphere and lower stratosphere atmospheric conditions than the mid and high latitude condition has also been revealed in Payan et al. [27] and in Errera et al. [54]. On the other hand, a large variability of water vapour in the upper troposphere and lower stratosphere in the tropics was reported by Schneider et al. [49] and by William et al. [11]. Moreover, there are also some studies that hypothesize that the large uncertainty of the MIPAS tropical CH_4 product by ESA is caused by the large variability of water vapour even though they did not quantify the contributions (e.g. [27]).

Therefore, this study aims to assess the large uncertainty of MIPAS_CH4_220 in the upper troposphere and lower stratosphere of the tropics and its relation to the variability of water vapour. Furthermore, we explore the reduction of uncertainty of MIPAS_CH4_224 in the tropics and analyze the relationship between these uncertainties and the variability of water vapor. The coincident measurements of H_2O, CH_4 and N_2O by MIPAS, ground-based FTIR and MLS were used to estimate the uncertainty of MIPAS_CH4_220 and MIPAS_CH4_224 vertical profiles and the natural variability of H_2O over the tropics. The specific objectives are:

- Retrieval of CH_4 and N_2O vertical profile from ground-based FTIR measurements;
- Intercomparison of ground-based FTIR with satellite observations CH_4 and N_2O; and
- Latitudinal variation of MIPAS_CH4_220 and MIPAS_CH4_224 uncertainty and their relation with water vapour variability in the lower stratosphere of the tropics.

The thesis is organized as follows. The upper troposphere and lower stratosphere characteristics such as the chemistry and other process taking place in the atmosphere are described in chapter 2. The basic principles for the retrieval of concentrations of atmospheric gases from spectra recorded by ground-based FTIR will be described in chapter 3. Brief description of instruments (FTIR, MIPAS, MLS and AIRS) is given in Chapter 4. Chapter 5 is dedicated to derive the vertical profiles and partial column of CH_4 and N_2O from FTIR. Comparisons

of the FTIR CH_4 and N_2O with MIPAS, MLS and AIRS are described in Chapter 6 and the impacts of H_2O variability on the uncertainty of MIPAS_CH4_220 and MIPAS_CH4_224 are discussed in chapter 7. Finally, a summary and conclusions are given in Chapter 8.

Chapter 2

The role of atmospheric dynamics and chemistry in CH_4 and N_2O budget

Chemical and dynamical processes in the Tropical Tropospheric Layer (TTL) determine the mixing ratios of air parcels entering the stratosphere. Chemically, the tropopause region is important because stratospheric trace gas distributions depend on the inter-play between dynamics and chemistry taking place near the tropopause. The concentrations and distribution of chemical species, CH_4 and N_2O in the atmosphere are controlled by transport and chemical processes. Chemical reactions in the atmosphere can lead to the formation and removal of species. Motions of the atmosphere, not just emissions and reactions, affect atmospheric composition, and the understanding of both must be coupled to evaluate distributions. Therefore, it is essential that long term monitoring of long lived trace gases are well used to understand the chemical and dynamical process that takes place in troposphere and stratosphere of the tropics. Hence, the role of atmospheric dynamics and chemistry in the budget of CH_4 and N_2O has been discussed in this chapter.

2.1 Atmospheric Transport

Transport is one of the causes with the movement of pollutants in the atmosphere by a time-averaged wind flow. The radiative imbalance of different parts of the globe was adjusted by atmospheric transport, for instance the tropical heat transported to polar vie thermal winds has maintained thermal balance in winter. Figure 2.1 depicts a theoretical circulation (Brewer–Dobson circulation) near the tropopause, which was inferred from horizontal fields of temperature, trends in O_3, tracers (CH_4 and N_2O), and estimated age of air. It is seen that, as tropical air enters the lower stratosphere from the upper troposphere, it is transported to

the mid-latitudes and polar areas. In mid-latitudes, air mass from the lower stratosphere is transported to the upper troposphere. In polar areas, air mass descends to the bottom of the stratosphere. The air flow from mid-latitude to polar region has been blocked at the time polar vortex is formed, the polar vortex forms when zonally averaged monthly mean wind speed exceeds 15 ms^{-1} .

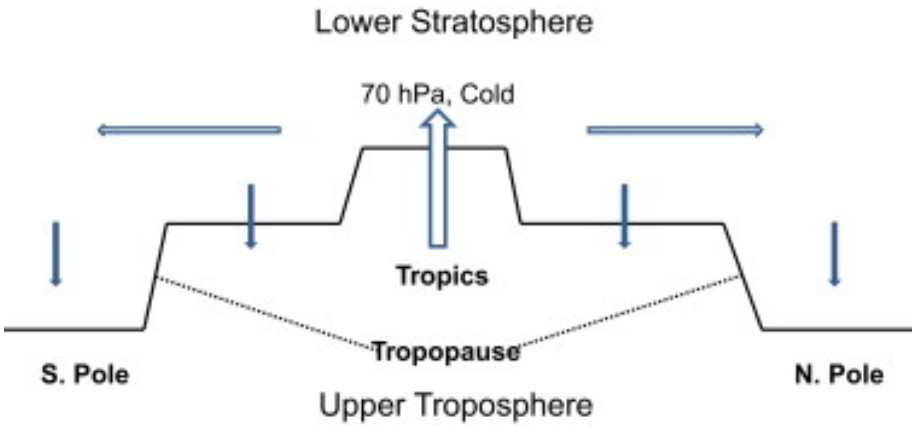

Fig. 2.1 Illustration of theoretical Brewer–Dobson circulation near the tropopause(source: https://www.sciencedirect.com/topics/earth-and-planetary-sciences/atmospheric-transport).

Methane is produced by biotic activity near the Earth's surface, transported into the stratosphere, and chemically destroyed (oxidized) above 35 km. The photochemical lifetime of CH_4 below 40 km is > 100 days, so that the distribution in the stratosphere and UTLS region is determined mainly by the circulation. The global budget and secular trends of atmospheric CH_4 have been discussed in Dlugokencky et al. [55] and Intergovernmental Panel on Climate Change [56].

Nitrous oxide (N_2O) is a long-lived species in the troposphere and lower stratosphere and can therefore be used as a tracer for atmospheric transport. N_2O is produced in the troposphere by natural (soils, wetlands) as well as by anthropogenic sources (industrial emissions, biomass burning), and is destroyed photochemically in the stratosphere. The N_2O abundance in the troposphere has increased rapidly due to anthropogenic emissions during the last centuries. The global mean lifetime of N_2O is 122 ± 24 yr in the troposphere [57] and decreases with altitude from several years in the lower stratosphere to $\sim$8 months in the middle stratosphere [58].

N_2O is transported via the Brewer–Dobson circulation to the polar regions after entering the lower stratosphere at the tropical tropopause (Brewer, 1949; Dobson, 1956). Thus, the

temporal and spatial distribution of stratospheric N_2O can be used as a diagnostic tool of global-scale transport processes at different time scales, from seasonal to decadal (e.g. [59]). Measurements of N_2O show that the zonally averaged lower stratospheric N_2O mixing ratios vary systematically with season, latitude, and altitude [60].

Greenhouse gases such as (H_2O), carbon dioxide (CO_2), methane (CH_4), nitrous oxide (N_2O) and chlorofluorocarbons (CFCs) are found mainly in the lower layer of the atmosphere, troposphere and heat the Earth by trapping additional IR radiation that would otherwise escape to space. N_2O and CFCs decline after reaching the stratosphere due to photo dissociation by UV light.

Fig. 2.2 shows the monthly and zonally mean distribution of methane and nitrous oxide in the upper troposphere and lower stratosphere measured by MIPAS in Feb, 2010. The highest values of CH_4 and N_2O are found in upper troposphere over tropics and in lower stratospheric over mid and high latitude. The bulge shape seen in the lower stratospheric contour lines over tropics are due to the ascending motion.

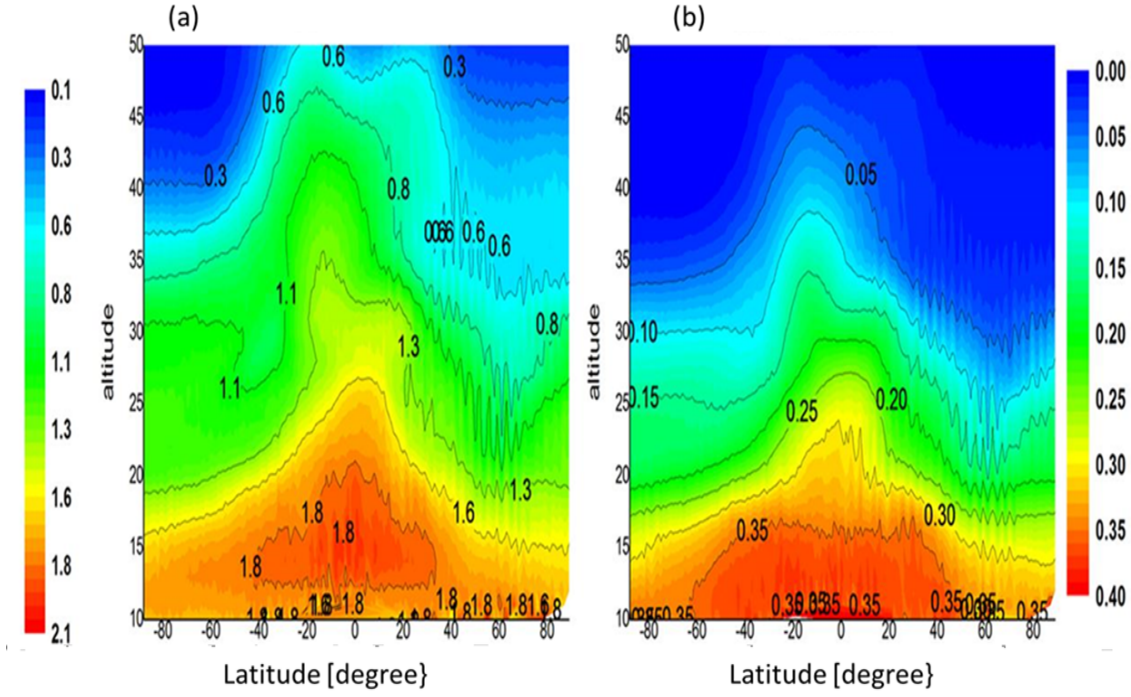

Fig. 2.2 Latitude & altitude Distribution of monthly mean (a) CH_4 in ppmv and (b) N_2O in ppmv (right) Volume mixing ratio for Feb, 2010 as measured by MIPAS.

Figure 2.3 shows the zonally averaged monthly mean of random uncertainty (noise) of MIPAS_CH4_220 with a spatial resolution of 15° (longitude) and 5° (latitude) for Feb., 2010

in five altitude levels (16, 17, 18, 19 and 20 km). Large uncertainty has been seen in the tropics in the upper troposphere and lower stratosphere of tropics in all the five layers and decline its value with altitude. Similarly, Fig. 2.4 shows the Zonally averaged monthly mean of water variability for Feb., 2010 of MIPAS_H2O_220 in five altitude levels. The variability of water vapour is high over the upper troposphere and lower stratosphere tropics as compared to mid-latitude with some exception on the central meridional edge of polar region.

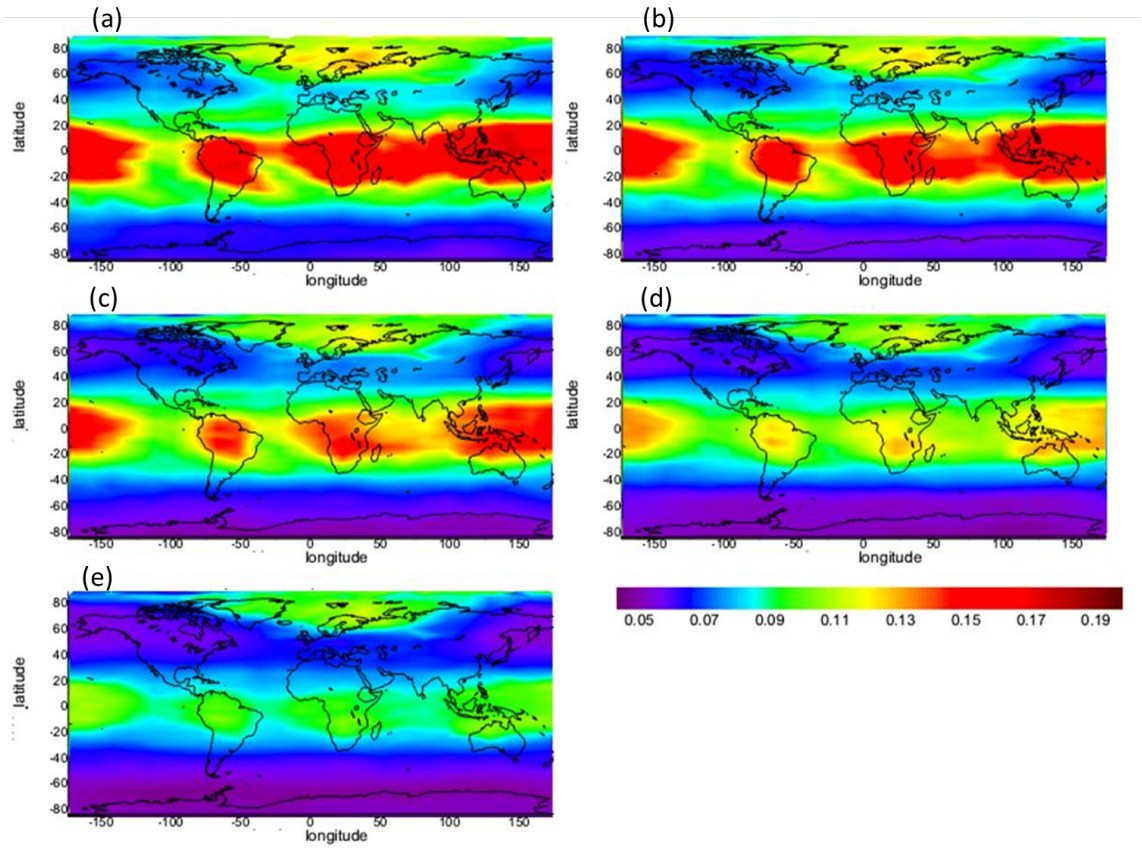

Fig. 2.3 Zonally averaged monthly mean of random uncertainty (noise) of MIPAS CH_4 with a spatial resolution of 15° (longitude) and 5° (latitude) for Feb., 2010 in five altitude levels (a) 16 km, (b) 17 km, (c) 18 km, (d) 19 km and (e) 20 km.

In the tropics, where the majority of transport from the troposphere into the stratosphere occurs through the up welling branch of the large-scale Brewer-Dobson circulation (Brewer, 1949; Dobson, 1956), the conversion of anthropogenic gases into reactive compounds is very efficient through enhanced photochemistry.

In the upper troposphere and lower stratosphere ($\geq$56 hPa - $\leq$146 hPa) the radiative and

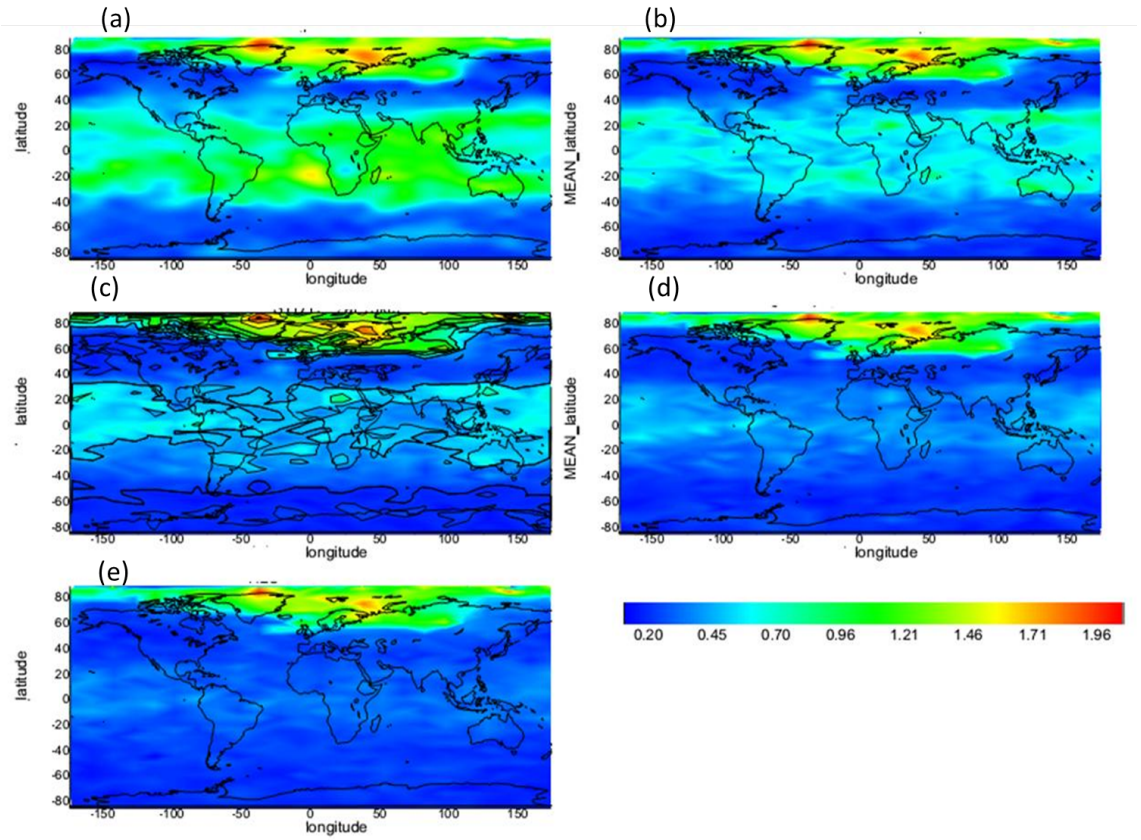

Fig. 2.4 Zonally averaged monthly mean of water variability with a spatial resolution of 15° (longitude) and 5° (latitude) for Feb., 2010 of MIPAS_H2O_220 in five altitude levels (a) 16 km, (b) 17 km, (c) 18 km, (d) 19 km and (e) 20 km.

chemical effects of water vapour are large and the concentration of H_2O varies considerably with the temperature and relative humidity. As a result, the satellite based measurements of atmospheric trace gases have large uncertainty [13, 21]. Moreover, the tropical tropopause layer (TTL) (16-20 km or 121 hpa to 56 hpa) is a layer at which the following is observed

- Transport of air mass horizontally;
- Chemistry;
- Lowest temperature; and
- Exchanges of air mass between troposphere and stratosphere.

Therefore, it is important to study the distribution of this climate gases in the layer along with the variability of water vapour in order to understand the dynamics and chemistry as well as quantify the large uncertainty of satellite measurements.

2.2 Tropospheric Chemistry of CH_4

Tropospheric chemistry is associated with the oxidation and subsequent transformation of chemical species released naturally from the biosphere or by anthropogenic activity to the troposphere. Hydroxyl is a free radical molecule having an unpaired electron that is a reactive species. The hydroxyl radical in the troposphere is removed by reaction with methane by producing H_2O. The main sink of atmospheric methane is the reaction with hydroxyl radical and about 90 % of methane is removed by oxidation in the troposphere [42].

$$OH + CH_4 \rightarrow CH_3 + H_2O \tag{2.1}$$

Tropospheric chemistry can be described as low temperature combustion system with the following reaction. This is not a thermal process, but a radical mediated process initiated photochemically:

$$CH_4 + 3O_2 \rightarrow CO_2 + 2H_2O \tag{2.2}$$

Thus, tropospheric chemistry has an impact on ozone in the stratosphere by controlling OH levels in the troposphere.

2.3 Stratospheric chemistry of CH_4

Methane oxidation chain of photochemical reaction as shown in Fig. 2.5 and H_2O is formed in the stratosphere with the oxidation of CH_4, leading to the observed increases of H_2O and decreases of CH_4 with altitude in the stratosphere [69]. This can happen directly due to the oxidation of CH_4 by OH radical or indirectly CH_4 would be oxidised by $O(^1D)$, Cl or other halogens to form formaldehyde (CH_2O), which is then oxidised to form H_2O vapour. Depending on NO_x levels, methane oxidation may either be a production or a destruction process for odd hydrogen. In general, high concentrations of nitrogen oxide are found in the polluted northern hemisphere or in boundary layer of the tropics, and low levels in the southern hemisphere. In regions of high levels of NO_x, methane oxidation primarily occurs via the sequence (see also Fig. 2.5)

$$CH_4 + OH \rightarrow CH_3 + H_2O \tag{2.3}$$

$$CH_3 + O_2 \underset{\nearrow}{M} CH_3O_2 \tag{2.4}$$

$$CH_3O_2 + NO \rightarrow CH_3 + NO_2 \tag{2.5}$$

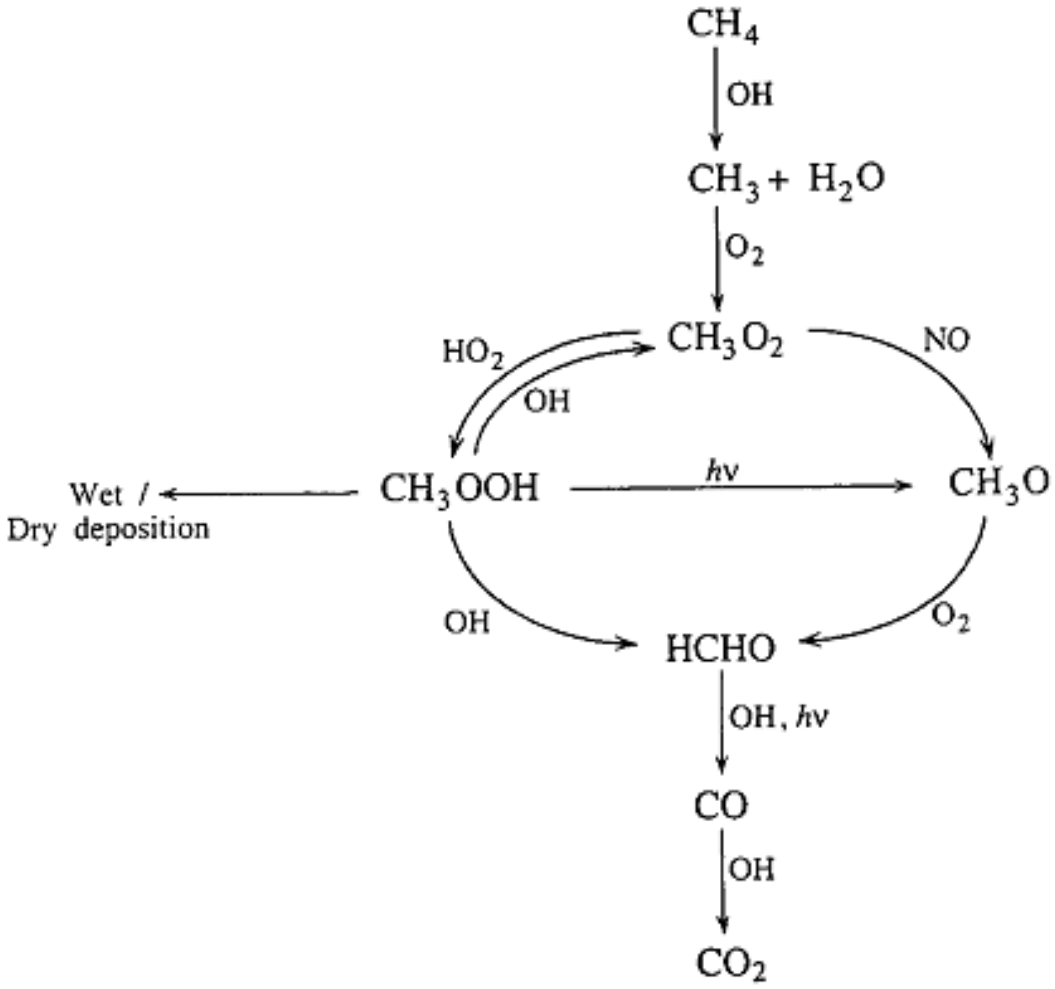

Fig. 2.5 Methane oxidation chain of photochemical reactions (Source: Seinfed J. H. and S. N. Pandis, Atmospheric Chemistry and Physics: From Air Pollution to Climate Change, 1998).

The oxidation of formaldehyde may also result in an end product of molecular hydrogen rather than H_2O. The oxidation of CH_4 results in roughly two molecules of H_2O for every molecule of CH_4 destroyed. The exact number varies with latitude and altitude, depending on the production of H_2O/H_2 from the oxidation of CH_2O. $H_2O + 2CH_4$ is called equivalent water that is constant in the stratosphere except air is significantly influenced by dehydration, like in the polar region, where air retains the cycle of tropopause temperatures. H_2O

produced in the stratosphere is less, since the oxidation of molecular hydrogen, which may disrupt the constancy of equivalent H_2O.

2.4 Stratospheric chemistry of N_2O

N_2O is produced in the troposphere by natural (soils, wetlands) as well as by anthropogenic sources (industrial emissions, biomass burning), and is destroyed photochemically in the stratosphere. The N_2O abundance in the troposphere has increased rapidly due to anthropogenic emissions during the last centuries.

In the stratosphere nitrous oxide is broken down to molecular nitrogen or odd nitrogen, 90 % through photolysis and about 10 % through attack by electronically excited oxygen atoms. N_2O is an important ozone-depleting and greenhouse gas [45]. N_2O emissions are not controlled by the Montreal Protocol, but it becomes One of the target in the Kyoto Protocol. The IPCC A2 scenario was used to compute the 21^{st} century and an 8 % ozone decrease by 2100 in the 20 to 40 km altitude range from changes in N_2O alone (these are estimated to be 0.8 ppb/yr) [61]. This will result in enhanced recovery of the depleted ozone layer and will reduce the anthropogenic forcing of the climate system. Nitrous oxide in the stratosphere is converted to nitric oxide that eventually oxidizes to nitric acid. This nitric acid diffuses down to the troposphere where it can be rained out.

Fig. 2.6 represents chemical processes of nitrogen oxide in stratosphere at which reactive species are inside the red circles, the source gases are in blue circles, ozone is also a source gas and those in cyan circles are reservoirs along the dot dot arrow shows the heterogeneous reaction.

N_2O is a very stable molecule which has no significant sinks in the troposphere and it is an inert gas with a lifetime of 120±30 years for which its destruction at lower stratosphere is not known. However, N_2O transported to the stratosphere where it encounters high concentrations of $O(^1D)$, allowing oxidation to NO which accounts for only about 5 % of loss of N_2O in the stratosphere and it affects the lifetime of N_2O [62].

$$N_2O + O(^1D) \rightarrow 2NO \tag{2.6}$$

$$N_2O + O(^1D \rightarrow N_2 + O_2$$

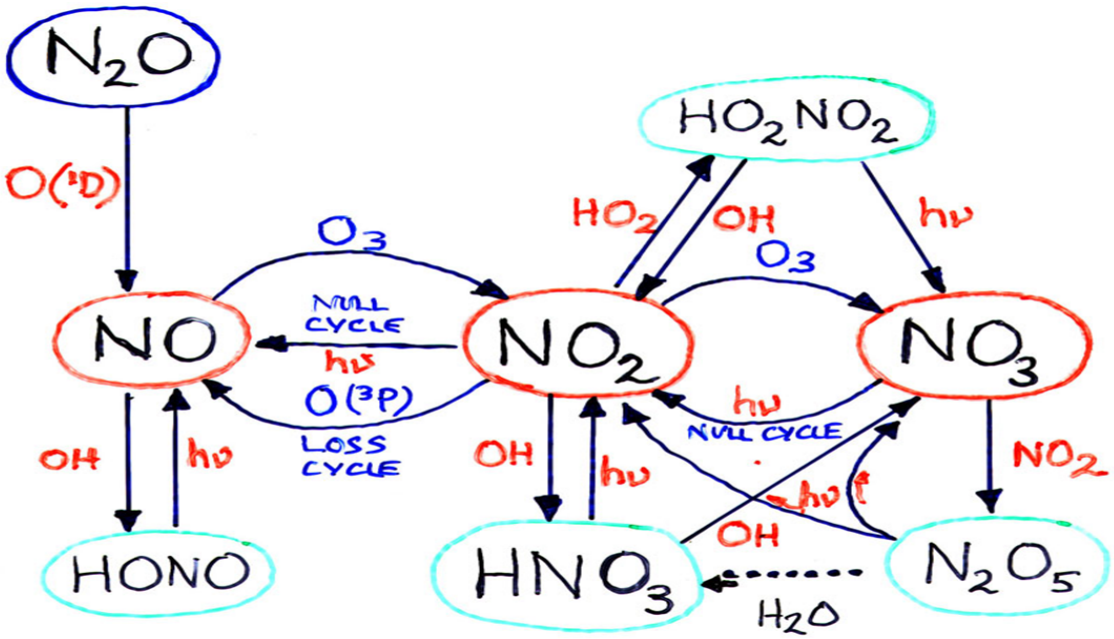

Fig. 2.6 Nitrogen oxides in the stratosphere (Source: https://www.slideserve.com/galahad/the-stratospheric-chemistry-and-the-ozone-layer).

The remaining 95 % are converted to N_2 by photolysis, which is

$$N_2O + h\nu \longrightarrow N_2 + O(^1D) \qquad \lambda < 398nm \tag{2.7}$$

Chapter 3

Fourier Transform Infrared Spectroscopy

Fourier transforms infrared spectroscopy is a powerful technique to study the atmospheric composition changes as it can measure different gases. As the major components of the atmosphere nitrogen, oxygen and argon are infrared inactive, thus technique has been significant to measure other trace gases. In ground-based solar fourier transform spectroscopy, the sun acts as the radiation source. The solar radiation reaching the top of the earth's atmosphere is in essence a black body curve at 5800 K with emission and absorption lines of gases in the solar atmosphere superimposed. Terrestrial atmospheric absorption lines contain information about the species of trace gases present in the atmosphere (line positions), the amounts of each gas present (line depths/areas) and some information about the altitude distribution of each gas (line shapes).

3.1 Fourier Transform Spectrometer

The Fourier transform spectrometer (FTS) is in principle a Michelson interferometer [63, 64]. The components of the fourier transform spectrometer are shown in Fig. 3.2. The light is separated into two beams by a beam splitter where some light is transmitted to a movable mirror and the remaining is reflected to a fixed mirror. Both beams are reflected by mirrors and then recombine at the beam splitter (BS) and interfere. Some recombined beam is transmitted to the light source and some is reflected to a detector. At the detector, the interference is recorded and converted to a digital signal. The optical path difference (OPD) is varied by moving the movable mirror. The pattern of the interference is called an interferogram which is used to calculate the spectrum of the incident radiation.

Infrared spectroscopy is a technique based on the vibrations of the atoms of a molecule that is commonly obtained by passing infrared radiation through a sample and determining what fraction of the incident radiation is absorbed at a particular energy. The energy at which any peak in an absorption spectrum appears corresponds to the frequency of a vibration of a part of a sample molecule. In this introductory chapter, the basic ideas and definitions associated with infrared spectroscopy will be described as these are crucial to the interpretation of infrared spectra. The radiation emerging from the source is passed through an interferometer to the sample before reaching a detector. Upon amplification of the signal, in which high-frequency contributions have been eliminated by a filter, the data are converted to digital form by an analog-to-digital converter and transferred to the computer for fourier-transformation.

3.1.1 Energy transitions

The three energy types, which are rotational, Vibrational and electronic energy are quantized and take only discrete values. The mid-infrared absorption spectra of molecules in the atmosphere are a result of simultaneous rotational and vibrational energy level transitions of these same molecules. Such spectra present themselves as bands of absorption with fine structure, where the central wave number of the band is determined by the type of vibrational transition taking place (fundamental, first overtone, etc.) while the band structure itself is determined by the allowed rotational transitions for that particular vibrational transition; the energy required to effect a rotational transition is much smaller than that required to effect a vibrational transition. We will now briefly consider rotational, vibrational and rotational-vibrational energy transitions in turn following the treatment made by Banwell and McCash in Banwell et.al., [65].

Nitrous oxide, N_2O is a triatomic molecule with a linear symmetrical configuration and having three vibrational modes: ν_1 for symmetric stretch, ν_2 for bending motion and ν_3 for antisymmetric. The nitrous oxide molecule has a linear and asymmetric structure, with the configuration NNO. Similar to carbon dioxide, it has a single rotational constant and a detectable rotational spectrum. Numerous bands produced by the fundamental, overtone, and combination frequencies exist in the infrared. The three fundamental frequencies are centered at $1285.6cm^{-1}(\nu_1)$, $588.8cm^{-1}(\nu_2)$ and $2223.5cm^{-1}(\nu_3)$. The ν_1 fundamental band of nitrous oxide overlaps the ν_4 fundamental band of methane.

Methane molecule has a spherical top configuration that has no permanent electric dipole moment or no pure rotational spectrum. There are four fundamental vibration modes and

only ν_3 and ν_4 that centered at 3020.3 and 1306.2cm^{-1} are active in the infrared spectrum. The ν_4 fundamental band of CH_4 is important in the climatic greenhouse effect. The inactive ν_1 and ν_2 fundamental bands are centered at 2914.2 and 1526cm^{-1}. Methane also possesses a rich spectrum of overtone and combination bands that have been identified in the solar spectrum.

Absorption lines of these anthropogenic trace gases are primarily located in the window region. Thus, their potential increase can make the atmospheric window "dirty" and may lead to significant greenhouse effects. The molecular symmetry of methane (CH_4) allows for highly active vibration-rotation excitation in the infrared absorption.

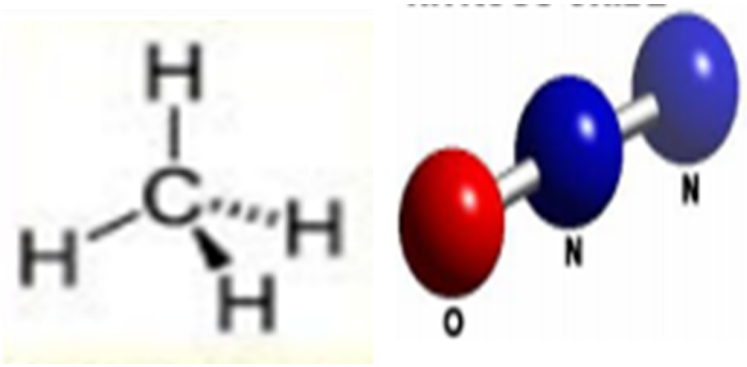

Fig. 3.1 Molecular structure of CH_4 (source: https://en.wikipedia.org/wiki/Alkane)and N_2O (source: https://www.webelements.com/compounds/nitrogen/nitrous_oxide.html) left to right respectively .

3.1.2 The Michelson Interferometer

The most common interferometer used in Fourier transform spectrometer is a Michelson interferometer, which consists of two perpendicular plane mirrors, one of which can travel in a direction perpendicular to the plane (Fig. 3.2).

If a collimated beam of monochromatic radiation of wavelength $\lambda(cm)$ is passed into an ideal beam splitter, 50 % of the incident radiation will be reflected to one of the mirrors while 50 % will be transmitted to the other mirror. The two beams are reflected from these mirrors, returning to the beam splitter where they recombine and interfere. The 50 % of the beam reflected from the fixed mirror is transmitted through the beam splitter while remaining 50 % is reflected back in the direction of the source. The beam which emerges from the

interferometer at 90° to the input beam is called the transmitted beam and this is the beam detected in FTIR spectrometers.

The moving mirror produces an optical path difference between the two arms of the interferometer. For path differences of $(n+1/2)\lambda$, the two beams interfere destructively in the case of the transmitted beam and constructively in the case of the reflected beam. The resultant interference pattern is shown in Fig. 3.2 for (a) a source of monochromatic radiation and (b) a source of polychromatic radiation. The former is a simple cosine function but the latter is of a more complicated form because it contains all the spectral information of the radiation falling on the detector.

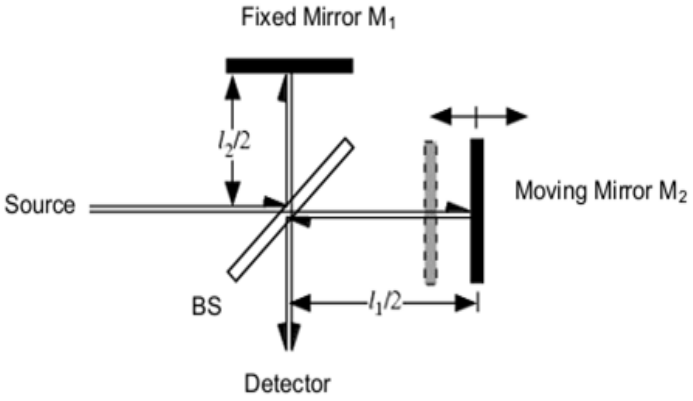

Fig. 3.2 A schematic diagram of a Michelson interferometer.

For a monochromatic light source which is single frequency with the interference created at the beam splitter due to the optical path difference x and the intensity of the interferogram can be written as

$$I(x) = B(\bar{\nu})[1 - cos(2\pi\bar{\nu}x)] \tag{3.1}$$

where $B(\bar{\nu})$ is the spectral intensity of the monochromatic source and $\bar{\nu}$ is wave number. Similarity, a polychromatic source of light which attains more than one frequency and the intensity of the interferogram can be written as

$$I(x) = \int_0^{+\infty} B(\bar{\nu})[1 - cos(2\pi\bar{\nu}x)]d\bar{\nu} \tag{3.2}$$

For a stable source the first term is constant represents the mean intensity of the interferom-

eter and the remaining term is AC component includes all the information in the spectrum

$$I(x) = \int_0^{+\infty} B(\bar{\nu}) cos(2\pi\bar{\nu}x) d\bar{\nu} \tag{3.3}$$

This is an essential equations for a Fourier-transformation relating the intensity falling on the detector, $I(x)$, to the spectral power density at a particular wave number, $\bar{\nu}$,given by $B(\bar{\nu})$ and this is one half of a cosine Fourier-transform pair, with the other being:

$$B(\bar{\nu}) = \int_{-\infty}^{+\infty} I(x) cos(2\pi\bar{\nu}x) dx \tag{3.4}$$

These two equations are interconvertible and are known as a Fourier-transform pair. The first shows the variation in power density as a function of the difference in path length, which is an interference pattern. The second shows the variation in intensity as a function of wave number. For real observations, only finite optical path differences can be attained and the above equation can be written as

$$B(\bar{\nu}) = \int_{-MOPD}^{+MOPD} I(x) cos(2\pi\bar{\nu}x) dx \tag{3.5}$$

where MOPD stands for maximum optical path difference and its value depends on the maximum distance that the moving mirror travels in the interferometer. Each FTS has a finite spectral resolution $\Delta\bar{\nu}$ due to its finite MOPD, the spectral resolution is defined as

$$\Delta\bar{\nu} = \frac{0.5}{MOPD} \tag{3.6}$$

3.2 Forward radiative transfer model

The signal reached to the sensor can be quantified using radiative transfer theory and expressed in terms of a physical quantity called Radiance. The two basic interactions held in the atmosphere are extinction and emission. Extinction includes all processes which reduce the radiant intensity is due to absorption and scattering. Moreover, this reduction of the radiance intensity were due to the constituent gases of the atmosphere. The radiation reaches an observing instrument through the atmosphere after traversing a thickness ds. Therefore, the change in the quantity I is given by

$$dI_\lambda = -k_\lambda n_a I_\lambda ds \tag{3.7}$$

Where n_a is the number density of an absorbing molecule and k_λ denotes the molecular extinction coefficient, which characterizes the interaction between the molecule and the radiation. Similarly, emission includes all processes which increase the radiant intensity. These processes include thermal emission and multiple scattering from the molecule that add radiance to the incident beam at the same frequency:

$$dI_\lambda = j_\lambda n_a ds \tag{3.8}$$

where j_λ is the emission coefficient, which characterizes the emission property of the molecules in the path. Both emission and absorption coefficient has been related using Kirchhof's law by assuming the local thermodynamics equilibrium of the layers and then at a given temperature, the two coefficients are related as follows:

$$J_\lambda(T) = \frac{j_\lambda}{k_\lambda}$$

Where J_λ is defined as the source function. The differential equation of radiative transfer is the combination of Equation (3.7) and (3.8), which is given by

$$dI_\lambda = -k_\lambda n_a I_\lambda ds + j_\lambda n_a ds \tag{3.9}$$

We introduce here an optical path of the medium to express Equation (3.9) in terms of the optical depth, The optical path measures the amount of extinction a beam of light experiences traveling between two points. When $\tau > 1$, the path is said to be optically thick. The most frequently used form of optical path is the optical depth. The optical depth τ is the vertical component of the optical path τ, i.e., τ measures extinction between vertical levels. For historical reasons, the optical depth in planetary atmospheres is defined as $\tau = 0$ at the top of the atmosphere and $\tau = \tau^*$ at the surface. Considering the optical depth between two levels $s_2 > s_1$ allows $s_2 \to \infty$:

$$\tau_\lambda(s_1, \infty) = \int_s^\infty k_\lambda \rho ds' \tag{3.10}$$

The radiative transfer Equation can be expressed in terms of the optical depth as follows:

$$\frac{dI_\lambda(s)}{d\tau_\lambda(s_1, s)} = -I_\lambda(s) + j_\lambda \tag{3.11}$$

Where τ_λ is a positive quantity and its first order differential equation with constant coefficient, integrating factor is $exp(-\tau_\lambda)$. After integrating using $\tau_\lambda = 0$, at the origin s_o is given by

$$I(s',s) = I(s_o,s)e^{-\tau(s_o,s)} + \int_0^{\tau(s_o,s)} J_\lambda(s',s)e^{-\tau(s',s)}d\tau_\lambda \tag{3.12}$$

The radiative transfer problem can be solved using equation (3.12) if the source function at a point and direction s is given and the source function is given by the planck function, $B_\lambda(T)$ under local thermodynamics conditions:

$$B_\lambda(T) = \frac{2h\nu^3}{c^2[exp(\frac{h\nu}{K_BT}) - 1]} \tag{3.13}$$

Where $\nu = \frac{c}{\lambda}$ and h is planck's constant, K_B is Boltzmann constant. At a given frequency, the source function depends only on temperature T, if the gas is in thermodynamic equilibrium. Different gas properties emitting and absorbing radiation at frequency ν are contained in their absorption or emission coefficient. One can also use transmission model equally well to describe the measurement The radiative transfer model in terms of total transmission has the form

$$I_\upsilon(t) = B_\nu T_s(t) \tag{3.14}$$

It is then noted that attenuation of radiation between arbitrary atmospheric layers bounded by s' and s is described as

$$I_\nu(t) = B_\nu(T_s \int_{s'}^{s} \frac{\partial t}{\partial s"} ds" \tag{3.15}$$

where now t is the total transmission after being attenuated by gases within layers bounded by $s"$ and $s" + ds"$. This is the general model for which explicit functional form of τ is not given, however, recalling the definition of optical thickness, the transmission can expressed as a function of s':

$$t_\nu(s',s) = exp(-\int_{s'}^{s} K_\nu(s")n_a(s")ds") \tag{3.16}$$

As there are many absorbers along the optical path, the absorption cross-section is weighted and given as

$$K_\nu(s') = \sum K_{\nu(m)(s')} y_m(s') \tag{3.17}$$

Where y_m(s') and $K_{\nu(m)(s')}$ denote volume mixing ratio (VMR) and absorption cross section of the species m with a total number M of different molecular species that absorb in the spectral region under consideration. By substituting equation (3.17) into equation (3.12),

the equation can be expressed as follows:

$$I_\nu(s',s) = I_\nu(s_o,s)[exp(-\int_{s_o}^{s}\sum K_{\nu(m)(s')}y_m(s')\rho(s')ds'] \tag{3.18}$$

Dividing equation (3.18) by $I_\nu(s_o,s)$ gives:

$$\frac{I_\nu(s',s)}{I_\nu(s_o,s)} = exp[-\int_{s_o}^{s}\sum K_{\nu(m)(s')}y_m(s')\rho(s')ds'] \tag{3.19}$$

Furthermore, the molecular species m may have several transitions which have different temperature and pressure dependence. The absorption cross-section of one molecular species m as a function of temperature and pressure is given by the following sum over all lines of the species (more details on the above discussion can be found in Fu et al. [26], Wunch et al. [29], Backus et al. [66]):

$$K_{\nu(m)}(T,P) = \sum_{i=1}^{lines} S_{m,i}(T)g_{m,i}(\nu-\nu_{m,i},T,P) \tag{3.20}$$

where $g_{m,i}(\nu-\nu_{m,i},T,P)$ is line shape function and $S_{m,i}(T)$ is spectral line strength.

3.3 Retrieval method

The focus of this work is on retrieval of methane (CH_4) and nitrous oxide (N_2O). The abundances of long-lived species has been determined from the ground-based FTIR for the mid and high latitudinal bands as reported in Holton and Gettelman [67]. For the retrieval of those species, We have also executed on 41 layer altitude grid starting from 2.45 km along with griding space of about 0.5 to 0.8 for the altitude range of lower tropospheric, which is 2.45 to 7.18 km and for the upper troposphere, 8 to 16 km the griding space between consecutive layers is about 0.9 to 1.2, for lower stratosphere is 1 to 1.8 griding space, which extends up to 34 km and finally for the upper layer the spacing is around 2 to 8 km.

Ideally, we can combine the observations and known information using a forward function, which describes all the necessary physics to relate the atmospheric state and the measured state.

In reality, we can never define perfectly, instead, we approximate by a forward model, **F(x,b)** that describes the physics of the measurement process and relates the measurement vector **y**

with m elements and the state vector $\mathbf{x}$ through

$$\mathbf{y} = \mathbf{F(x,b)} + \varepsilon \tag{3.21}$$

where $\mathbf{b}$ is a model parameter influencing the retrieval (temperature, pressure, absorbtion cross section of species and spectroscopic parameters) and ε is the error vector including the error in the observation, in the forward model and model parameters. Equation (3.21) can be linearized about the a priori state, $\mathbf{X}_a$:

$$\mathbf{y} = \mathbf{F}(\mathbf{x}_a, \mathbf{b}) + \mathbf{K}(\mathbf{x} - \mathbf{x}_a) + \varepsilon \tag{3.22}$$

where

$$\mathbf{K} = \frac{\partial \mathbf{F}(\mathbf{x}, \mathbf{b})}{\partial \mathbf{x}}$$

is an m by n matrix. Equation (3.22) can be further expanded to

$$\begin{aligned} \mathbf{y} =& \mathbf{F}(x_a, b) + \frac{\partial \mathbf{F}}{\partial \mathbf{x}}(x - x_a) + \frac{\partial \mathbf{F}}{\partial b}(b - b_a) + \varepsilon \\ =& \mathbf{F}(x_a, b_a) + K(x - x_a) + K_b(b - b_a) + \varepsilon \end{aligned} \tag{3.23}$$

$\mathbf{K}$ contains the sensitivity of the forward model to the true state of VMR, and $\mathbf{K}_b$ defines the sensitivity of the forward model to the model parameters. $\mathbf{K}$ is called the weighting function matrix or Jacobian matrix. It is possible to determine an inverse model $\mathbf{R}$ which relates the spectra $\mathbf{y}$ to the desired estimate of the atmospheric state, $\hat{\mathbf{x}}$:

$$\hat{\mathbf{x}} = \mathbf{R}(\mathbf{y}, \mathbf{b}) \tag{3.24}$$

The inverse model can also be linearized as

$$\begin{aligned} \hat{\mathbf{x}} =& \mathbf{R}(\mathbf{y}_a, b_a) + \frac{\partial \mathbf{R}}{\partial \mathbf{y}}(\mathbf{y} - \mathbf{y}_a) + \frac{\partial \mathbf{R}}{\partial \mathbf{b}}(\mathbf{b} - \mathbf{b}_a) \\ =& \mathbf{R}(\mathbf{y}_a, \mathbf{b}_a) + \mathbf{G}(\mathbf{y} - \mathbf{y}_a) + \mathbf{G}_b(\mathbf{b} - \mathbf{b}_a) \end{aligned} \tag{3.25}$$

About the measurement $\mathbf{y}_a$, which is expected from the measured spectrum when the VMR profile in the given atmosphere is $\mathbf{x}_a$. $\mathbf{G}$ is an n by m matrix called the gain or contribution function matrix, since it shows the contribution to the solution due to a unit change in the corresponding element of $\mathbf{y}$. $\mathbf{G}_b$ represents the sensitivity of the inverse model to its model parameters. The retrieved profile $\hat{\mathbf{x}}$ can be related to the true profile $\mathbf{x}$ using a transfer

function **T**,

$$\hat{\mathbf{x}} = \mathbf{R}(\mathbf{F}(\mathbf{x},\mathbf{b}),\mathbf{b}) = \mathbf{T}(\mathbf{x},\mathbf{b}) \tag{3.26}$$

By ignoring the errors in the measurements and model parameters. Equation (3.26) can be linearized about the a priori state, $\mathbf{x}_a$.

$$\hat{\mathbf{x}} = \mathbf{T}(x_a,b) + \frac{\partial \mathbf{T}}{\partial \mathbf{x}}(x-x_a) = \mathbf{T}(x_a,b) + \frac{\partial \mathbf{R}}{\partial F}\frac{\partial \mathbf{F}}{\partial x}(x-x_a) \quad = \mathbf{T}(x_a,b) + \mathbf{GK}(x-x_a) \tag{3.27}$$

Since $\mathbf{T}(\mathbf{x}_a,\mathbf{b}) = \mathbf{x}_a$, Equation (3.27) can be further simplified to

$$\hat{\mathbf{x}} = \mathbf{x}_a + \mathbf{GK}(\mathbf{x}-\mathbf{x}_a) = \mathbf{x}_a + \mathbf{A}(\mathbf{x}-\mathbf{x}_a) = \mathbf{A}\mathbf{x} + (\mathbf{I}-\mathbf{A})\mathbf{x}_a \tag{3.28}$$

with **A** defined as **GK**. Thus, $\hat{\mathbf{x}}$ is the solution of the retrieval, which is weighted by the matrix $\mathbf{A} = \mathbf{GK} = \frac{\partial \mathbf{R}}{\partial \mathbf{F}}\frac{\partial \mathbf{F}}{\partial \mathbf{x}} = \frac{\partial \hat{\mathbf{x}}}{\partial \mathbf{x}}$. The rows of the square matrix **A** are called the averaging kernel, and they represent the sensitivity of the retrieved state to the true state. The algorithm iterates until the cost function J(x) is minimized by solving for $\nabla_x J(x) = 0$ as shown below

$$\nabla_x J(x) = 2s_a^{-1}(x-x_a) + 2K^T s_a^{-1}(Kx-y) = 0 \tag{3.29}$$

Where S_a and S_ε are the a priori error and observational error covariance matrices respectively (the matrix equivalents of ε_a and ε). Note that observational error includes errors in the forward model as well as spectral noise and that in many instances it is the forward model error that dominates the S_ε matrix. The solution to Equation (3.28) yields the optimal estimate or retrieval $\hat{x}$ and is given by

$$\hat{x} = x_a + G(y - Kx_a) \tag{3.30}$$

where G is known as the gain matrix and describes the sensitivity of the retrieval to the observations, i.e.$G = \frac{\partial \hat{x}}{\partial y}$, and is given by: $G = (K^T s_a^{-1} K + s_a^{-1})^{-1} K^T s_a^{-1}$ and the averaging kernel matrix or resolving kernel $\mathbf{A} = \mathbf{GK}$. The rows of the nXm **G** matrix are commonly referred to as the contribution functions and represent the sensitivity of the retrieved state to the measurements. The rows of the mXn **K** matrix are commonly referred to as weighting functions and represent the sensitivity of the forward model to the true state. By definition, the rows of the nXn **A** matrix give the sensitivity of the retrieved state to the true state:

$$A = GK = \frac{\partial \hat{x}}{\partial y}\frac{\partial F(x)}{\partial x} = \frac{\partial \hat{x}}{\partial x} \tag{3.31}$$

For a measurement system that resolves each element of the retrieved state vector with perfect sensitivity, A equal the identity matrix. The *n* row of **A** then corresponds to a delta function response to the n element of the retrieved state vector. The 'n' column of **A** is the impulse response to a perturbation in the element of the true state vector.
In ground-based FTIR measurements the diagonal elements of **A** are not unity (representing imperfect sensitivity to the true state at all heights). The above results are strictly valid where the measurement and state vectors are linearly related and where the measurement and a priori error covariance statistics are Gaussian [68]. In this case the optimal solution is obtained using Newtonian iteration and is given by

$$x_{i+1} = x_a + (K_i^T s_\varepsilon^{-1} K_1 + s_a^{-1})^{-1} K_i^T s_\varepsilon^{-1} [(y - y_1) - K_i(x_a - x_i)] \tag{3.32}$$

where K_i is taken to mean K evaluated at x_i and $y_i = F(x_i)$. The number of state vector elements that are independently resolved is calculated by taking the trace of **A** and is referred to as the degrees of freedom for signal in the measurement, $d_a = tr(A)$.
By taking the trace of **A** over a certain vertical range of the atmosphere, we determine the number of independently resolved pieces of information present in the partial column derived from this region. The information content may be defined in terms of the degrees of freedom for signal which is the trace of the averaging kernel. Mathematically this is the sum of the diagonal elements of the averaging kernel matrix [69].

3.4 Retrieval Characterization

In this section, we give an overview of our retrieval approach for two target molecules, followed by a discussion of the characteristics of the derived profiles and the FTIR measurements of CH_4 and N_2O for the tropical atmospheric conditions.

3.4.1 Vertical resolution and sensitivity assessment

Averaging kernel is the most important quantities, which characterize the retrieval results weather the information comes from the measurement or the a priori. Taking the summation of individual elements of the row averaging kernels estimates the amount of measurement information in the retrieved results. Thus, $\hat{\mathbf{x}}$, which is the solution of the retrieval as mathematically expressed in Equation (3.28) is a combination of a priori profile $\mathbf{x}_a$ and the measurements.

The spectral resolution of a measurement affects the amount of vertical information derived from the spectral line shape of a measured species [31]. The vertical resolution of the instruments in the ideal case representees the vertical layer spacing. However, in reality the vertical layer spacing couldn't represent the vertical resolution of the measurements. Hence, **A** is different from identity matrix, which shows presence of contribution of the assumed a priori profile information in the retrieved profiles. The vertical resolution is defined as full width at half maximum (FWHM) of the row averaging kernels of the species.

The trace of the averaging kernel matrix **A**, called the degrees of freedom for Signal($DOFS$) in the measurement determines the number of independently resolved pieces of information in the atmosphere obtained from the measurement.

3.4.2 Retrieval Error Analysis

The retrieved results are affected by statistical, systematic errors, the a priori and the spectrum solar zenith angle. This section provides a brief description of the error estimation, which includes measurement, smoothing and interfering species error. The retrieved state vector related to the a priori and the true state vectors $\mathbf{x}_a$ and $\mathbf{x}$ by taking the error in to account in Equation (3.28).

$$\hat{\mathbf{x}} = \mathbf{A}\mathbf{x} + (\mathbf{I} - \mathbf{A})\mathbf{x}_a + \boldsymbol{\varepsilon} \tag{3.33}$$

The error estimation analysis based on the analytical method suggested by Rodgers (2000) is expressed as follows

$$\hat{\mathbf{x}} - \mathbf{x} = (\mathbf{A} - \mathbf{I})(\mathbf{x} - \mathbf{x}_a) + \mathbf{G}\mathbf{K}_b(\mathbf{b} - \mathbf{b}_a) + \mathbf{G}\triangle f(\mathbf{x}, \mathbf{b}, \mathbf{b}^{'}) + \mathbf{G}\boldsymbol{\varepsilon} \tag{3.34}$$

where **A** is the averaging kernel matrix as defined in Section 3.3 and Eq. (3.31), **I** is the identity matrix, **G** is the gain matrix representing the sensitivity of the retrieved parameters to the measurement, $\mathbf{K}_b$ the sensitivity matrix of the spectrum to the forward model parameters **b**. As long as we do not know the real VMR profile in the atmosphere, only the error covariance matrix can be obtained as

$$\mathbf{S}_s = (\mathbf{A} - \mathbf{I})\mathbf{S}_a(\mathbf{A} - \mathbf{I})^T \tag{3.35}$$

$$\mathbf{S}_F = \mathbf{G}\mathbf{K}_b\mathbf{S}_b\mathbf{K}_b^T\mathbf{G}^T \tag{3.36}$$

$$\mathbf{S}_M = \mathbf{G}\mathbf{S}_\varepsilon\mathbf{G} \tag{3.37}$$

The total error obtained in the retrieved profile can be described as the combination of three different error sources, i.e. the smoothing error, the forward model parameter error including the temperature error, and the measurement error. The retrievals of CH_4 and N_2O vertical profiles have been made using PROFFIT algorithm that stated its detailed in chapter five of this paper.

3.5 Retrievals Using PROFFIT algorithm

The retrieval code used which is based on optimal estimation method (OEM) is PROFFIT 95 [70]. The first step in retrieval is to calculate synthetic spectrum based on model atmosphere using forward code (PROFFWD) and derivatives for error estimation. This software performs a radiative transfer calculation for a given set of relevant atmospheric temperature, pressure and mixing ratio. Pressure and temperature dependent absorption line parameters are obtained from the high-resolution transmission molecular absorption (HITRAN) and auxiliary (SZA, ILS) input quantities for the spectral micro windows are selected for analysis. The derivative of the spectrum with respect to the target and auxiliary quantities are allowed to vary in the process of searching the best estimate of the atmospheric state. The second step, the inversion model (PROFFIT), which processes the PROFFWD model output and suggests improved solution, restarts forward model with updated variables, and cycles until convergence is reached. In short, PROFFIT determines a best estimate of the observed atmospheric state by improving fit quality to recorded spectrum iteratively.

The model includes a model of the instrumental effects and a layered model of the atmosphere with assumptions about environmental parameters such as the pressure, temperature and composition of each layer.

Methane and nitrous oxide vertical profiles over Addis Ababa has been obtained by fitting five and four Micro windows respectively. The retrieved state vector contains the retrieved volume mixing ratios of the target gas defined in 41 layers of the tropical atmospheric conditions.

PROFFIT includes various retrieval options such as scaling of a priori profile, the Tikhonov-Phillips [32, 37], or the optimal estimation method [31]. In this study, an optimized retrieval strategy for Addis Ababa has been established for CH_4 and N_2O by applying it first to single spectra, as test cases, and later routinely to the full set of measurements. Partly, the strategy

to optimally retrieval of the total columns of CH_4 and N_2O are to search for a set of spectra micro-windows, constraint, initial guess and a priori profile are chosen in such a way that all the structures visible in the retrieved distributions originate from the measurements and are not artifacts due to any constraints. At the Addis Ababa site, we did not use the a priori covariance matrix as an optimal estimation. However, the Tikhonov-type L_1 regularization method [33] on a logarithmic scale is used during the retrieval of CH_4 and N_2O. The retrieval is performed on a fine vertical grid from 2.45 to 85 km and is stabilized by a first order Tikhonov constraint, $R = \alpha L^T L$, where α is the strength of the constraint and L_1 is the first order derivative [34], which smooths the solution without biasing it towards the a priori profile. The parameter determines the weight of regularization and it is also important to choose appropriate to the problem. One way to fix this parameter is the L-curve method [36]. The regularization strength α, is determined by finding a trade-off between the number of degrees of freedom (a measure of the amount of information in methane and nitrous oxide retrieval), which is given by the trace of row averaging kernel and the noise induced error [31]. A regularization strength α, of 2.5 $\times 10^4$ was found optimum for CH_4 and N_2O retrieval.

Chapter 4

Instrumentations and site descriptions

4.1 Instrumentations

4.1.1 NDACC FTIR experiments

Network for the Detection for Stratospheric Change (NDACC) is a global network community that monitors changes in atmospheric composition. FTIR spectrometers are operated at various stations worldwide on a regular basis and provides long-term observations of many trace gases to assess their impact on global climate. In this work, we will present results from data recorded at Addis Ababa, Ethiopia (9.01° N, 38.77° E, 2443 m a.s.l.), Jungfraujoch, Switzerland (46.5° N, 8.0° E, 3580 m a.s.l.) and Ny-Ålesund, Spitsbergen (78.92° N, 11.9° E, 20 m a.s.l.) as stations located in three different latitude bands. The time periods under considerations were starting May, 2009 to Feb, 2011 for Addis Ababa, Jan., 2009 to Feb., 2011 for Jungfraujoch and March, 2009 to April, 2011 for Ny-Ålesund are considered in this paper. FTIR measurements have been used successfully for the validation of SCIAMACHY CO, CH_4, CO_2 and N_2O columns [38] and for the validation of upper troposphere/lower stratosphere measurements by ENVISAT MIPAS [71, 72].
The ground-based NDACC FTIR stations used in this study are shown in Table 4.1. Hence, the large uncertainty of satellite observations of methane in upper troposphere and lower stratosphere over tropics will be investigated as well impacts of water vapour variabilities on the large uncertainty are also studied (see Chapter 7).

In this project, we use data products of CH_4 derived from two NDACC FTIR site that represents the mid and high latitudes of northern hemisphere to explore the large uncertainty of MIPAS methane in tropics for May, 2009 to Feb, 2011. The profiles were retrieved using the inversion code PROFFIT (PROFile FIT) [70] for Addis Ababa, but the retrievals of the

remaining two stations have been performed using the SFIT2 algorithm. PROFFIT and SFIT2 codes have been cross-validated successfully [70]. The detail description of the two NDACC FTIR sites are reported in different articles (eg. [27]) and the description of Addis Ababa FTIR experiment is also reported in the previous works [24, 25]. Therefore, only the main features of Addis Ababa FTIR is briefly described in the following section. Fig. 4.1 shows the location of FTIR sites.

Table 4.1 Three locations, which are representing the three norther hemispheric atmospheric conditions

FTIR Sit	Latitude	Longitude	Elevation (m)
Addis Ababa, Ethiopia	9.03°N	38.77°E	2443
Jungfraujoch, Switzerland	46.55°N	7.98°E	3580
NyÅlesund, Spitsbergen	78.92°N	11.93°E	15

Addis Ababa FTIR

The high-resolution FTIR Spectrometer, Bruker IFS120M upgraded with 125M electronics, from the Bruker Optics Company in Germany was installed in May, 2009 at the Addis Ababa site. The spectral coverage of the IFS120M instrument at Addis Ababa site is 750-4000 cm^{-1} with seven filters. This interferometer is equipped with indium-antimonide (InSb) detector, which allow the coverage of the 1500-4400 cm^{-1} spectral interval. In this spectral interval, a very large number of species that reside in the atmosphere can be detected. PROFFIT Ver 95 algorithm has been used to derive the VMR profiles and column amounts of CH_4 and N_2O from measured spectra in the microwindows that span spectral range of 2400-3100 cm^{-1}. Fig. 4.2 shows various components of the instrumental set up. The vertical profiles over Addis Ababa have been obtained by fitting five and four selected spectral regions (microwindows) for CH_4 and N_2O respectively. The retrieved state vector contains the retrieval volume mixing ratios of the target gas defined in 41 layers of the tropical atmosphere.

4.1.2 Michelson Interferometer for Passive Atmospheric Sounding (MIPAS)

Michelson Interferometer for Passive Atmospheric Sounding (MIPAS) instrument is a high-resolution atmospheric limb sounder aboard ESA's ENVISAT launched in March 2002 and

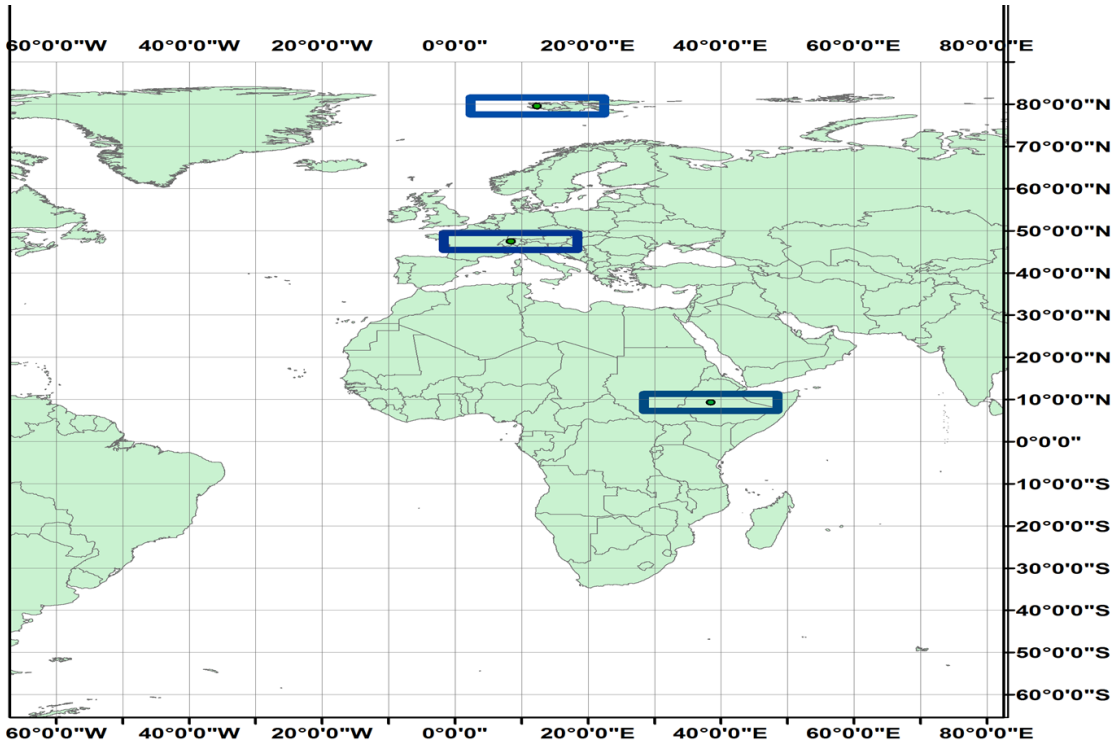

Fig. 4.1 The three spatial locations of FTIR site considered in this study. The box on the map encloses the spatial area considered for validation with satellites (see also Chapters 5-6).

operating in a sun−synchroneous orbit, which delivered limb spectra of atmospheric infrared range of 685 cm^{-1} to 2410 cm^{-1} along with a resolution of 0.035 cm^{-1} [73]. It aims at global and simultaneous measurements of the chemical composition of the middle atmosphere and upper troposphere. The pointing system allows MIPAS to observe atmospheric parameters in a maximum altitude range of 5-160 km with a vertical spacing of 1-8 km depending on the altitude and the measurement mode. Water vapor is retrieved on a fixed altitude grid, using a grid width of 1 km from 0 to 44 km, 2 km from 44 to 70 km, 5 km from 70 to 80 km, 10 km from 80 to 120 km. The infrared limb spectra are inverted to provide profiles of numerous trace gases, including CH_4 and N_2O [43].

In this study, we have used the reduced spectral resolution (Institute for Meteorology and Climate Research) MIPAS IMK/IAA V5R_CH4_224, V5R_N2O_224 and V5R_H2O_220 [48, 53] and the previous version data products V5R_CH4_220, V5R_N2O_220 [73]. The lower limit altitude to obtain the profiles of climate gases from MIPAS is different for different atmospheric conditions. For instance, lower altitude in tropics is around 10 km, and around 6 km for both mid latitude and polar region.The infrared limb spectra are inverted to

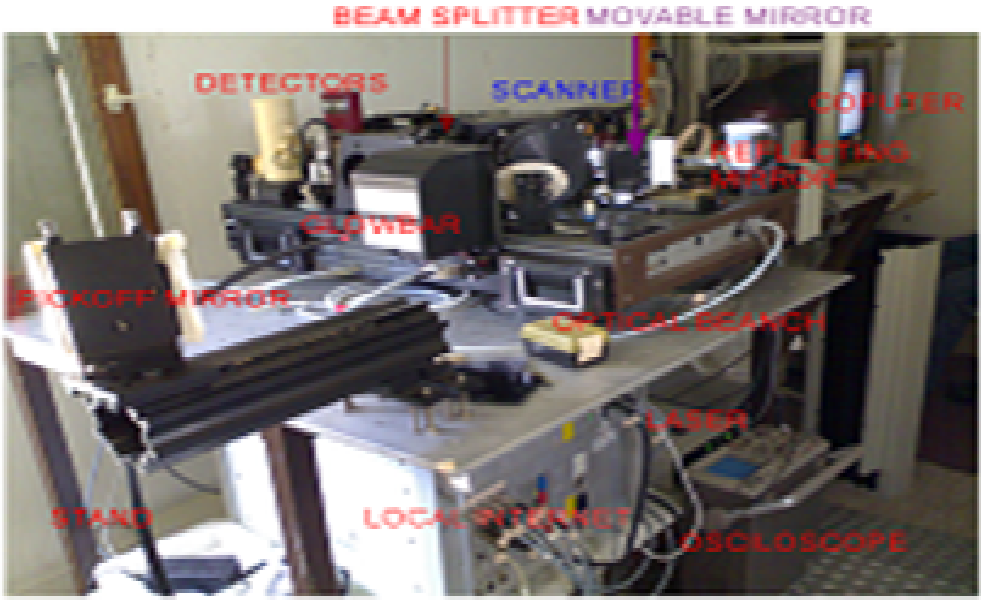

Fig. 4.2 The FTIR spectrometer at measurement site in Addis Ababa and its principle (Source: Endale Gemechu, OBSERVATION AND VALIDATION OF METHANE FROM FTTIR OVER ADDIS ABABA, http://etd.aau.edu.et/bitstream/handle/123456789/2692,pg66,2011).

provide profiles of numerous trace gases, including CH_4 and N_2O [43].

4.1.3 Microwave Limb Sounder (MLS)

The Earth Observing System (EOS) Microwave Limb Sounder (MLS) is one of four instruments on the NASA's EOS Aura satellite and launched on July 15, 2004 into a near polar sun-synchronous orbit at 705 km altitude [74]. MLS scans the earth's limb in the forward direction of flight and observes thermal microwave far infrared emission from the Earth's atmosphere in five spectral regions, 118, 190, 240 and 640 GHz and 2.5 THz [75]. The vertical profiles of O_3, H_2O, BrO, ClO, HCl, HOCl, OH, HO_2, HCN, CO, HNO_3, N_2O and SO_2 mixing ratios have been derived from the spectra measured by MLS. In addition to the measurements of mixing ratios relative humidity with respect to ice, cloud water, geo potential height and temperature have also been obtained from this instrument. The spatial coverage of this instrument is nearly global (-82°S to 82°N) and individual profile is spaced at 1.5^o or 165 km along the orbit track. Roughly the satellite covers this latitudinal bands

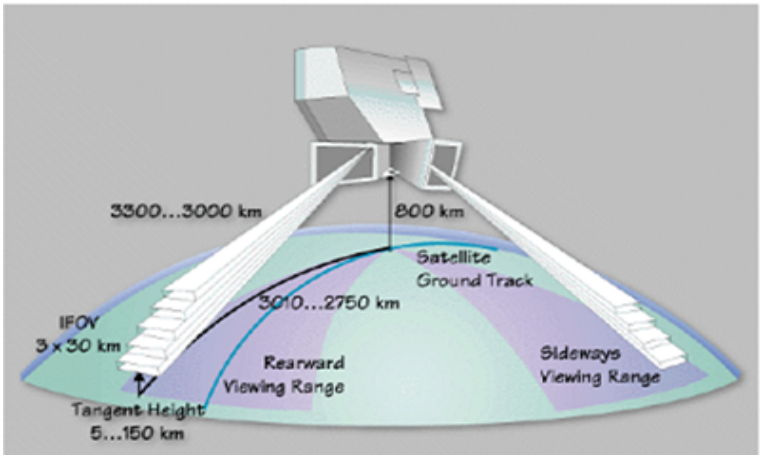

Fig. 4.3 Scanning possibilities for MIPAS (Source: European Space Agency, Envisat MIPAS product handbook, Issue 2.2, 27 February 2007).

with 15 orbit per day or around 3500 vertical profiles per day. This instrument ascending equatorial region at local time of around 13:45 hour [76]. MLS version 3.3 (v3.3) data have been used. The retrieval scheme is based on the Optimal Estimation Method and retrieval approach is detailed in Livesey et al. [77]. The vertical resolution of MLS CH_4 is between 4 and 5 km; the vertical resolution of N_2O is 4 to 6 km; the vertical resolution for H_2O is 1.5 km at 316 hpa increasing to 3.3-3.5 at 147 hPa. H_2O is retrieved from measurements of the 183 GHz H_2O rotational line spectrum [24, 78]. From the UT (220 hPa) to the LS (31 hPa), the precision and accuracy range of H_2O are from 40 to 6 % and from 25 to 4 % respectively, for a vertical resolution from 2.5 to 3.2 km, although the entire useful pressure range spans from 316 to 0.002 hPa [79].

In this work, we have used version 3.3 MLS of N_2O data set to validate a ground-based FTIR results. However, the methane (CH_4) data contain vertical profiles of between 100 and 0.1 hPa pressure which are derived using coincident measurements of atmospheric water vapor (H_2O), carbon monoxide (CO) and nitrous oxide (N_2O) from the EOS MLS (Earth Observing System Microwave Limb Sounder) instrument on the NASA Aura satellite and detail of the derivation are in Minschwaner et al. [80]. More details regarding the MLS experiment and data screening are provided in the above references in detail and at http://mls.jpl.nasa.gov/data/datadocs.php. Nitrous oxide derived from MLS v2.2 has been taken from the 640 GHz (Core+R4B) retrieval and validated in Lambert et al. [78] and reported that MLS N_2O precision is 24-14 ppbv (9-41 %) and the accuracy is to be 70-3 ppbv (9-25 %) in the pressure range 100-4.6 hPa [79].

Table 4.2 Summary on the characteristics of the satellite based instruments and measurement systems of CH_4 and N_2O used in this study

Instruments	FTIR	MLS	MIPAS	AIRS
Platform	Ground-based	Satellite	Satellite	Satellite
Observation geometry	upward	limb	limb	nadir
Observation mode	absorption	emission	emission	emission
Vertical resolution(km)	∼9-15	3-4	3-5	greater than ∼6
Spectral resolution	0.009 cm^{-1}	6-96 MHz	0.0625 cm^{-1}	2 cm^{-1}
Spectral domain	600-4400 cm^{-1}	∼80,000 cm^{-1} (∼240 GHz)	685 2410 cm^{-1}	650-2700 cm^{-1}

4.1.4 Atmospheric Infrared Sounder (AIRS)

Operating in nadir sounding geometry, the Atmospheric Infrared Sounder (AIRS) on board the Aqua satellite launched into Earth orbit in May 2002 [81]. AIRS is a medium-resolution infrared grating spectroradiometer and a diffraction grating disperses the incoming infrared radiation into 17 linear detector arrays comprising 2378 spectral samples. The satellite crosses the equator at approximately 1:30 A.M. and 1:30 P.M. local time, resulting in near global coverage twice a day. AIRS 2378 channels covers from 649 to 1136, 1217–1613 and 2169–2674 cm^{-1}. It also measures trace gases such as O_3, CO and to some extent CO_2. AIRS CH_4 and N_2O retrievals have been characterized and validated by [82] and [83] respectively.

4.2 Measurement site description

The Addis Ababa FTIR spectroscopy site was established to acquire high-quality long-term measurements of trace gases for the purpose of understanding chemical and dynamical processes in the atmosphere and to validate models and satellite measurements of atmospheric constituents. The geographic position of the observatory is (9.01°N, 38.76°E, 2443 m altitude above sea level) and its suitability has been confirmed from the measurements of tropical stratospheric ozone, precipitable water vapour and isotopic composition of water

vapour [20–24]. Addis Ababa is a tropical high altitude observing site and as such extremely important to understand processes near the tropical tropopause. Physical process in tropics, mainly around tropopause layer has a vital role in climate change and the general circulation of the tropical troposphere, which would control the transport of energy, water vapour and trace gases in the climate system derived by the deep convection [67]. Ethiopian

Fig. 4.4 FTIR measurement site at Addis Ababa inside Addis Ababa university, Science faculty campus (Source: Endale Gemechu, OBSERVATION AND VALIDATION OF METHANE FROM FTTIR OVER ADDIS ABABA, http://etd.aau.edu.et/bitstream/handle/123456789/2692,pg66,2011.

is characterized by high rainfall and temperature variability on both spatial and temporal scales. The variability in distribution is related to altitude, latitude, humidity and winds, which are the significant factors in affecting the weather system of the country. Therefore, measurements and interpretation of atmospheric trace gas (CH_4 and N_2O) composition of tropics are vital for a better understanding of the budgets, sources and sinks of trace gases in the atmosphere and their effects on atmospheric chemistry, greenhouse effect and climate changes globally. The retrieval of CH_4 and N_2O from the Addis Ababa FTIR observatory and the characterization of the averaging kernel and error analysis will be discussed in chapter five and their intercomparison results with the instruments stated in this chapter have been used to assess the quality of the observations made by FTIR at the Addis Ababa site and presented in chapter six of this study.

Chapter 5

Observations of CH_4 and N_2O from ground-based FTIR over Addis Ababa

5.1 Introduction

Ground-based high-resolution Fourier transform infrared (FTIR) is one of the power full remote sensing techniques used to derive the concentration of atmospheric trace gases. Spectra recorded at the Addis Ababa observatory were analyzed using inversion code PROFFIT version 95 and its description is reported in Hase et al. [70]. The algorithm has been developed based on semi empirical Optimal Estimation Method to derive the VMR profiles and column amounts of CH_4 and N_2O from the measured spectra in the microwindows that span spectral range of 2400-3100 cm^{-1} (3.3-4.1 μm). A detailed description of the retrieval strategy, information content and corresponding full error budget evaluation of methane (CH_4) and nitrous oxide (N_2O) are presented.

5.2 Spectral Analysis and Retrievals parameters

5.2.1 Spectroscopic data and a priori profiles

Interfering species (see Table 5.1) were scaled together with the inversion of the target gas profile. A priori profiles based on available data sets from the Whole Atmosphere Community Climate Model (WACCM, http://www2.cesm.ucar.edu/working-groups) for Addis Ababa site, which has been recommended by the NDACC/IRWG Group.
Daily profiles of pressure and temperature were taken from the NCEP reanalysis are made available through the NASA Goddard Space Flight Centre auto mailer from http://hyperion:

gsfc:nasa:gov/. The spectroscopic parameters were chosen from the High Resolution Transmission (HITRAN) database version 2004 with the 2009 and 2012 updates [84, 85]. The updated HITRAN data of 2009 for H_2O and HITRAN 2012 for CO_2, CH_4, NO_2 and hit08 of N_2O were used during retrieval of CH_4 and N_2O. The contribution of pressure and temperature uncertainty to the overall error budget in retrieval of trace gases from ground-based FTIR absorption spectra is insignificant. Nevertheless, the microwindows selected are due to their strong sensitivity to pressure broadening [86].

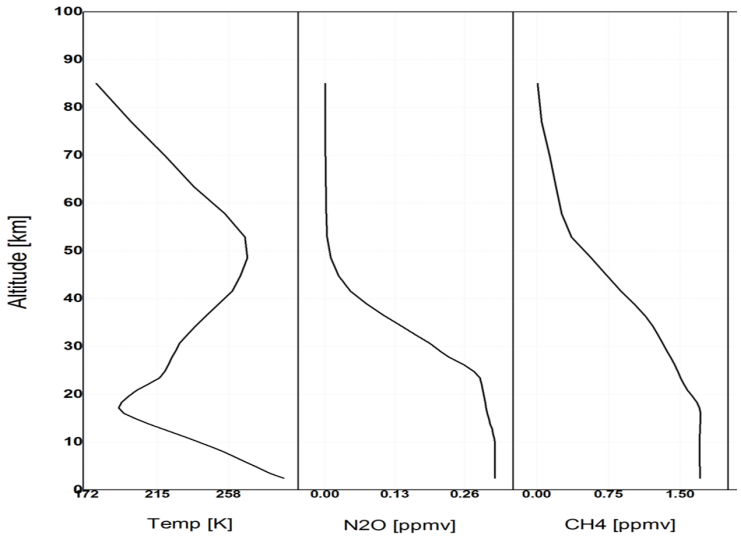

Fig. 5.1 a priori profile of N_2O and CH_4 (second and third column) and temperature (first column) at Addis Ababa site.

Figure 5.1 shows a priori profile of N_2O and CH_4 for tropical atmospheric conditions along with the temperature profiles. Methane is well-mixed in the troposphere and its VMR decreases with height and remains negligible with no variation above 55 km. The vertical variation of CH_4 in the stratosphere is characterized by large vertical gradient.

The spectral micro-windows used for the retrieval are selected such that the absorption features of the target species along with a minimal number of interfering absorption lines are presented. The microwindows have been adopted from different sources [25, 87, 91]. The microwindows as well as interfering gases for the two target species in this paper are shown in Table 5.1. However, the microwindows are somehow modified for tropics from the windows recommended by NDACC as mentioned in a result of work done Within the EU projects UTFIR (www.nilu.no/uftir) and HYMN (www.knmi.nl/samenw/hymn).

The spectral fit and residual between measured and simulated spectra at five and four mi-

crowindows for CH_4 and N_2O respectively are depicted in Fig. 5.2 and Fig. 5.3 for example the spectra recorded on Feb 26, 2013 and Dec 31, 2009 at Addis Ababa respectively. The last column of Table 5.1 provides typical values for the degrees of freedom for signal (DOFS) and it indicates the possible independent pieces of information of the target gases distribution. Magnitudes of residuals of the spectral fits are less than 1 % with both positive and negative signs (CH_4: 0.64 % and N_2O: 0.34 %). An optimized retrieval strategy for tropics has been established within the framework of this thesis for the retrieval of CH_4 and N_2O by applying it first to single spectra as test cases, and later routinely to the full set of measurements. Concentrations of CH_4 and N_2O were derived from 166 spectra in c region recorded from Dec. 2009 to March 2013. From the forward modeled value of the spectrum, the

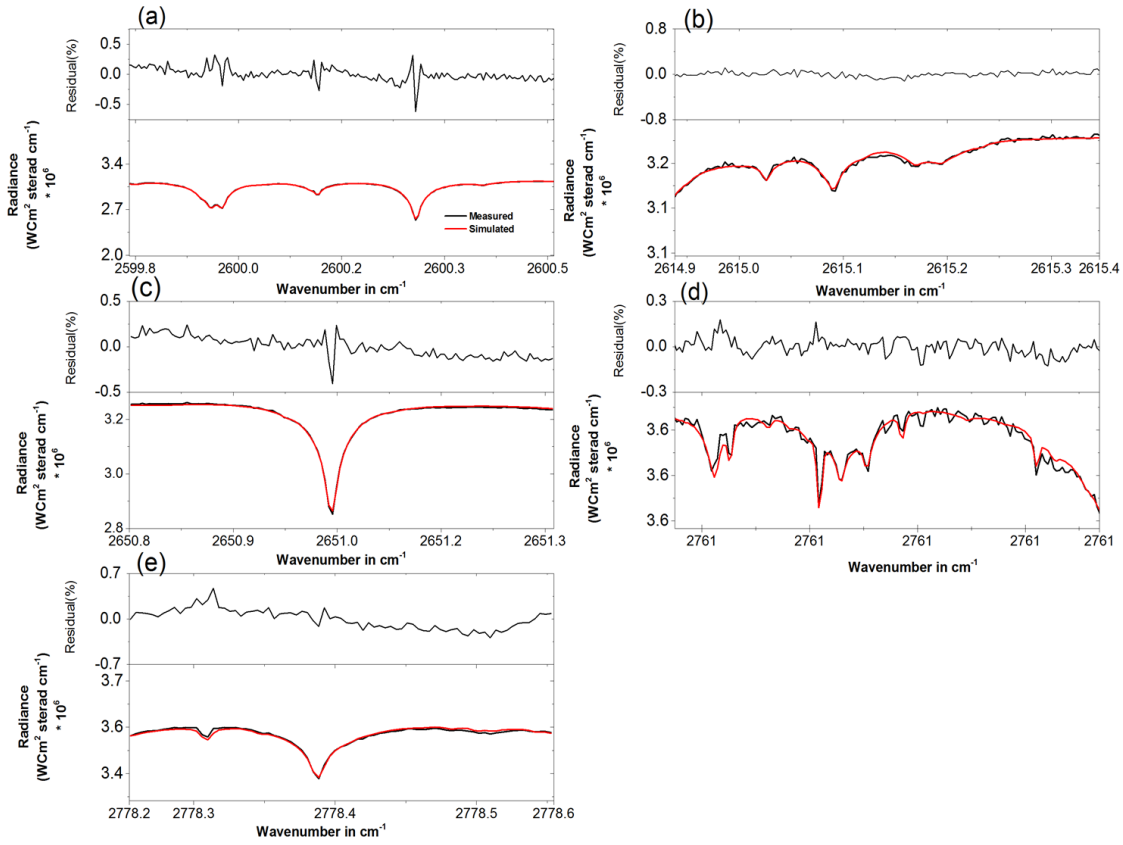

Fig. 5.2 The five spectral micro-windows used for retrieval of CH_4, with the measured spectrum in red, the simulated spectrum in black, and residuals on top of the respective microwindow. The spectrum was recorded on Feb 26, 2013, time: 10h17m15s, root mean square (RMS) =0.1189, solar zenith angle (SZA)= 20.6° , Optimal Path Difference (OPD)=116.1, DOF = 2.23, Field Of View (FOV)=2.27 mrad.

weighting function matrix, **G** can be determined. Figure 5.5 show the weighting function

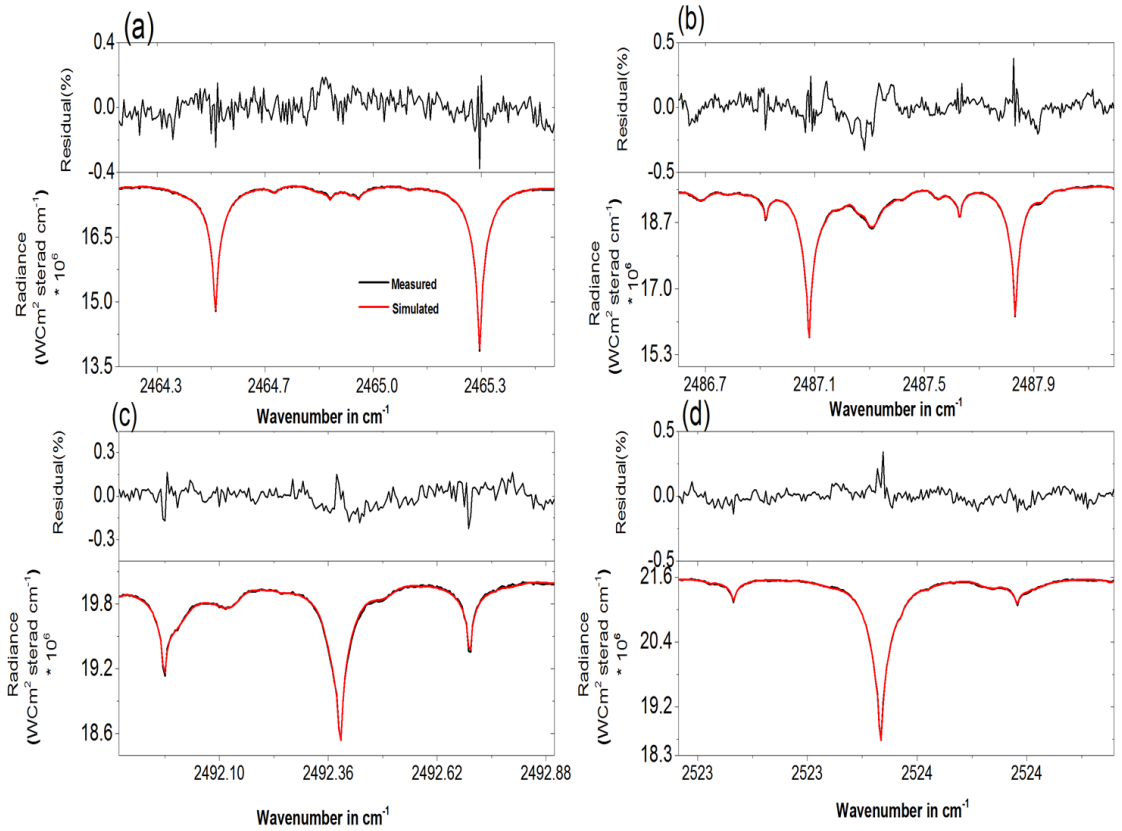

Fig. 5.3 The four spectral micro-windows used for retrieval of N_2O, with the measured spectrum in red, the simulated spectrum in black, and residuals on top of the respective microwindow. The spectrum was recorded on Dec 31, 2009, time: 09h3m727s,solar zenith angle (SZA) = 13.4°, Optimal Path Difference (OPD) =100, DOF = 3.35.

matrix for the fit in Fig. 5.3. The relative strength of the contours indicates what part of the spectral lines weight the retrieval or the sensitivity of the retrieved profiles of N_2O at Addis Ababa observatory with respect to observations.

The retrievals were affected by statistical, systematic errors, a priori and the spectrum solar zenith angle; therefore, the results presented in this section are representative of the whole spectrum, and indeed, all retrievals performed with similar constraints. The information content of the retrieval will strongly depend on the choice of the absorption lines and use of accurate pressure and temperature profiles [86].

An optimized retrieval strategy has been established within the frame of this work for the retrieval of CH_4 and N_2O as shown in Table 5.1. The micro windows used in this work, which are applicable for the retrieval of those gases of tropical atmospheric conditions, are

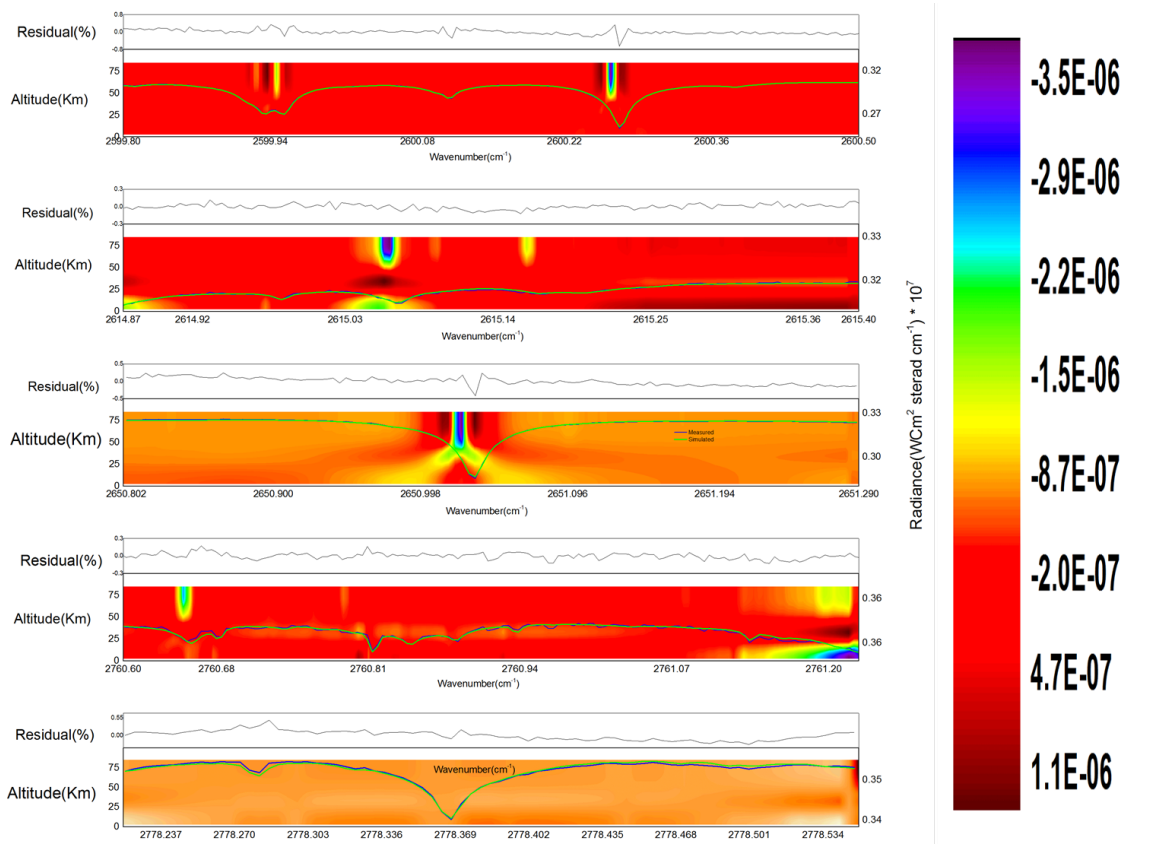

Fig. 5.4 weighting function matrix calculated for the CH_4 infrared absorption spectral micro windows used (see Table5.1). This was calculated for the spectrum shown in Fig. 5.2, which was recorded on Feb. 26, 2013.

Table 5.1 Micro windows, interfering gases and their DOFs listed in the table are used for the retrieval of VMR profiles and column amounts of CH_4 and N_2O from FTIR spectra recorded at Addis Ababa.

Target Gases	Micro windows(cm^{-1})	interfering gases	DOFS
CH_4	(2599.8,2600.5) (2614.87,2615.4) (2650.8,2651.29) (2760.6,2761.23) (2778.22,2778.55)	H_2O, CO_2, NO_2	2.045 $\pm$0.18
N_2O	(2464.2,2465.57) (2486.55,2488.18) (2491.86,2492.9) (2522.95,2524.1)	CH_4 H_2O, CO_2, CH_4 H_2O H_2O, CH_4	3.38 $\pm$0.15

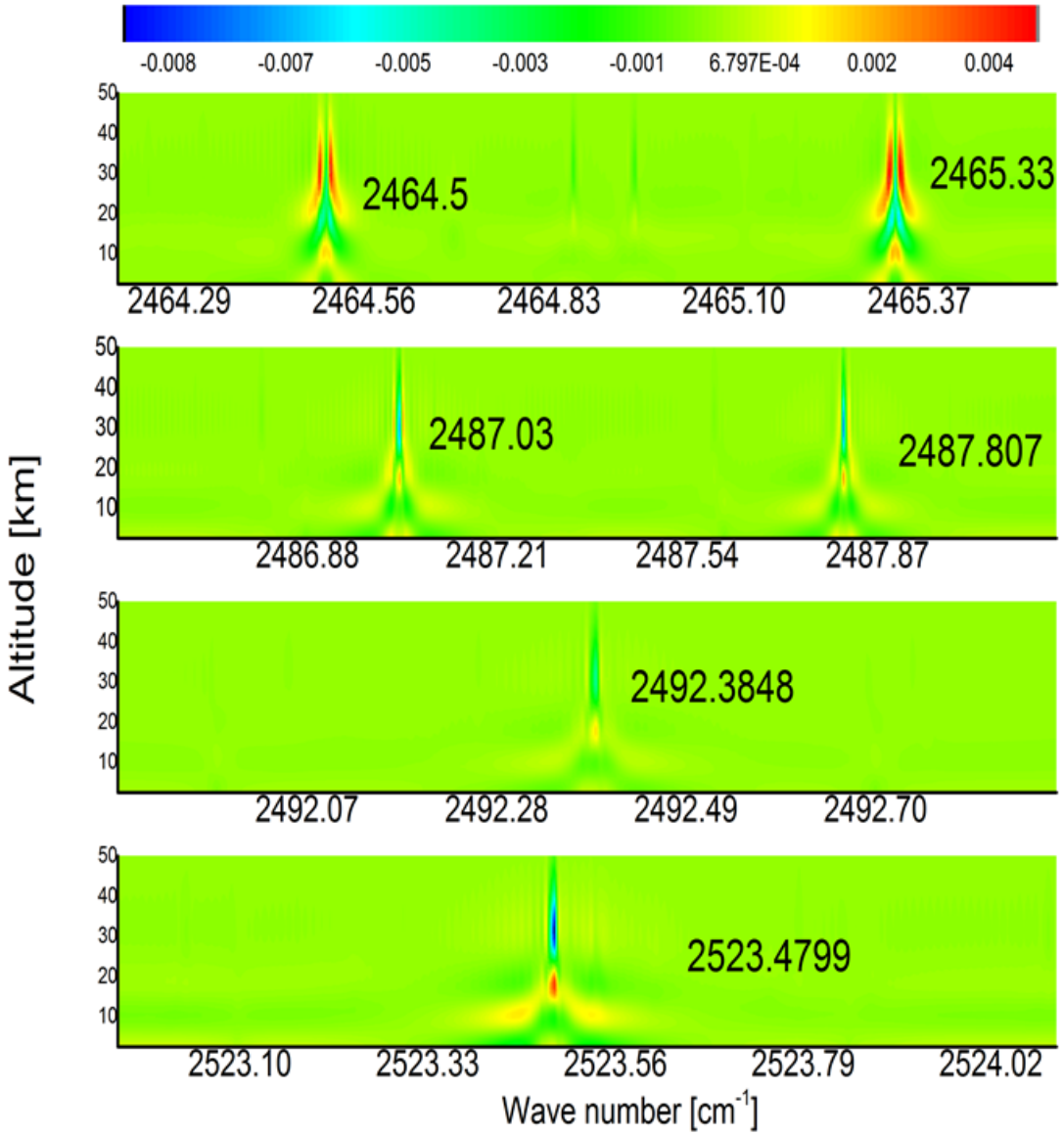

Fig. 5.5 weighting function matrix calculated for the N_2O infrared absorption spectral micro windows used (see Table5.1). This was calculated for the spectrum shown in Fig. 5.3, which was recorded on Dec 31, 2009.

also summarized in Table 5.1. The characteristics of the retrieved profiles of CH_4 and N_2O will be given in section 5.3.

5.3 Characterization of Retrievals

In this section, we give an overview of our retrieval approach followed by a discussion of the characteristics of the derived profiles of CH_4 and N_2O.

5.3.1 Vertical resolution and sensitivity assessment of CH_4 and N_2O

The spectral resolution of a measurement affects the amount of vertical information derived from the spectral line shape of a measured species [63]. Figure 5.6 show averaging kernel matrices for the retrieval of the vertical profiles of CH_4 and N_2O mixing ratios from the FTIR measurements at the Addis Ababa site. Figure 5.6 (right panel) represents the rows of the averaging kernel matrices at selected altitudes which indicate the sensitivity of retrieved CH_4 and N_2O values at the level to true mixing ratios. The dotted line represents the sum of all the rows of the averaging kernel, which represents the overall sensitivity of the FTIR measurement to observe CH_4 and N_2O.

Figure 5.6 shows a strong sensitivity in the altitude range of the troposphere and lower stratosphere, i.e. 2.45 km up to 27 km, since the sum of rows of **A** for all the retrieval values of CH_4 is greater than 0.5. The trace of this averaging kernel, which is 2.25 for the spectra recorded on Feb. 26, 2013 and 2.11 $\pm$ 0.06 for the whole data which implies that partial columns representing two different altitude ranges in the atmosphere can be obtained from the observations of CH_4 in tropical atmospheric conditions.

Figure 5.6 (right panel) shows that the ground-based FTIR measurements of N_2O at Addis Ababa have a sensitivity larger than 0.5 from the ground to about 27 km altitude. The altitude range with better sensitivity does not only depend on the species considered, but it is also different at the various stations in agreement with the different values for DOFS found from the output. This can also be seen in the right panel of Fig. 5.6, where the partial columns averaging kernel for N_2O molecule are given. The averaging kernels peak in the right altitude ranges, therefore the partial column comparisons will not have any biases induced by the limited vertical resolution of the ground-based FTIR. The amplitude of the averaging kernels indicates the sensitivity of the retrieval and the full widths at half maximum (FWHM) indicate the vertical resolution of the corresponding layer. We also ignore the altitude range where the resolution of the instrument becomes beyond 20 km,

which has been computed using the reciprocal of the diagonal values of averaging kernels and multiplying by the intervals of the layers as reported in Rinsland et al. [88].

The amplitude of the averaging kernels indicates the sensitivity of the retrieval, the full widths at half maximum (FWHM) indicates the vertical resolution of the corresponding layer (see Fig. 5.7). The altitude range where the resolution of the instrument becomes beyond 20 km has not been taken in the discussion. The vertical resolution is less than 20 km for the altitude below around 26 km (see Fig 5.7). Furthermore, the vertical resolution of the corresponding layer can also be computed using the reciprocal of the diagonal values of averaging kernels and multiplying by the intervals of the layers as reported in Rinsland et al. [88] and found similar results.

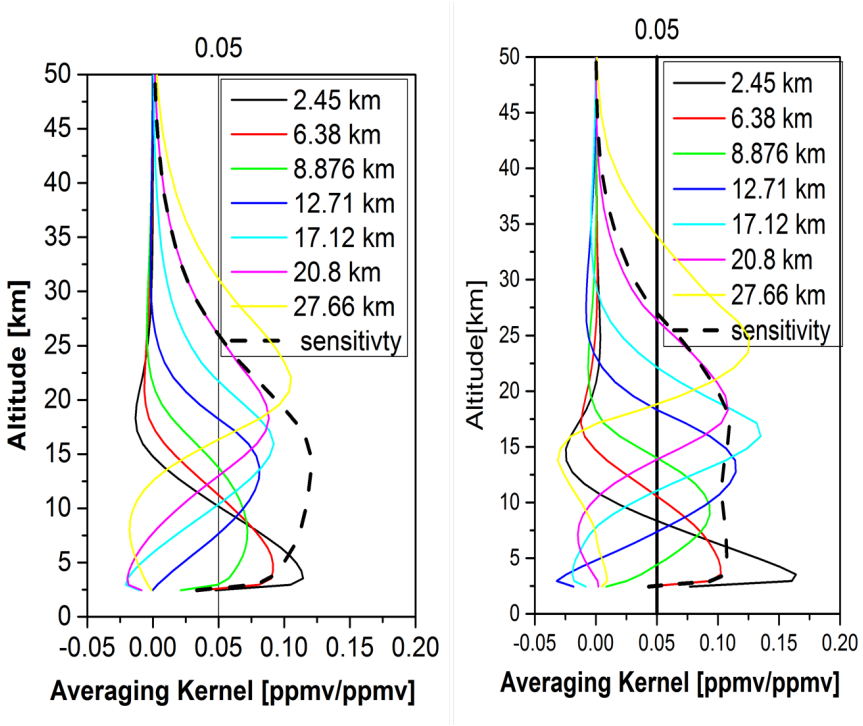

Fig. 5.6 Sensitivity analysis of the retrieved profiles of CH_4 (left) and N_2O (right) at Addis Ababa using the selected rows of the averaging kernels as a function of altitude. The dotted lines are the sum of the rows of the averaging kernels for a spectrum measured on Feb. 26, 2013 for CH_4 and Dec 31, 2009 for N_2O.

5.3.2 Error Estimation

The error calculations conducted here are based on the error estimation package incorporated in the PROFFIT retrieval algorithm that was developed based on the analytical method

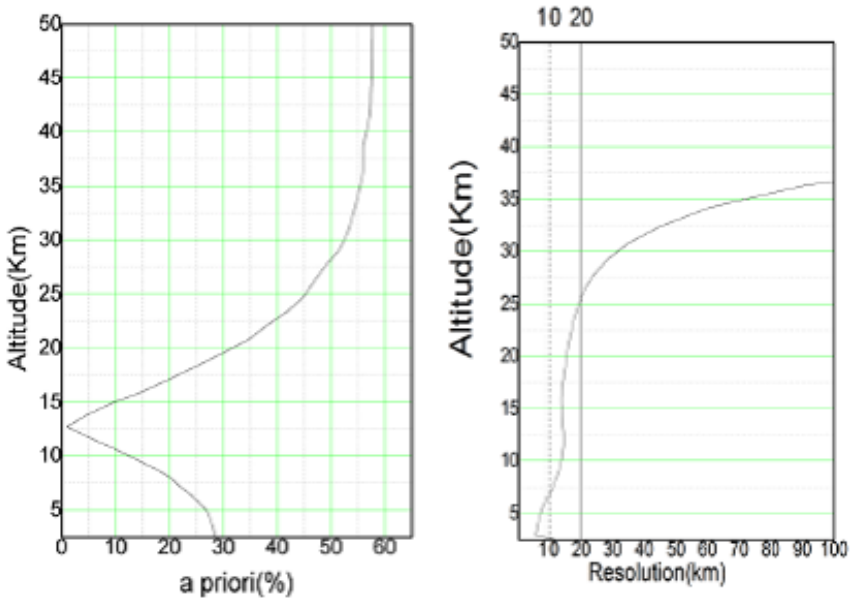

Fig. 5.7 Contribution of a priori information to CH_4 retrieval results (left). Vertical resolution of the observation for tropical atmospheric condition (right).

suggested by Rodgers [31]. The quantified sources of errors are temperature, measurement noise, instrumental line shape, solar lines, line of sight, zero baselines offset, and spectroscopy. It has been observed that baseline and atmospheric temperature uncertainties are the leading contributing to the total uncertainty. Details about the evaluation of the individual contributions to the error budget are provided in Senten et al. [28] and detailed descriptions of interfering error in Sussmann et al. [89].

Figure 5.8, shows the statistical error (left panel) and systematic error (middle panel) profiles for a typical CH_4 retrieval. One can note from Fig. 5.8 that the main systematic error source is the uncertainty of spectroscopic parameters, whereas the major statistical error source is a baseline. The estimated random and systematic errors for the profile retrieval of CH_4 from FTIR station at Addis Ababa is shown in Fig. 5.8 (left and middle panel) respectively. We observe that in the troposphere the random errors are dominated by the baseline offset uncertainty and the measurement noise. The total estimated random error due to parameter uncertainties is depicted as a dark yellow line in Fig. 5.8 (left panel). It is about 0.07 ppm (4.4 %) in the lower troposphere and about 0.04 ppm (2.25 %) in the UT/LS region. Concerning systematic errors, spectroscopic uncertainties are the dominant uncertainty sources and estimated total systematic error is depicted as a dark yellow line in

Table 5.2 Assumed uncertainty sources used for our error estimation. The second column gives the uncertainty value and the third column the partitioning of this uncertainty between statistical and systematic sources for the CH_4 and N_2O.

Error sources	Uncertainty	Statistical/ systematic
Measurement noise		100/0
Baseline (channelling and offset)		50/50
Mod. eff. and pha. err.	10 % and 0.1rad	50/50
Temperature profile	1K	70/30
Line of sight	0.1^{O}	90/10
Solar lines (intensity and ν- scale)	1 % and 10^6	80 /20
Spectroscopic parameters (S and)	2 %	0/100

Fig. 5.8. They are about 0.05 ppm (3.5 %) and 0.1 ppm (7.2 %) for the lower troposphere and the UT/LS region, respectively. The precision of the mid-infrared FTIR measurements of CH_4 is 3 % and the relative accuracy of 7 % as reported in Dils et al. [90] using the NDACC data.

Figure 5.9 shows the statistical error (left panel) and systematic error (middle panel) profiles for a typical N_2O retrieval. One can note from Fig. 5.9 that the main systematic error source is the uncertainty of spectroscopic parameters, whereas the major statistical error source is a baseline. The estimated random and systematic errors for the profile retrieval of N_2O from FTIR station at the Addis Ababa is shown in Fig. 5.9(left and middle panel) respectively. In the troposphere the random errors are dominated by the baseline offset uncertainty and the measurement temperature. The total estimated random error due to parameter uncertainties is depicted as a dark yellow line in Fig. 5.9(left panel). The total statistical error in middle and upper troposphere is between 0.009 ppm(3.5 %) and 0.03 ppm(9 %) and its major source is the baseline. Concerning systematic errors, spectroscopic parameters, baseline and temperature are the dominating uncertainty sources. The estimated total systematic error is depicted as dark yellow line in Fig. 5.9 and it is less than 0.025 ppm (8 %) in the altitude below around 22 km. The total statistical error is larger than that of total systematic error mainly in the troposphere and lower stratosphere and the average values are 8 % and 5 % respectively. In the stratosphere the systematic error dominated statistical error and their average values are 9 % and 7 %.

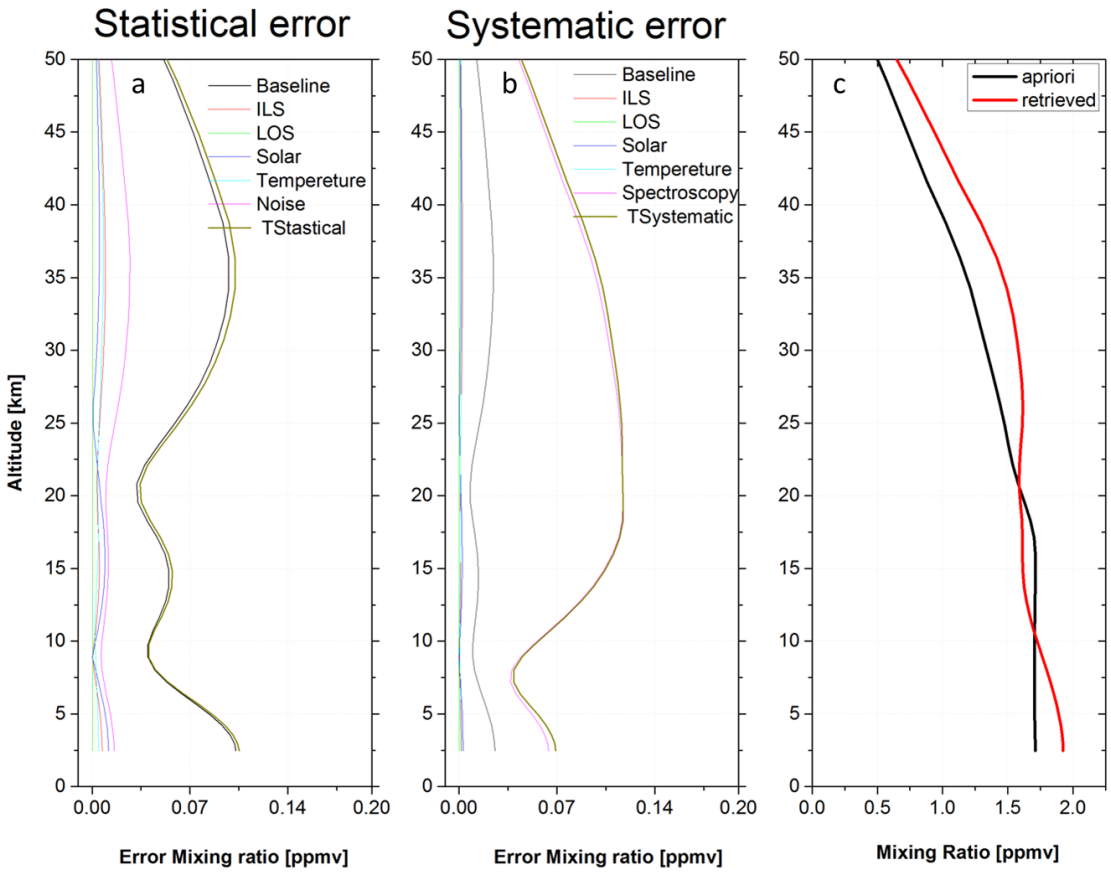

Fig. 5.8 Error estimates for tropical atmospheric conditions of CH_4: Estimated uncertainty profiles for statistical error (left), Systematic error contributions (middle) and retrieved profile (right).

Column amount

Figure 5.10 shows the time series of the retrieved total column amounts (in molecules/cm^2) of CH_4 and N_2O species obtained from the Addis Ababa FTIR measurements from 2009-2013. The mean total column amounts of CH_4 and N_2O measured at Addis Ababa are 2.9×10^{19} molecules/cm$^2\pm$3.4 % and 5.23×10^{18} molecules/cm$^2\pm$6.93 % respectively. The sensitivity of the observation in measuring CH_4 and N_2O trace gases is limited to an altitude of around 27 km as explained using the averaging kernel row of the measurement. The mean partial column of CH_4 and N_2O within the sensitivity range of the instrument, which is from the surface to around 27 km is determined as 2.85×10^{19} molecules/cm$^2\pm$5.3 % and 5.16×10^{18} molecules/cm$^2\pm$6.95 % respectively.

The ground-based FTIR sensitivity is used to determine the upper altitude limit, which is

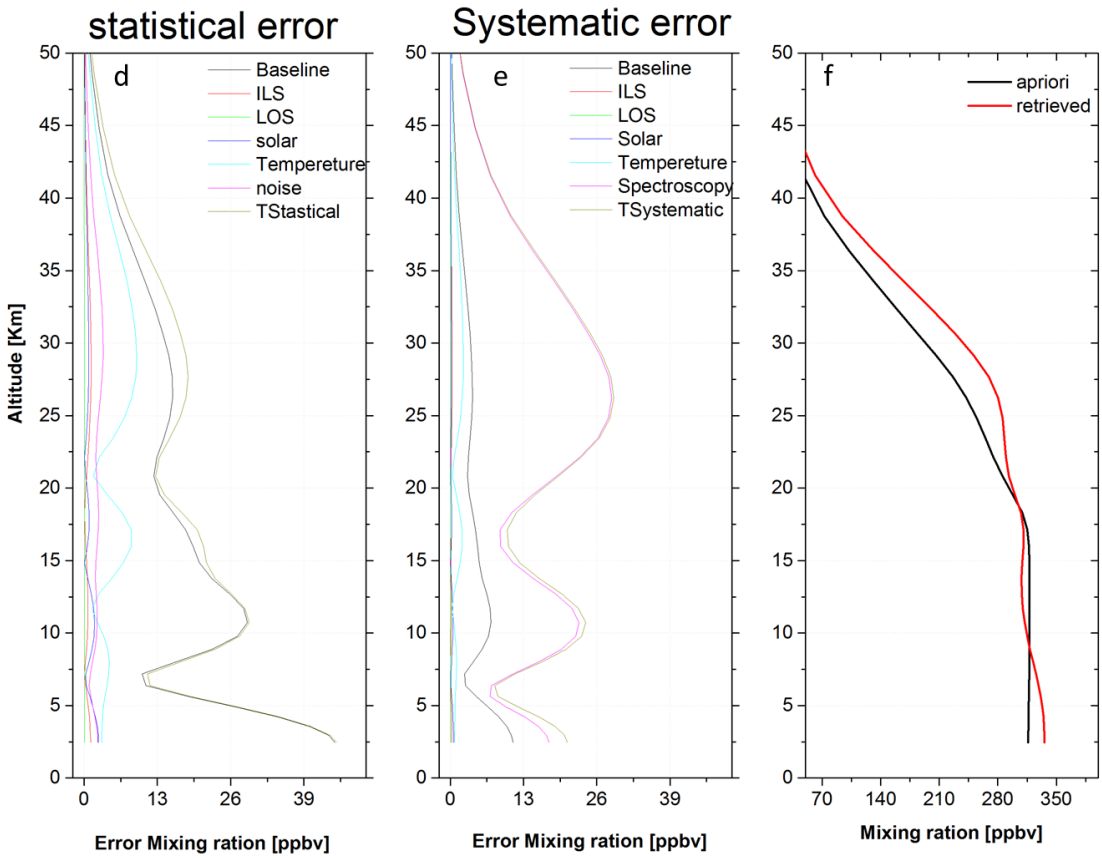

Fig. 5.9 Error estimates for tropical atmospheric conditions of N_2O: Estimated uncertainty profiles for statistical error (left), Systematic error contributions (middle) and retrieved profile (right).

reasonable up to around 27 km for both CH_4 and N_2O in the tropical atmospheric condition. The DOFS within these partial columns limits are about 1.03 for CH_4 and 1.27 for N_2O. Error analysis indicates the statistical error accounts for 2.3 % in the total column amounts of CH_4 and 2.0 % in total columns of N_2O. Similarly, the systematic error accounts for 2.1 % in total column of CH_4 and 2.26 % in the total columns of N_2O. Generally, the overall contribution of both statistical and systematic errors to the total error during the retrieval of CH_4 and N_2O from ground-based FTIR are 3.1 % and 3 % respectively.

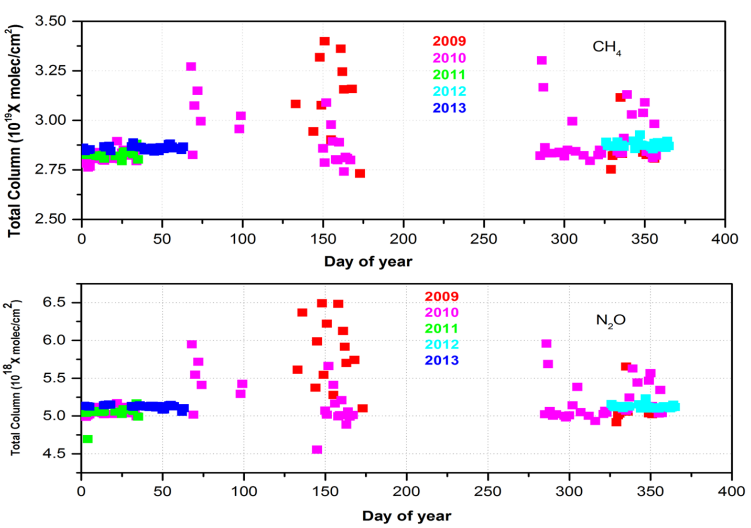

Fig. 5.10 Partial columns of CH_4 (top) and N_2O (bottom) gases over Addis Ababa in the altitude range of 2.45 to 27 km.

Table 5.3 Characterization of the retrieved profiles of N_2O and CH_4 at Addis Ababa station: statistical mean and standard deviation (1σ) for five years of measurements of the Degrees of Freedom for Signal (DOFS), and Sensitivity Range (S.R.) of the ground-based FTIR retrievals (Gd: ground; TC: total column; PC: partial column). See Sect. 4.3 for definitions

Species	TC.DOFS	S.R(km)	PC.range	PC.DOFS
CH_4	2.11±0.06	Gd-27	Gd-27	1.03
N_2O	3.4±0.15	Gd-27	Gd-27	1.27

5.3.3 A posteriori correction of CH_4

The tropospheric kernels (red lines) peak mainly in the troposphere and the stratospheric kernels (blue lines peak) mainly in the stratosphere (see Fig. 5.11). However, the plot also indicates contributions of the UT/LS to the retrieved tropospheric CH_4 (negative values above 15 km for the red tropospheric kernels). This means that the stratospheric CH_4 variations might significantly affect the retrieved tropospheric CH_4 signals.

Figure 5.11 (left panel) shows the negative value of tropospheric kernel in the lower stratosphere and this indicates influence of stratospheric CH_4 variations on the retrieved tropospheric amounts of CH_4 and such influence creates an error on the retrieved profiles of tropospheric CH_4. The effects of the stratospheric CH_4 variation can be minimized by applying a posteriori correction method using the averaging Kernel of the retrieved results of

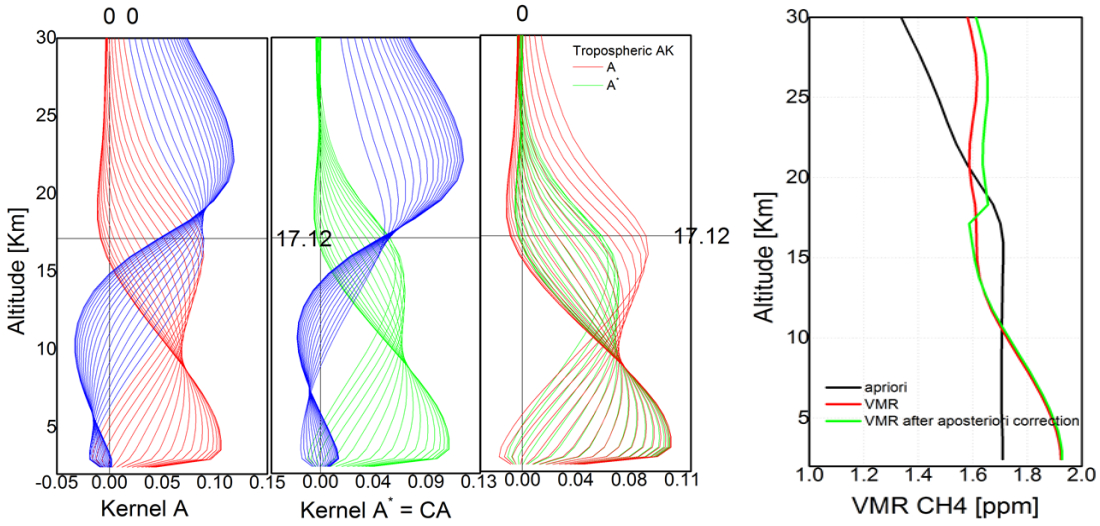

Fig. 5.11 Row averaging kernels of CH_4 observation from FTIR at Addis Ababa site. Left panel: kernels **A** obtained from the Tikhonov Phillips profile retrieval (red: tropospheric kernels, blue: UT/LS kernels). Central panel: kernels $\mathbf{A}^*$ obtained after applying the a posteriori correction (green: tropospheric kernels, blue: UT/LS kernels). Right panel: comparison of the surface row kernels **A** (red line) and A^*(green line). The typical altitude where the UT/LS starts is indicated by the horizontal black line (17.12 km)and the last to the right is VMR after using the a posteriori correction.

CH_4 from FTIR as stated in Sussmann et al. [91];

$$A = \begin{pmatrix} A_{TT} & A_{ST} \\ A_{TS} & A_{SS} \end{pmatrix} \tag{5.1}$$

where A_{TT} describes tropospheric CH_4 signal on retrieved tropospheric amounts and A_{SS} is stratospheric CH_4 signal on the retrieved stratospheric amounts. A_{ST} and A_{TS} describe the cross-dependencies of the retrieved tropospheric amounts on the stratospheric signal and of the retrieved stratospheric amounts on the tropospheric signal, respectively. The a posteriori correction method will be constructed using the two cross-entries and can be written as

$$C = \begin{pmatrix} I & A_{ST} \\ A_{TS} & I \end{pmatrix} \tag{5.2}$$

Therefore, the averaging Kernel of the retrieved results of CH_4 from FTIR can be corrected by multiplying it using C and then the a posteriori corrected averaging kernel A^* is given as

$$A^* = \mathrm{C} \times A \tag{5.3}$$

The retrieved CH_4 profile amount can be corrected by the following equation

$$\hat{x}^* = C(\hat{x} - x_a) + x_a \tag{5.4}$$

All the original retrieved values of FTIR CH_4 as well as the statistical and systematic errors have been changed after applying the a posteriori correction. The impacts of local signal on the retrieval results of FTIR CH_4, which is mainly signals coming from the lower stratosphere affects the concentration of methane retrieved from the troposphere.

5.4 Summary

In this chapter, the vertical profiles and total columns of CH_4 and N_2O over Addis Ababa, Ethiopia are presented. The overall contribution of both statistical and systematic errors to the total error during the retrieval of CH_4 and N_2O from ground-based FTIR are 3.1 % and 3 % respectively. The mean total column amounts of CH_4 and N_2O measured at Addis Ababa are $2.9 \times 10^{19} \pm 3.4\%$ and $5.23 \times 10^{18} \pm 6.93\%$ respectively. The mean partial column of CH_4 and N_2O with in the sensitivity ranges of the instrument, which is from the surface to around 27 km is determined as $2.85 \times 10^{19} \pm 5.3\%$ and $5.16 \times 10^{18} \pm 6.95\%$ respectively. The apostriori correction is only applicable to the retrieved profiles of methane since other molecules are not affected by locale signal as well as the vertical gradient of methane in UP/LS is large.

Comparisons with correlative data from IMK/IAA MIPAS-ENVISAT CH_4 and N_2O data products for the MIPAS (version V5R_CH4_220, V5R_CH4_224, V5R_N2O_220 and V5R_N2O_224), the Microwave Limb Sounder on board of the Aura satellite (Aura/MLS) (MLS v3.3 of CH_4 and N_2O) and the Atmospheric Infrared Sounder (AIRS) (CH_4) measurements are given to confirm the results and to validate the instrument performance in the next chapter.

Chapter 6

Comparison of FTIR CH_4 and N_2O with satellite data

6.1 Introduction

This chapter describes the validation of ground-based FTIR profiles of CH_4 and N_2O. The quality of ground-based FTIR measurements of atmospheric trace gases and their use to understand various lower and middle atmospheric processes have been reported in a number of previous studies [20–22, 24, 68]. H_2O VMR profiles and integrated column amounts from ground-based FTIR measurements of the Addis Ababa site were also compared with the coincident satellite observations of Tropospheric Emission Spectrometer (TES), Atmospheric Infrared Sounding (AIRS) and Modular Earth Sub model System (MESSy) model and the result confirmed reasonably good agreement [25]. Laeng et al. [64] found that the MIPAS CH_4 profiles below 20–25 km are biased high.

The ground-based FTIR CH_4 and N_2O retrieved vertical profiles and partial columns from the Addis Ababa site have been stated in chapter 5. Furthermore, the comparison of results will be presented and discussed in this chapter. The intercomparison of the FTIR CH_4 and N_2O with MIPAS (version V5R_CH4_220, V5R_CH4_224, V5R_N2O_220 and V5R_N2O_224), the Microwave Limb Sounder on board of the Aura satellite (Aura/MLS) (MLS v3.3 of CH_4 and N_2O) and the Atmospheric Infrared Sounder (AIRS) (CH_4) will be presented and analysed using the statistical tools detailed in von Clarmann [38]. The satellite data (MIPAS, MLS, and AIRS) have a considerably better vertical resolution than ground-based FTIR profiles due to observation geometry, spectral windows, and measurement techniques. Thus, analysis of the comparison between volume mixing ratio values derived from FTIR and MIPAS were performed for the data sets collected on May 2009 to

December 2010. Furthermore, the comparison of FTIR (CH_4 and N_2O) with MLS (CH_4 and N_2O) and AIRS (CH_4) for the time period of May 2009 to February 2013 has also been applied to assess quality of the data derived from FTIR.

6.2 Methodology

Comparisons of daily averaged ground-based FTIR measurement of CH_4 and N_2O with that of MIPAS were performed for time period of May, 2009 to Feb., 2011. However, FTIR comparison with MLS retrievals for time period of May, 2009 to March, 2013 were used after averaging data obtained within coincidence criteria of $\pm 2^{\circ}$ of latitude and $\pm 10^{\circ}$ of longitude from the ground-based FTIR site in Addis Ababa and within time difference of $\pm$24hr.

MIPAS MLS and AIRS were used in the following comparisons as they have better vertical resolution than ground-based FTIR profiles and high temporal and spatial coverage in the tropics. Hence, the profiles from MIPAS, MLS and AIRS have been degraded to make a comparison between the FTIR and satellite observations. Therefore, satellite measurement profiles are smoothed using the FTIR averaging kernels of individual species obtained from the ground-based FTIR retrieval by applying the procedures reported in [92] and given as

$$\mathbf{x}_s = \mathbf{x}_a + \mathbf{A}(\mathbf{x}_i - \mathbf{x}_a) \tag{6.1}$$

Where $\mathbf{x}_s$ is the smoothed profile, $\mathbf{x}_a$ and $\mathbf{A}$ represents the a priori and averaging kernel for CH_4 and N_2O obtained from the ground-based FTIR instrument respectively and $\mathbf{x}_i$ is the initial retrieved profile obtained from satellite measurements after we interpolated it to the FTIR grid spacing.

We also calculate the following; error parameters that can characterize the features of the instruments and parameters to be observed, such as the bias between the instruments using the difference (absolute or relative) of the daily mean of a pair profile. The absolute or relative difference at each altitude layers of a pair profile is calculated using

$$\delta_i(z) = [\mathrm{FTIR}_i(z) - \mathrm{Sat}_i(z)] \tag{6.2}$$

The mean squares error can be express as

$$MSE_i(z) = \sqrt{\frac{1}{N(z)-1}\sum_{i=1}^{N(Z)}[\delta_i(z)]^2} \tag{6.3}$$

and the relative difference of a paired profile can be given in percentage as

$$\delta_i(z) = 100(\%) \times \frac{[\mathrm{FTIR}_i(z) - \mathrm{Sat}_i(z)]}{[\mathrm{FTIR}_i(z) + \mathrm{Sat}_i(z)]/2} \tag{6.4}$$

The mean difference (absolute or relative) for a complete set of coincident pairs of profiles obtained from the ground-based FTIR and the correlative satellites (MIPAS and MLS) is expressed as

$$\triangle_{\mathrm{rel}}(z) = \frac{1}{N(z)}\sum_{i=1}^{N(z)}\delta_i(z) \tag{6.5}$$

where $\delta_i(z)$ is the difference (absolute or relative), $N(z)$ is the number of coincidences at z, $\mathrm{FTIR}_i(z)$ is the FTIR VMR at z and the corresponding $\mathrm{Sat}_i(z)$ volume mixing ratio derived from satellite instruments (MIPAS, MLS). The standard deviation from the mean differences (absolute or relative) $\sigma_{diff}(z)$ is important to partially characterizes the measurement error by instruments. As reported in von Clarmann [38], some literatures use de−biased standard deviation, which measures the combined precision of the instruments instead of the standard deviation of the mean differences. The statistical data that we obtained from the following equations uses the entire observation period of the paired instruments:

$$\sigma_{diff}(z) = \sqrt{\frac{1}{N(z)-1}\sum_{i=1}^{N(Z)}[\delta_i(z) - \triangle_{\mathrm{abs}}(z)]^2} \tag{6.6}$$

where $\delta_i(z)$ is the difference (absolute or relative) for the i^{th} coincident pair calculated using Eq. 7.4 and Eq. 6.4. The statistical uncertainty of the mean differences (absolute or relative), which is standard error of the mean (SEM) is the quantity used to judge the statistical significance of the estimated biases and it can be expressed in terms of the standard deviation of the mean:

$$SEM(Z) = \frac{\sigma(z)}{\sqrt{N(Z)}} \tag{6.7}$$

Furthermore, we can also conduct the partial columns comparison of ground-based FTIR CH_4 and N_2O with MIPAS_CH4_220, MIPAS_CH4_224, MIPAS_N2O_220 and MIPAS_N2O_224. Hence, the relative difference between ground-based FTIR and smoothed MIPAS partial

columns of CH_4 and N_2O by taking into account the lower altitude limit of MIPAS observations and upper altitude limit of ground-based FTIR sensitivity has been calculated using:

$$\mathrm{RDiff}(\%) = 200 * (\frac{\mathrm{PC_{FTIR}} - \mathrm{PC_{Sat}}}{\mathrm{PC_{FTIR}} + \mathrm{PC_{Sat}}}) \tag{6.8}$$

where PC is partial column of FTIR and the corresponding satellite measurements, MIPAS.

6.3 Comparison of FTIR and MIPAS_CH4_220, N2O_220 vertical profiles

The results of comparisons of ground-based FTIR vertical profiles of CH_4 and N_2O with satellite based observations of MIPAS_CH4_220, MIPAS_CH4_224, MIPAS_N2O_220 and MIPAS_N2O_224 will be presented and discussed. For daily average ground-based FTIR CH_4 and N_2O were performed for time period of May, 2009 to Feb., 2011.

FTIR CH_4 mixing ratio comparison result is shown in Fig. 6.1 for the MIPAS Comparison, The mean profiles of both FTIR and MIPAS results show a maximam at around 17 km and decline smoothly as altitude increases. The VMR of MIPAS mixing ratio is higher than that of FTIR in the altitude below 27 km at which the sensitivity of FTIR is maxima. Comparison of FTIR CH_4 profiles to MIPAS_CH4_220 products using 61 coincident data (see Fig 6.1) indicates that no significant bias in FTIR CH_4 data is present between 32 and 42 km as its bias $\pm\ \sigma(z)$ includes zero. Around the tropopause layer the comparison indicates that there is a strong low bias of FTIR CH_4, which are 0.06 to 0.27 ppm in upper troposphere and lower stratosphere along with maximum at tropopause.

Figure 6.1 (middle panel) shows the mean absolute and relative difference of CH_4 between the VMR value derived from ground-based FTIR and MIPAS_CH4_220 which is 15 % (-0.27 ppm) at the tropopause layer (17 km) and 3.8 % (-0.06 ppm) at around 27 km. The bias below 24 km is larger than the FTIR systematic errors, this means that the differences cannot be explained by known systematic uncertainties of FTIR. The standard deviation of the difference is larger than the combined error of the two instruments through out the altitude above 18 km, it is twice in the altitude 20-24 km and less below 20 km as shown in right panel of Fig. 6.1.

Comparison of FTIR N_2O profiles to MIPAS_N2O_220 (see Fig 6.2) indicates that no significant bias in FTIR N_2O data is present below 18 km and above 45 km. A positive bias is present in the stratosphere and this comparison indicates that strong high positive bias of FTIR N_2O as FTIR N_2O values are higher by 0.004 ppm (1.5 %) to 0.02 ppm (8 %) in the

altitude range between 18 to 30 km.

Figure 6.2 (middle panel) shows the mean absolute difference of N_2O between the VMR value derived from ground-based FTIR and MIPAS which is 8 % (0.02 ppm) and by 0.004 ppm (1.5 %) at around 18 km, and statistically significant in the altitude between 18 to 45 km as the standard error of the mean is smaller than the mean bias. The bias in the altitude between 18 km to 30 km is smaller than the FTIR systematic errors, indicating the bias can be explained by known systematic uncertainties of FTIR. The standard deviation of the difference is larger than the combined error of the two instruments in the altitude above 18 km. Figure 6.2 (right panel) shows the standard deviation of the difference which agrees with the estimated combined random error in the altitude ranges between 18 to 30 km. For the altitude range of below 18 km, the estimated combined random error is overestimated.

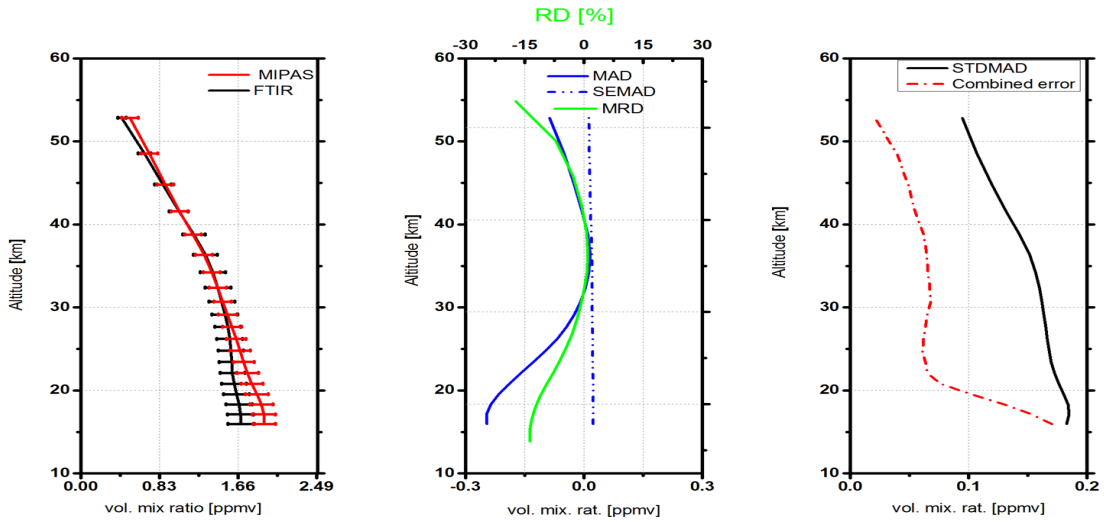

Fig. 6.1 Comparison of CH_4 from MIPAS reduced resolution (V5R_CH4_220) and FTIR. Left panel: mean profiles of MIPAS (red) and FTIR (black) and their standard deviation (horizontal bars). Middle panel: mean difference FTIR minus MIPAS (blue solid), standard error of the difference (blue dotted), mean relative differences FTIR minus MIPAS relative to their averaged (green, upper axis). Right panel: combined mean estimated statistical error of the difference (red dotted, contains MIPAS instrument noise error and FTIR random error budget), standard deviation of the difference (black solid).

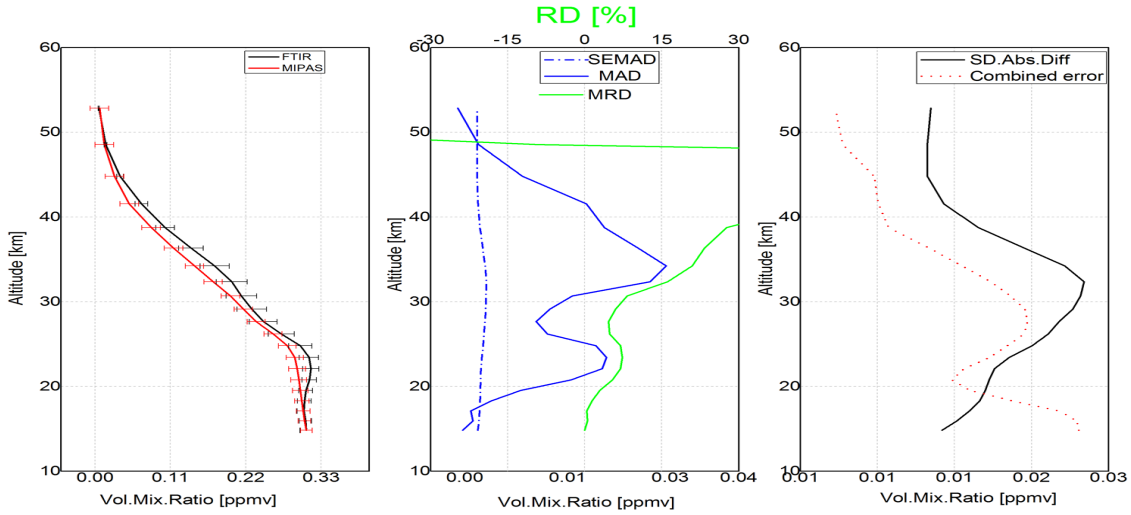

Fig. 6.2 Same as Fig. 6.1, but for N_2O profiles of FTIR with MIPAS_N2O_220. For a more detailed description see Fig. 6.1.

6.4 Comparison of FTIR and MIPAS_CH4_224 and MIPAS_N2O_224 vertical profiles

The new version of MIPAS-IMK has also used to validate ground-based FTIR data of Addis Ababa site and comparison has made using 29 coincident data for a time period between Nov., 2009 and Dec., 2010. Middle panel of Fig. 6.3 indicates that a negative bias of -4.8 % at around 16 km and declined to -2 % at 22 km are obtained and followed with statistically not significant bias at around 22 to 23 km as standard error of the mean is somehow greater than the mean difference. Between 23 and 27 km the FTIR value is higher than MIPAS values. The mean differences show that the FTIR mixing ratio is lower below 27 km with value of the difference increase as altitude increases from 23 to 27 km (4.6 %) at 27 km maximum. Moreover, the bias in the FTIR observations of CH_4 declined while we employed the new version of MIPAS products as compared to the old version of MIPAS. This declined of the bias is due to the employment of relaxed of off diagonal regularization matrix in the new version of MIPAS produces [93]. A large negative bias in FTIR CH_4 is obtained, i.e., FTIR CH_4 values are lower by 0.07 (4.8 %) to 0.04 ppmv (2.2 %). MIPAS V5R_CH4_222 profiles is biased high (14 %) below 20-25 km as compared with other instruments Laeng et al. [53] meanwhile the positive bias in the lowermost stratosphere and upper troposphere MIPAS-ENVISAT CH_4 and N_2O profiles version MIPAS_CH4_21 and MIPAS_N2O_21 and MIPAS_CH4_224, MIPAS_CH4_225, MIPAS_N2O_224 and MIPAS_N2O_225 prod-

ucts has been largely reduced [48, 93].

Figure 6.3 (right panel) indicates that the standard deviation of the mean differences is larger than the combined random error of the two instruments throughout the altitude. For instance, it is twice the combined standard deviation in the altitude above 20 km and less below 20 km, which indicates the underestimation of random errors of one or both of the instruments. In addition, the overestimation of standard deviation of the difference may result from not taking all the error budget of MIPAS into account and the spatial and temporal criteria sets used to collect the coincidence data of MIPAS can create a discrepancy as well. The natural variation of the methane have also contributed to the overestimation of a standard deviation of the difference as biases are vary with seasons as reported in Gavrilov et al. [30].

Comparison of FTIR N_2O profiles to MIPAS (V5R_N2O_224) measurements (see Fig. 6.4

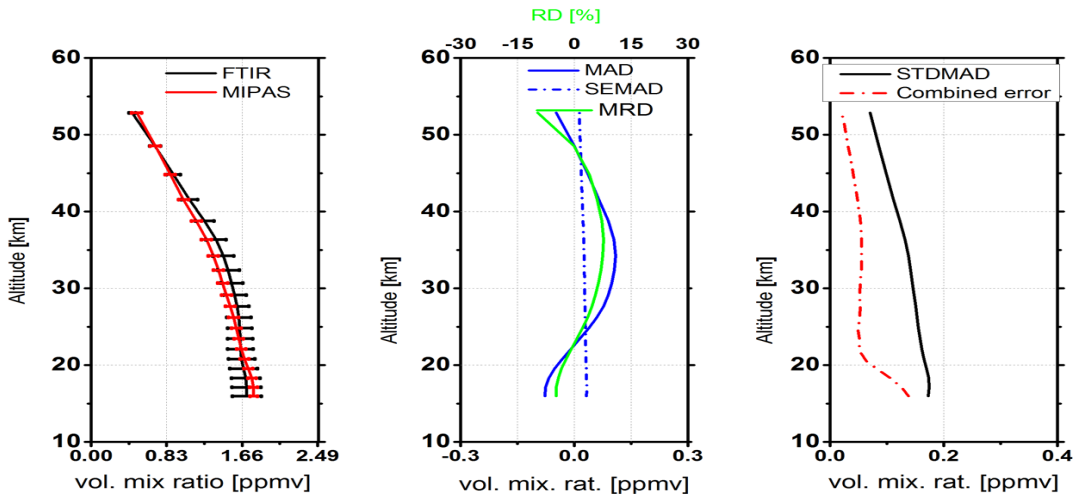

Fig. 6.3 Comparison of CH_4 from MIPAS (V5R_CH4_224) and FTIR. Details as in Fig. 6.1

(middle panel)) indicates that FTIR value is higher than the MIPAS above 20 km and the maximum mean absolute difference of N_2O is 15 % (0.04 ppmv) at around 24 km while, the FTIR value is less in altitude below 20 km with a maximum difference of -7 % (-0.02) at around 17 km. The bias at 19 km is not statistically significant as the standard error of the mean is larger than the bias. Since, the bias in altitude between 20 to 27 km is smaller than the FTIR systematic errors, the bias can be explained in terms of systematic uncertainties in FTIR (see Fig. 5 (bottom middle panel)). The standard deviation of the difference is larger than the combined error of the two instruments in the altitude above 20 km (see Fig. 6.4, right panel) and the standard deviation of the difference agrees with the estimated combined

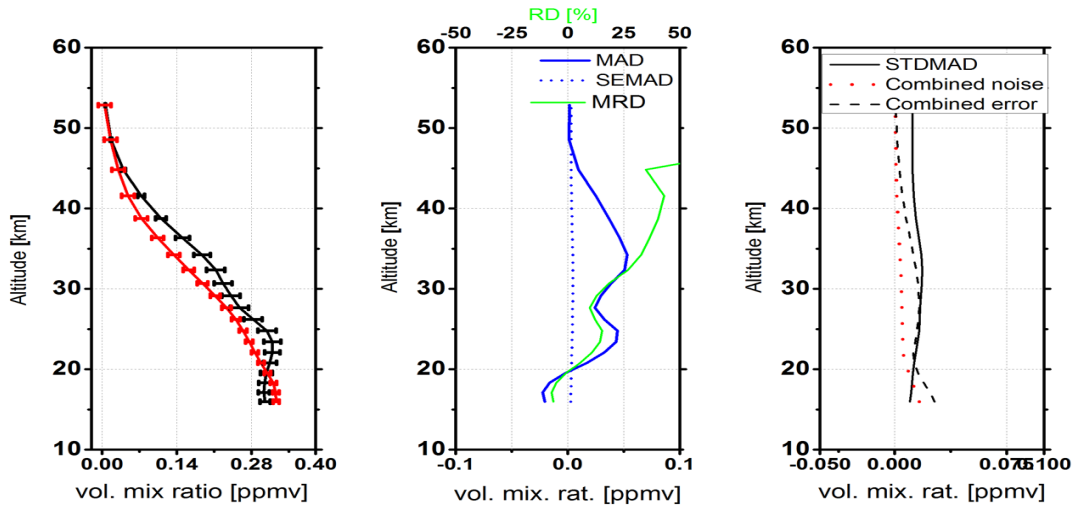

Fig. 6.4 Comparison of N_2O from MIPAS (V5R_N2O_224) and FTIR. Details as in Fig. 6.1

random error in the altitude ranges between 20 to 27 km. The estimated combined random error is overestimated below 20 km.

6.4.1 Time series comparisons of CH_4 and N_2O from FTIR with MIPAS

If the standard deviation of the mean relative difference is comparable to the estimated error of one instrument, the contribution of the second instrument to the systematic bias is very small.

The standard deviation of the FTIR and MIPAS mean profiles of CH_4 for the tropical atmospheric conditions, which shows the altitude range where the two instruments attained a maximum STD at the tropopause layer around 17 km that confirms both instruments measured air masses with similar variability with a discrepancy in the STD of FTIR is somehow higher than the STD of MIPAS, since the sensitivity of FTIR on the retrieval is influenced by a local signal.

6.4.2 Comparison of FTIR and MIPAS CH_4 and N_2O columns

The FTIR CH_4 and N_2O were with in the altitude ranges $2.45 - 27$ km (as seen in subsection 5.3.1 Fig. 5.7) and that of satellite measurements, MIPAS extended down to 12 km, even though we have some profiles extended up to 12 km, but most of the measurements were

Table 6.1 Comparison of ground-based FTIR measurements of CH_4 and N_2O partial column (PC) with MIPAS_CH4_220 and V5R_N2O_220 for the tropics.

species	mean square error(%)	Mean error(%)	STD from Mean error(%)	N
CH_4	14.95	-11.7	9.4	57
N_2O	5.55	2.39	5.57	61

ascertain down to 15 km for N_2O.

For the partial column comparisons of FTIR with MIPAS, it is vital to take in to account the lower altitude limit of MIPAS, which is 12 Km. The ground-based FTIR sensitivity is used to determine the upper altitude limit, which is reasonable up to around $\sim$ 27 km for CH_4 and N_2O, but the sensitivity of MIPAS measurements of both CH_4 and N_2O are 12 km and 14 km respectively. Therefore the PC that we use in the comparison is limited to the altitude ranges covered by both instruments.

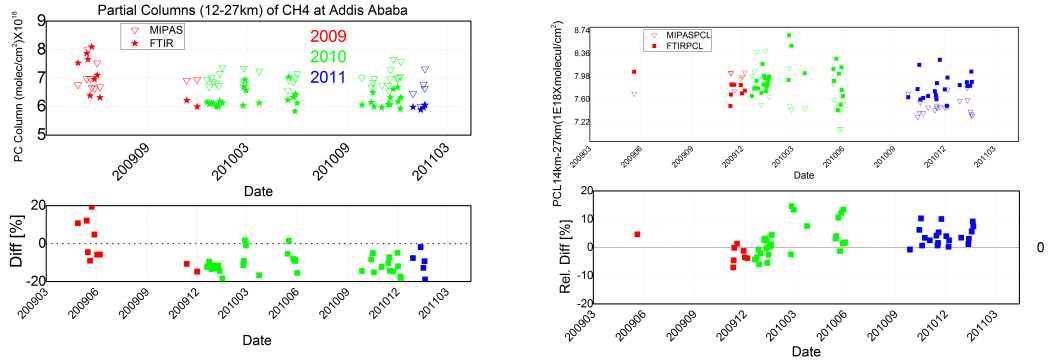

Fig. 6.5 Time series of CH_4 and N_2O partial column comparisons: Upper panel: ground-based FTIR (stars) and MIPAS (triangular) (V5R_CH4_220 and V5R_N2O_220) partial columns for collocated measurements at Addis Ababa. Lower panel: relative differences between ground-based FTIR and MIPAS partial columns.

Therefore the PC used in the comparison is limited to the altitude ranges covered by both instruments. Figure 6.6 shows the time series of the partial columns and relative differences of CH_4 (upper panel) and N_2O (lower panel). The partial column comparison of CH_4 between values of FTIR and MIPAS_CH4_224 and V5R_N2O_224 revealed a mean error of -5.5 %, mean square error of 7.4 % and a standard deviation from the mean error of 5 %. Similarly, N_2O values between FTIR and MIPAS revealed a mean error of 0.5 %, mean square error of 3.7 % and standard deviation from mean error of 3.8 %.

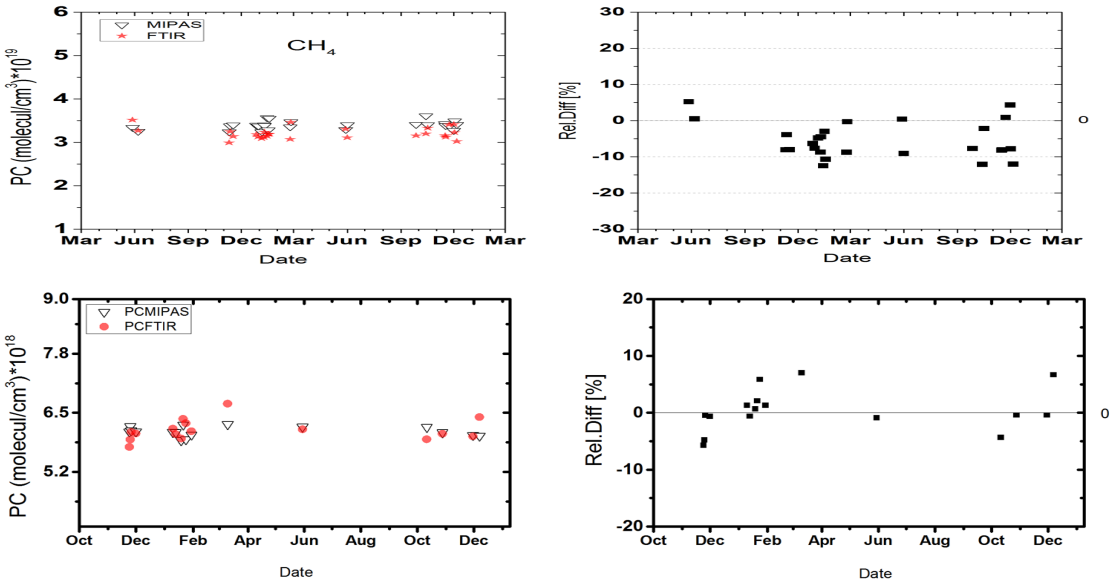

Fig. 6.6 Time series of CH_4 and N_2O partial column comparisons: ground-based FTIR (stars) and MIPAS (V5R_CH4_224 (upper left panel) and FTIR (stars) and V5R_N2O_224) (triangular) (upper right panel) partial columns. Relative differences between ground-based FTIR and MIPAS (V5R_CH4_224 (bottom left panel) and V5R_N2O_224 (bottom right panel)) partial columns.

Table 6.2 Comparison of ground-based FTIR CH_4 and N_2O partial column (PC) with MIPAS_CH4_224 and V5R_N2O_224 for the tropics, Addis Ababa.

species	mean square error(%)	Mean error(%)	STD from Mean error(%)	N
CH_4	7.4	-5.5	5	29
N_2O	3.7	0.5	3.8	16

6.5 Comparison of CH_4 and N_2O from FTIR with MLS

Figure 6.7 (middle panel) shows the comparison between FTIR CH_4 profiles and CH_4 derived from MLS measurements and indicates that no significant bias in FTIR CH_4 data is present between 22 and 27 km. In the tropopause layer the comparison indicates that strong low bias of FTIR CH_4 (at 18.31 km). The bias below 19 km and above 29 km can not explained by the systematic errors of FTIR as the bias is larger than the systematic errors of FTIR. Further the standard deviation of the difference is larger than the combined random errors of the instruments. The bias within 19 km to 29 km can be explained by the systematic error of FTIR. The combined error of this comparison indicates that all the er-

ror contribution to both instruments have not taken in to account which might be the main sources of the deviation of standard deviation of the mean difference from the combined error. The spatial and temporal criteria sets used to collect the coincidence date might also contribute towards observed discrepancy.

The left panel of Fig. 6.8 represents the mean profiles of N_2O derived from the coincident pairs of FTIR and MLS N_2O. The FTIR values of N_2O is larger than the MLS N_2O by a factor of 1.3 at around 30 km and by a factor of 1.1 at around 21 km. The mean relative difference of FTIR and MLS N_2O value increases as altitude increases. The positive bias is statistically significant as the mean difference of the comparison is larger than the standard error of the mean.

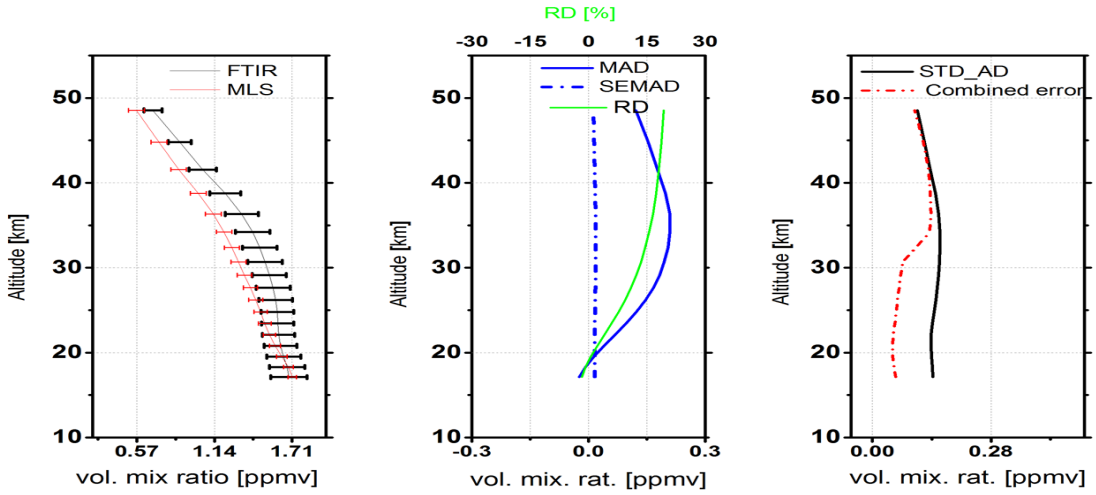

Fig. 6.7 Mean profiles, bias and standard deviation of the differences versus estimated combined retrieval error for MLS and FTIR methane retrievals.

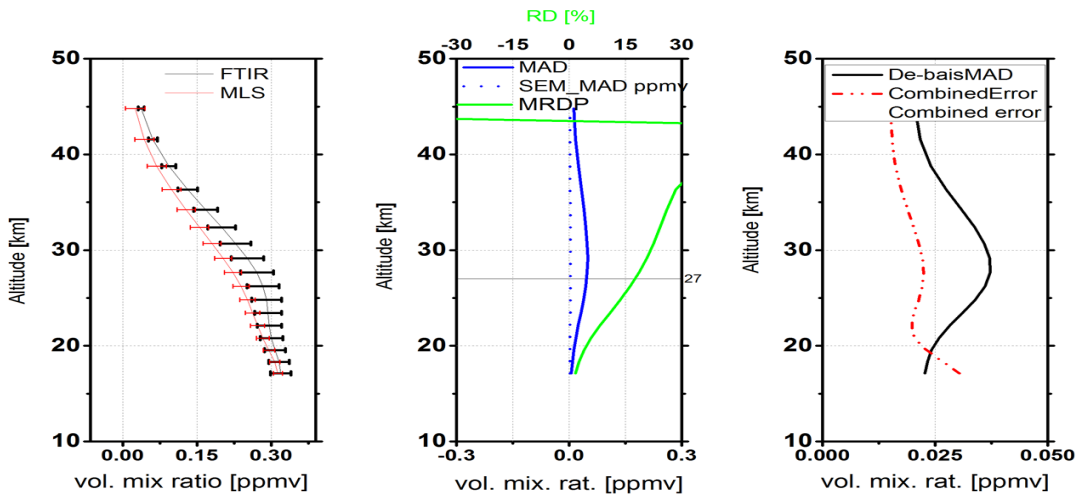

Fig. 6.8 Mean profiles, bias and standard deviation of the differences versus estimated combined retrieval error for MLS and FTIR N2O retrievals.

6.6 Comparison of CH_4 from FTIR with AIRS

In Fig. 6.9 mean profiles, mean differences and estimated error versus deviation of the difference between FTIR and AIRS mixing ratios are shown. The largest negative bias is found in altitude between 11-19 km with a maximum difference of -0.08 ppmv at around 15 km. A negative bias that AIRS mixing ratio of CH_4 is higher than the FTIR as shown in Fig. 6.9. A positive bias existed at altitude between 7-9 km and similarly, it also shown in altitude between 21-27 km with a maximum value at around 27 km and its bias is 0.14 ppmv (9 %). The standard deviation of the difference agree to the combined random error in altitude below 20 km and it overestimate above 20 km.

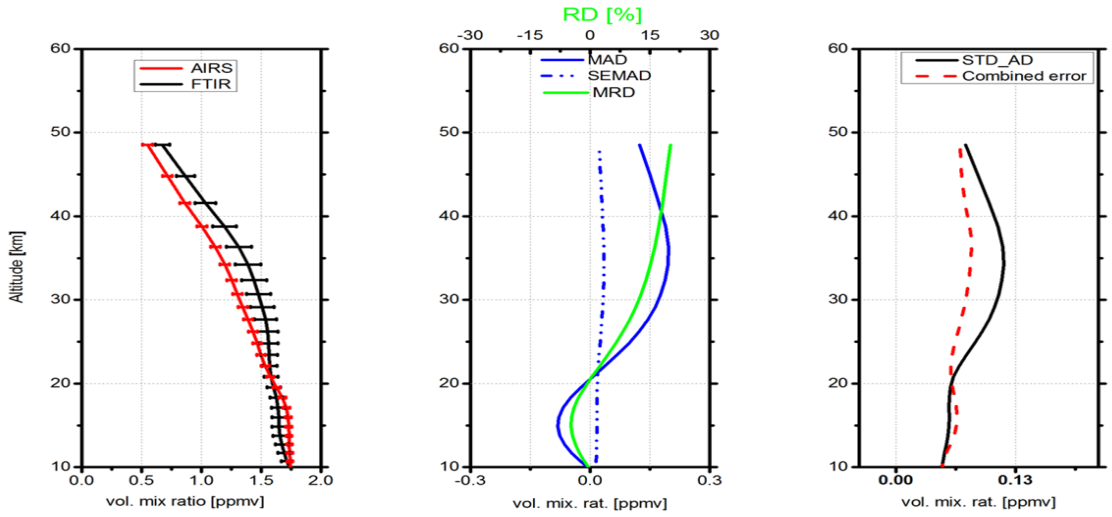

Fig. 6.9 Comparison of CH_4 from AIRS and FTIR. Details as in Fig. 6.1

6.7 Correlation plots of CH_4 and N_2O derived from FTIR, MIPAS and MLS

The scattering plot of the data sets between FTIR (CH_4 and N_2O) and MIPAS_CH4_220, MIPAS_N2O_220 is shown in Fig. 6.10 in the altitude range of 15-30 km, color bar has been represented for 3 km space (blue, cyan, green, yellow and red). The correlation coefficients between FTIR CH_4 Vs MIPAS_CH4_220 and FTIR N_2O Vs MIPAS_N2O_220 in the altitude range 15-22 km are 0.05 and 0.65 respectively. Whereas, the scattering plot between FTIR (CH_4 and N_2O) and the new data version of MIPAS_CH4_224 and MIPAS_N2O_224 are 0.18 and 0.2 respectively (see Fig. 6.11). Here, we found that the data points of the new data version coincide better with the line with unity slope than the older version. The latter tend to lie above this line for altitudes below 22 km for Addid Ababa measurements. This confirms the findings of the previous section that low altitude methane of MIPAS_CH4_220 is biased high and this bias has been reduced in MIPAS_CH4_224.

The correlation coefficients between FTIR Vs MLS values of N_2O and CH_4 are 0.94 and 0.75 in the altitude range of 17-48 km respectively (Fig.6.12). The scatter plot of the ground-based FTIR vs MLS of N_2O and CH_4 confirms what has been seen in the comparison of mean profiles: the data points are mainly found near the reference line with unity slope, indicating that both instruments agree reasonably well. Particularly the data points referring to altitudes below 20 km (orange and red data points) have a tendency to fall below the

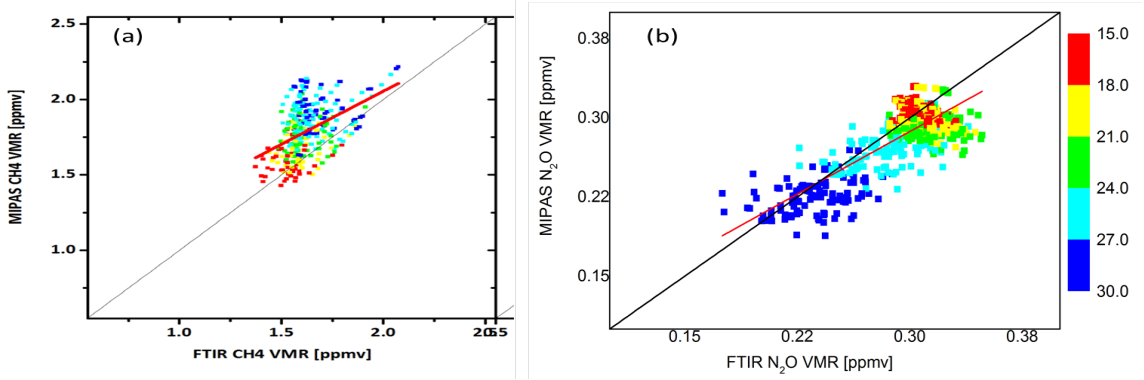

Fig. 6.10 A scatter plot of daily mean values of FTIR CH_4 of Addis Ababa Vs MIPAS_CH4_220 (left), FTIR N_2O Vs MIPAS_N2O_220 (right). The colour bar represents the altitude in Km. The thick red line is the best fit straight line while the black line would be obtained for a perfect agreement (FTIR = MIPAS). The correlation coefficients r of the FTIR and MIPAS series are summarized in table 1 (15-22 km).

Table 6.3 Averaged statistical means (M) and standard deviations (STD) of the relative differences $(2 \times \frac{MIPAS-FTIR}{FTIR+MIPAS})$ [%] defined in altitude range of 15-22 km. R is correlation coefficient with in 15 to 22. The number of coincidences (N) within a spatiotemporal criteria of $\pm 2^\circ$ of latitude and $\pm$ 10° of longitude and time difference of $\pm$24hr. This is for FTIR and MIPAS_CH4_220, MIPAS_CH4_224.

FTIR Vs	Residual	R	Slope	Intercept	$M \pm STD$[%]	period	N
MIPAS_CH4_220	4.6	0.05	0.31	1.4	-12.3±9.8	Jun 2009-Feb 2011	57
MIPAS_CH4_224	0.4	0.18	0.13	1.5	3.4± 9.5	Jun 2009-Feb 2011	29
MIPAS_N2O_220	0.21	0.65	0.8	0.05	2.5± 5.5	Jun 2009-Feb 2011	61
MIPAS_N2O_224	0.005	0.2	-0.3	0.4	2.5± 5.5	Jun 2009-Feb 2011	18

reference line, confirming the high bias of MIPAS at the low altitudes.

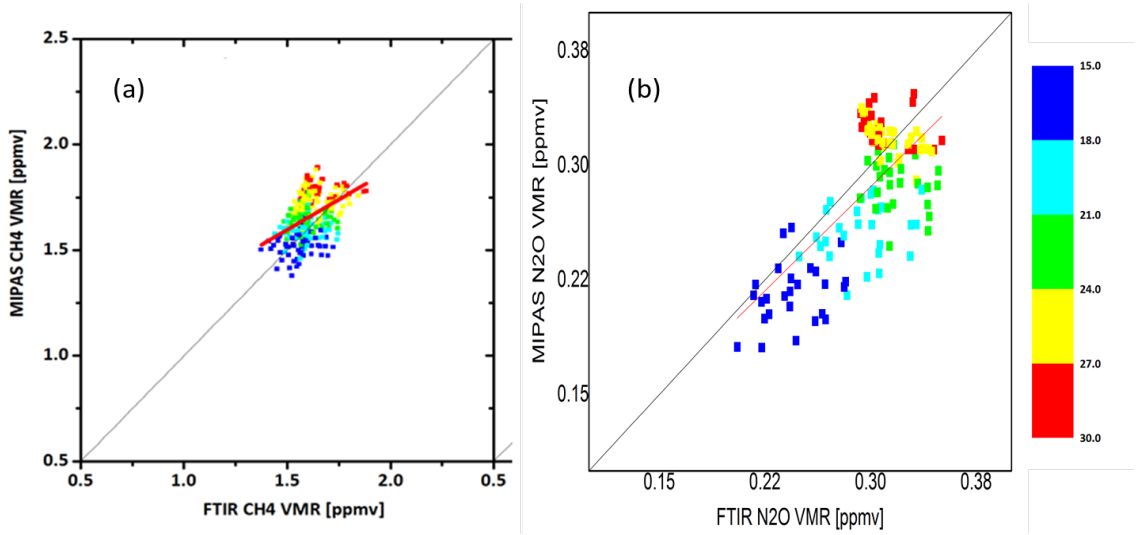

Fig. 6.11 Scattering plots between FTIR CH_4 and MIPAS_CH4_224 (left) and FTIR N_2O and MIPAS_N2O_224 (right). The colour bar represents the altitude in Km. The thick red line is the best fit straight line while the black line would be obtained for a perfect agreement (FTIR = MIPAS). The correlation coefficients r of the FTIR and MIPAS series are summarized in table 1 (15-22 km).

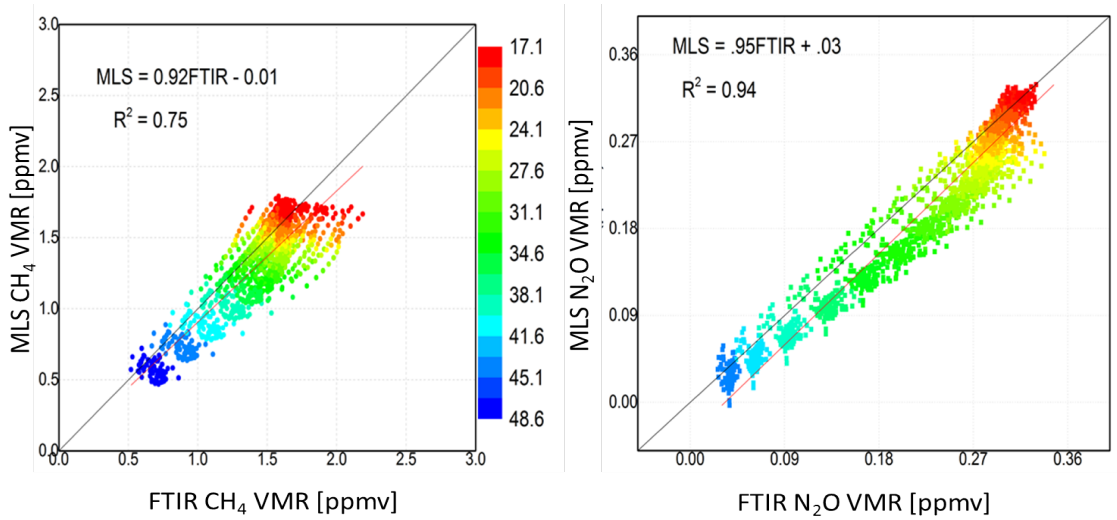

Fig. 6.12 Daily scattering plot of FTIR Vs MLS of CH_4 (left) and N_2O (right).

6.8 Summary

Here, the FTIR products of CH_4 and N_2O have been compared to coincident volume mixing ratio (VMR) measurements obtained from the reduced spectral resolution (Institute of Meteorology and Climate Research) IMK/IAA MIPAS satellite instrument (Version V5R_CH4_220, V5R_N2O_220 and Version V5R_CH4_224, V5R_N2O_224), the Microwave Limb Sounder on board of the Aura satellite (Aura/MLS) (MLS v3.3 of N_2O and CH_4 derived from MLS v3.3 products of CO, N_2O and H_2O) and the Atmospheric Infrared Sounder (AIRS)of CH_4.

For CH_4 comparisons, we obtain a statistically significant negative bias of -15 % to -3.8 % in the altitude ranges of 12 km to 27 km between FTIR and MIPAS_CH4_220, mainly upper troposphere and lower-middle stratosphere profiles with the maximum value of difference is at tropopause and a standard deviation of 7 to 8 %. No statistically significant bias is seen with in 27 up to 42 km. For N_2O comparisons, statistically significant positive bias is seen between FTIR and MIPAS_N2O_220 within 2 to 5 % in altitude range 15-20 km and its difference is within 5-10 % in altitude 20-30 km. below 18 km, the standard deviation of the mean relative difference is within 7 to 10 % and above 20 up to 30 km, the standard deviation of the mean relative difference is with in 10 to 15 %. However, the comparison of FTIR CH_4 and IMK/IAA MIPAS V5R_CH4_224 and V5R_N2O_224 products has been discussed, a statistically significant maximum negative bias of -4.8 % in altitude 15 km that extends to 21 km and maximum positive bias of 4.6 % in altitude 27 km were obtained. Whereas in the case of FTIR and MIPAS V5R_N2O_224, a significant positive bias of less than 15 % in the altitude range 22-27 km with a maximum value at around 25 km and a negative bias of -7 % at 17 km has been obtained. The largest negative bias is found in altitude between 11-19 km with a maximum difference of -0.08 ppmv (-4.8 %) at around 15 km and a positive bias of less than 0.14 ppmv (9 %) is found in altitude between 21-27 km with a maximum value at around 27 km in FTIR CH_4 comparison with AIRS. On the other hand, comparison of FTIR CH_4 profiles with MLS measurement indicates that no significant bias in FTIR CH_4 data is present between 22 and 27 km. The mean absolute and relative difference shows positive bias, FTIR CH_4 values are lower in average of 0.15 ppmv (9 %) below 22 km and higher above to 0.12 ppmv (8 %) in 27 km. The standard deviation of the difference is larger than the combined random errors of the instruments through out the altitude, but maximum variation is existed below 31 km. the value of standard deviation of difference is larger by a factor of around 0.1 ppmv for altitude below 31 km. Since we did not take in to account all the source of random uncertainties of the measurements, the standard deviation of the difference is overestimated. The atmospheric variability due to the

coincidence criteria might contribute the overestimation of standard deviation of absolute difference.

For N_2O derived from the coincident pairs of FTIR and MLS N_2O the value derived from FTIR is overestimated through out the altitude or the FTIR values of N_2O is larger than the MLS values of N_2O by a factor of 1.3 at around 30 km and by a factor of 1.1 at around 21 km. The mean relative difference of FTIR and MLS N_2O value is statistically significant positive bias that increases as altitude increases, its value is less than 20 % for the altitude below 30 km. Therefore, the ground-based FTIR spectrometer can be recommended for CH_4 and N_2O satellite data (MIPAS, MLS and AIRS) validation

The large negative bias at upper troposphere and lower stratosphere of the tropics obtained in this chapter, mainly for the intercomparison of FTIR CH_4 with MIPAS_CH4_220 and its reduction in the new data version MIPAS_CH4_224 has been investigated in the next chapter.

Chapter 7

Impacts of H_2O Variability on accuracy of CH_4 observations from MIPAS measurements over the tropics

7.1 Introduction

Uncertainty of an instrument measuring atmospheric parameter in a global scale is expected to be equal. However, the primary noise observed from limb sound recorded on February 2010 has been shown large noise in the upper troposphere and lower stratosphere of tropics. Furthermore, different literatures have suggested that the large uncertainty of satellite observations of methane in the upper troposphere and lower stratosphere of tropics and this might be related to water vapour variability [27]. In this work, we showed the large uncertainties of MIPAS_CH4_220 and MIPAS_CH4_224 in the upper troposphere and lower stratosphere of tropics with reduced the value in the new version.

Different methods have been applied to determine uncertainty of MIPAS_CH4_220, MIPAS_CH4_224 measurements and variability of water vapour at the three latitudinal bands. Intercomparison of methane measured by MIPAS with the ground-based FTIR products obtained from the Addis Ababa FTIR observatory and other two NDACC FTIR sites representing the mid and high latitude sites (Jungfraujoch, Switzerland and Ny-Ålesund, Spitsbergen) are performed. The standard deviation of mean difference and the combined random uncertainty of instruments are compared to explore the magnitude of natural variability of water vapour. Natural variability of water vapour and the uncertainties of MIPAS methane can also be determined using the differential method proposed by Fioletov

et al. [94] and applied on different literatures (e.g. [39, 40]) for the three atmospheric conditions using at least two different measurement techniques. Furthermore, correlation analysis between MIPAS_CH4_220 and MIPAS_N2O_220, MIPAS_CH4_220 and MLS CH_4, MIPAS_CH4_224 and MIPAS_N2O_224 and between MIPAS_CH4_220 and MLS CH_4 have been applied to explore the variation of the uncertainty of MIPAS CH_4 as a function of latitude and altitude in a global scale. It is also used to show a large uncertainty in the lower stratosphere of of tropics in the MIPAS_CH4_220 and reduced in MIPAS_CH4_224. Finally, the cause of high uncertainty of MIPAS_CH4_220 and its reduction in MIPAS_CH4_224 at the lower stratosphere of the tropics has been assessed through its relation with water vapour variability using a regression analysis method.
In this chapter, we discuss different established methods for random uncertainty variation as a function of latitude in the lower stratosphere and their applicability to MIPAS_CH4_220, MIPAS_CH4_224 and natural variability of water vapour. Like, bias evaluation, differential method and correlation coefficient analysis methods were used and then the cause of the latitudinal variation has been revealed by taking three selected atmospheric conditions or ground based FTIR sites.

7.2 Preliminary observations

Figure 7.1 (middle and left panel) shows the latitudinal variation of MIPAS_CH4_220 and MIPAS V5R_CH4_224 uncertainty, which is noisy on Feb. 2010. Hence, the random uncertainty of the instrument taking in to account is noise only as this is the only sources of the random uncertainty provided with the IMK/IAA retrieved products obtained from Institute of Meteorology and Climate Research. It indicates that random uncertainty of MIPAS CH_4 profile is large in the altitude range of upper troposphere and lower stratosphere of tropics (below 20 km). This latitudinal variation of the IMK/IAA retrieved products, MIPAS CH_4 random uncertainty is also shown on the MIPAS ESA retrieved value of CH_4. However, the random uncertainty of the MIPAS ESA products from Oxford university includes all the sources of error contributed to the random uncertainty. Similarly, the variability of H_2O as a function of latitude and altitude is shown in right panel of Fig. 7.1.
Therefore, the preliminary results observed from the measurements of methane by MIPAS that is processed at Institute of Meteorology and Climate Research, IMK/IAA MIPAS_CH4_220 and MIPAS_CH4_224 as well as the retrieved data products adapted from Oxford MIPAS page (www.atm.ox.ac.uk/group/mipas/err) shows the latitudinal variation of the uncertainty with a large value in tropics. Different literatures indicates the appearance

of high random uncertainty of methane measurements in tropical atmospheric conditions. The total random uncertainty of methane is high in the upper troposphere and lower stratospheric of tropics as compared with mid and high latitude bands at altitude range of 15 to 21 km. The random uncertainty of the measurement is less than 11 %, 6 % and 4 % in tropics, mid and high latitude respectively.

Noise is large at upper tropospheric and lower stratosphere of tropics and its noise value reaches 0.17 ppmv and decline in mid and high latitudes to less than 0.1 ppmv. Moreover, high variability of H_2O are inspected in upper troposphere and lower stratosphere of tropics with a maximum value of 3 ppmv and variability of less than 2 ppmv on the other latitudinal bands. This leads us to investigate the relation between water vapour variabilities with uncertainty of MIPAS_CH4_220 and MIPAS_CH4_224 at upper troposphere and lower stratosphere of different latitudinal bands.

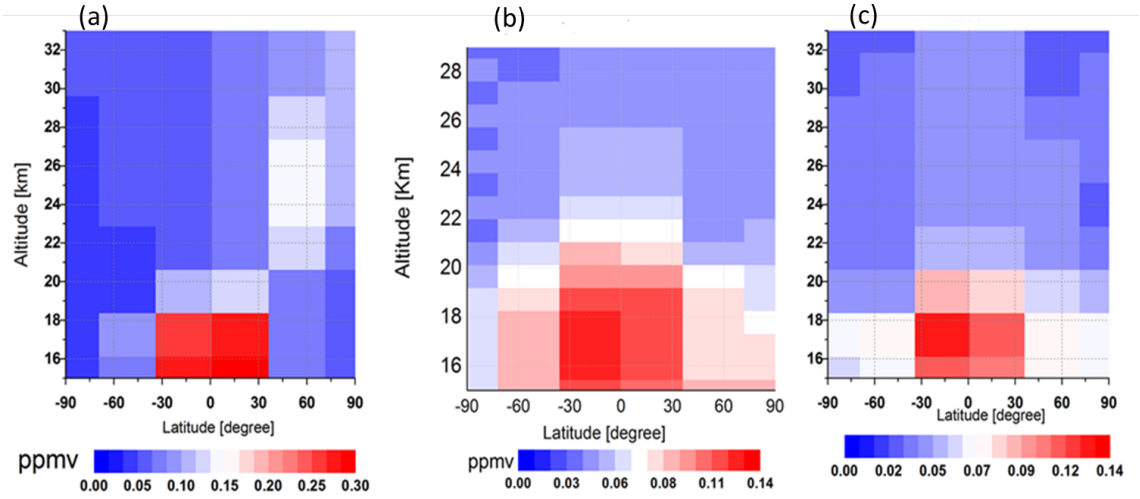

Fig. 7.1 Latitude/ altitude distribution of (a) natural variability of H_2O in ppmv, (b) uncertainty of MIPAS_CH4_220 in ppmv and (c) uncertainty of MIPAS_CH4_224 in ppmv for Feb, 2010.

7.3 Methodology

For bias and precision validation of MIPAS CH_4 we use established methodology. The bias is calculated as the mean difference between the data sets, and its significance is assessed via the standard deviation of the mean difference of collocated measurements [38]. The precision is estimated as the standard deviation of the differences between the collocated

measurements [95]. Furthermore, we use the method proposed by Fioletov et al. [94] which estimates both the natural variability of a state variable and the random uncertainties of two systems measuring this state variable in the same latitude band.

7.3.1 Bias evaluation

Bias evaluation of CH_4 volume mixing ratios derived from MIPAS is considered as a technique to determine the uncertainty of the instrument and the natural variability of water vapour by comparing the bias obtained for the three latitudinal bands. From the intercomparison results of MIPAS_CH4_220 and V5R_CH4_224 with Microwave Limb Sounder (MLS) and ground-based FTIR products obtained from Addis Ababa FTIR observatory and other two NDACC FTIR sites representing the mid and high latitude sites (Jungfraujoch, Switzerland and Ny-Ålesund, Spitsbergen) using the statistical analysis methods detailed in von Clarmann [38] and corresponding noise of MIPAS CH_4 were considered as the random error that represent the uncertainty of the instrument [64]. To estimate the uncertainty of MIPAS data sets of CH_4, the standard deviation of bias has been taken as it represents a combined random errors of the two instruments [95]. We can call this as bias evaluation method. we consider the MIPAS CH_4 with coincident criteria of $\pm 2^\circ$ of latitude and $\pm 10^\circ$ longitude from the locations of FTIR at Addis Ababa, Jungfraujoch and Nylesund respectively for the three atmospheric conditions.

In the case of bias evaluation, the vertical profiles MIPAS_CH4_220, V5R_CH4_224 and MLS version 3.3 CH_4 are smoothed using the FTIR averaging kernels of individual species obtained from the ground-based FTIR retrieval by applying the procedures reported in Rodgers and Connor [92] and given as

$$\mathbf{x}_s = \mathbf{x}_a + \mathbf{A}(\mathbf{x}_i - \mathbf{x}_a) \tag{7.1}$$

where $\mathbf{x}_s$ is the smoothed profile, $\mathbf{x}_a$ and $\mathbf{A}$ represents the a priori and averaging kernel for CH_4 and N_2O obtained from the ground-based FTIR instrument respectively. The $\mathbf{x}_i$ is the initial retrieved profile obtained from satellite measurements (MIPAS and MLS) after we interpolated it to the FTIR grid spacing. We then compare with the FTIR measurements at the geolocations of the respective FTIR sites within coincidence criteria of $\pm 2^\circ$ of latitude and $\pm 10^\circ$ of longitude and time difference of $\pm$24hr.

7.3.2 Differential method

The Fioletev method is applied to MIPAS, MLS and ground-based FTIR measurements of CH_4 and H_2O. It uses variances of the trace gas measurements in latitude bins which can be considered as fairly homogeneous, such that sampling artifacts in the variances can be excluded. We further assume that the measured values of H_2O, CH_4 and the errors associated with these measurements are independent. Then the sample variance $\sigma^2(M_i)$ of the measurements of one gas by instrument i can be understood as

$$\sigma^2(M_i) = \sigma^2(X_t) + \sigma^2(\varepsilon_i) \tag{7.2}$$

where X_t is the true value of the measured quantity and ε_i is the measurement error of the i^{th} instrument. Since, putting sampling artefact aside, the natural variability is the same, regardless by which instrument the atmosphere is observed, and since random errors of two independent measurement systems are usually uncorrelated, the variance of the differences between collocated profile measurements by the two instruments depends only on the random errors:

$$\sigma^2(X_{t1} - X_{t2}) + \sigma^2(M_1 - M_2) = \sigma^2(\varepsilon_1) + \sigma^2(\varepsilon_2) \tag{7.3}$$

The terms $\sigma^2(M_1 - M_2), \sigma^2(M_1)$ and$\sigma^2(M_2)$ are available from the observations, and Eqs (7.2-7.3) can be rearranged to give the natural variability (NV) and the random error of each of the two measurements.

$$\begin{aligned}
\sigma^2_{NV}(X) &= \frac{1}{2}(\sigma^2(M_1) + \sigma^2(M_2) - \sigma^2(M_1 - M_2)) \\
\sigma^2(\varepsilon_1) &= \frac{1}{2}(\sigma^2(M_1) - \sigma^2(M_2) + \sigma^2(M_1 - M_2)) \\
\sigma^2(\varepsilon_2) &= \frac{1}{2}(\sigma^2(M_2) - \sigma^2(M_1) + \sigma^2(M_1 - M_2))
\end{aligned} \tag{7.4}$$

where M_1 represents MIPAS and M_2 the MLS or FTIR measurement, depending on the application. Both the estimated standard deviation (SD) of instrument uncertainty (i.e. MIPAS CH_4) and standard deviation of water variability for a given location, time of year, and layer were obtained using equations (7.4). Applying equation (7.4) to these data sources creates two sets of the SD of MIPAS CH_4 uncertainty estimates. Similarly, SD of water vapour variability were obtained for each of the three latitudinal bands. The value estimated SD uncertainty of MIPAS CH_4 was calculated as the square root of mean variance estimates

from the two data sources.

In addition to the above methods employed in this paper, as the UT/LS, mixing ratios of these long-lived trace gases are largely controlled by dynamical processes, generally resulting in compact tracer-tracer correlations. These correlations are usually more compact in high and mid-latitudes, while in the tropics a somewhat larger scatter is observed (see e.g., [27, 52]). We used such methods to show the variation of MIPAS_CH4_220 and MIPAS_CH4_224 uncertainty with high value at LS of the tropics and its reduction in MIPAS_CH4_224 as a function of latitude and altitude in a global scale using corresponding values MIPAS_N2O_220, MIPAS_N2O_224 for February 2010. In addition, both version data sets of MIPAS CH_4 and MLS CH_4 version 3.3 for February 2010 have been discussed too. These correlations are calculated on latitude bin space by 30 and on an altitude grid with 7 levels and spacing of 2 km.

7.4 Results and Discussion

The bias in MIPAS_CH4_220 and MIPAS V5R_CH4_224 can be quantified by comparison with the ground-based FTIR CH_4 at the three selected sites, representing the three latitude bands mentioned. Similarly, the variability of H_2O over these three sites has been presented and discussed using the standard deviation of the bias and combined random errors of the instruments between MIPAS and MLS.

Figure 7.2 (panel a, b and c) shows the results from the comparison between MIPAS_CH4_220 and FTIR methane profiles. There are 61 coincident measurements in the tropics, 80 in mid-latitudes and 15 in high latitude. The mean relative differences range from 13.7 % to 3.0 % in altitude range 15 to 27 km for the tropical site, they are in ranges 10 % to 1 % and -2.7 % to 2.2 % for mid and high latitudes respectively. We found that the bias is largest in tropical site relative to the mid and high latitude bands, with positive peak value at tropopause. The averaged mean relative differences and their standard deviations in the altitude range of 15-22 km are 12.3 % $\pm$ 9.9 %, 8.9 % $\pm$ 5 % and -1.2 % $\pm$ 6.7 % for Addis Ababa, Jungfraujoch and Ny-Ålesund sites respectively (see Table 7.1).

Figure 7.2 (panel d, e and f) shows the same type of comparison, but for the new version MIPAS V5R_CH4_224 and FTIR methane profiles over three sites. There are 29 coincident measurements in Addis Ababa, 17 in Jungfraujoch and 16 in Ny-Ålesund. The mean relative differences range from 4.8 % to -4.6 % at the altitude range of 15 to 27 km for Addis Ababa with a positive bias at altitudes below 22 km and a negative bias above 22 km. They are -2.5 % to 4.9 % and -3.8 % to 1 % for the Jungfraujoch and Ny-Ålesund site respectively.

We found that the bias is largest for the tropical site, Addis Ababa, relative to the mid and high latitudes with a positive peak value at tropopause. The values reported in the sixth column of Table 7.2 are averaged mean relative differences and their standard deviations in the altitude ranges of 15 to 22 km.

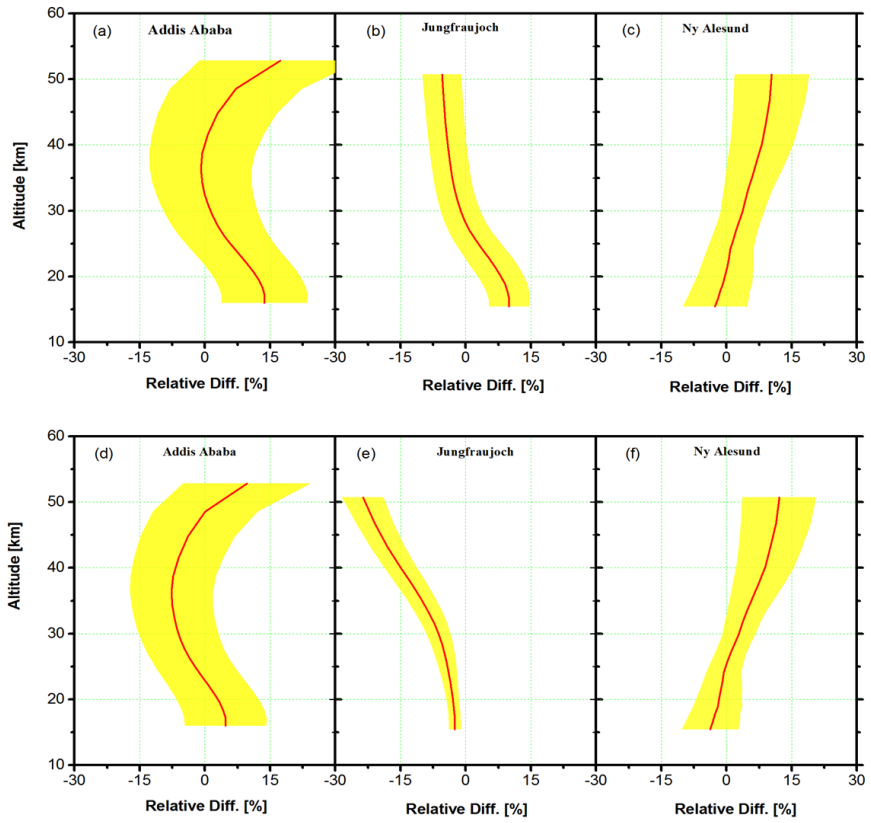

Fig. 7.2 Comparisons of MIPAS_CH4_220 profile with FTIR values (upper panel) and MIPAS_CH4_224 profile with FTIR (lower panel). The relative differences $(2 \times \frac{MIPAS-FTIR}{FTIR+MIPAS})$ [%] averaged over Addis Ababa, Jungfraujoch and Ny-Ålesund sites. The shaded area is the standard deviation of the mean relative differences.

To explore the precision of MIPAS_CH4_220 and MIPAS_CH4_224 vmr measurements, the coincidence of MIPAS and FTIR CH_4 at the three latitudinal bands have been used. The scatter plots that are shown in Fig. 7.4 in the altitude range 15-30 km, color bar has been represented for 3 km space (blue, cyan, green, yellow and red). The high correlation at Jungfraujoch and Ny-Ålesund indicate that the instrument uncertainties are low relative to the methane variability for both MIPAS_CH4_220, MIPAS_CH4_224 with reduced the bias in the MIPAS_CH4_224 at Jungfraujoch. However, the correlation is less at Addis Ababa that indicates large instrument uncertainties relative to the methane variability. The

correlation coefficients are shown in table 1 for altitude range 15-22 km, those are 0.84 (MIPAS_CH4_220) and 0.98 (MIPAS_CH4_224) for Jungfraujoch , 0.9 (MIPAS_CH4_220) and 0.89 (MIPAS_CH4_224) for Ny-Ålesund and less than 0.3 for both MIPAS_CH4_220, MIPAS_CH4_224 at Addis Ababa. Further, the data points of the new data version coincide better with the line with unity slope than the older version. The latter tend to lie above this line for altitudes below 22 km for Addid Ababa and Jungfraujoch measurements. This confirms the findings of the previous section that low altitude methane in MIPAS_CH4_220 MIPAS data is biased high and this bias has been reduced in MIPAS_CH4_224.
The standard deviation of mean relative differences between MIPAS_CH4_220 and FTIR stated in the previous section also shows the precision and it is in the order of 4 to 8 % in altitude between 15 and 27 km of all the three sites and this is comparable to the estimated precision reported by von Clarmann [38]. On the other hand, the precision between MIPAS_CH4_224 and FTIR is in the order of 1 to 5 %, maximum at Addis Ababa, tropics. Thus the effect of water vapour variability on the uncertainty of MIPAS CH_4 (mainly on MIPAS_CH4_220) at tropics is required to assess in this work.

Table 7.1 Averaged statistical means (M) and standard deviations (STD) of the relative differences $(2 \times \frac{MIPAS-FTIR}{FTIR+MIPAS})$ [%] defined in altitude range of 15-22 km. R is correlation coefficient with in 15 to 22. The number of coincidences (N) within a spatiotemporal criteria of $\pm 2^\circ$ of latitude and $\pm$ 10° of longitude and time difference of $\pm$24hr. This is for MIPAS_CH4_220 and FTIR.

Site	Residual	R	Slope	intercept	$M \pm STD$	period	N
Addis Ababa 9.03° N	5.9	0.32	0.4	1.22	12.3± 10.1	Jun 2009-Feb 2011	57
Jungfraujoch 46.55° N	3.6	0.84	1.2	-0.07	8.9± 5	Jan 2009-Dec 2009	12
Ny-Ålesund 78.92° N	1.1	0.9	0.99	0.03	-1.2 ± 6.7	Mar 2009-Apr 2011	33

Natural variability of H_2O

MIPAS water vapour observations over the three measurement sites in January 2010 were compared to Aura MLS version 3.3 water vapour. The coincidences criteria were 7° N to 11° N, 45° N to 49° N and 77° N to 81° N and we ascertain 9, 12 and 14 coincidences between MIPAS and Aura/MLS respectively, their temporal coincident is ± 12 hr. Version 3.3 of Aura/MLS and IMK/IAA MIPAS V5R_H2O_220 data product were used to analyze the intercomparison result.
Figure 7.4 shows a plot of the standard deviations of mean absolute differences and the

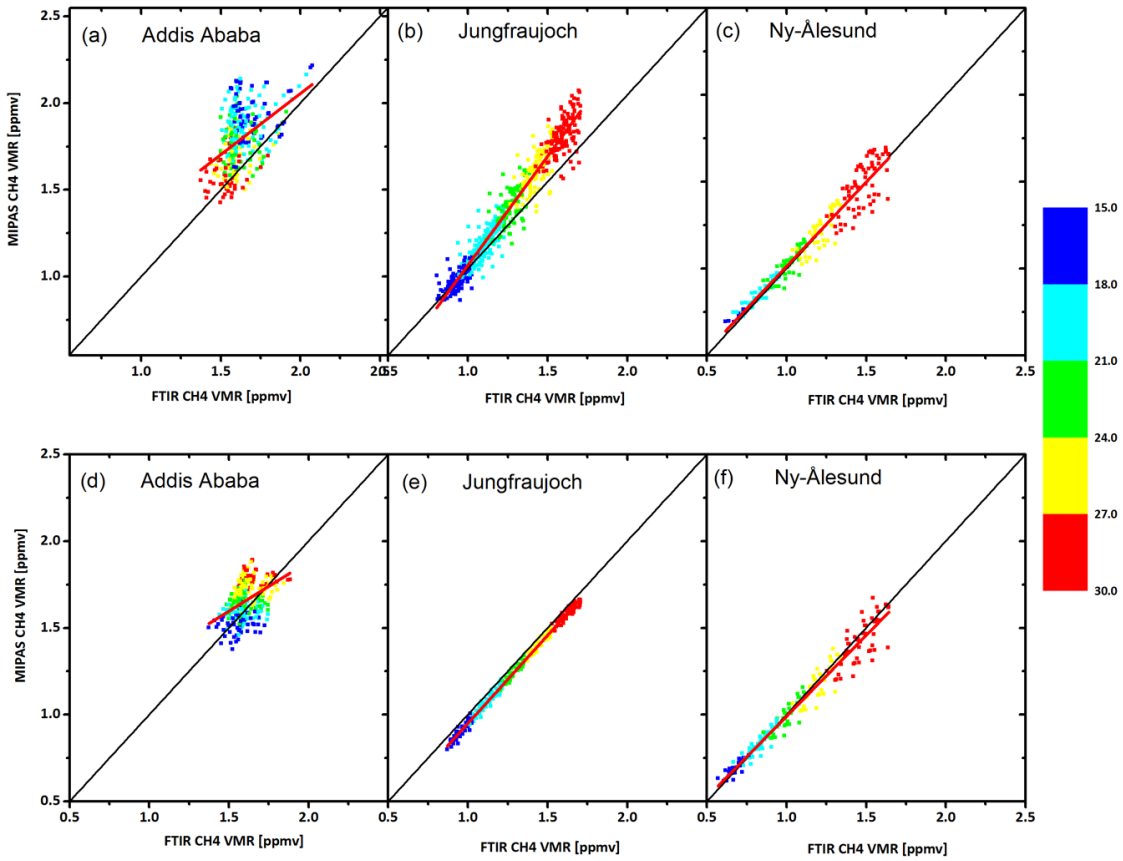

Fig. 7.3 A scatter plot of daily mean values of MIPAS_CH4_220 (upper panel) and V5R_CH4_224 (lower panel) vs FTIR CH_4 of Addis Ababa, Jungfraujoch and Ny-Ålesund sites from left to right respectively. The colour bar represents the altitude in Km. The thick red line is the best fit straight line while the black line would be obtained for a perfect agreement (CH_4 (MIPAS) = CH_4 (FTIR)). The correlation coefficients r of the MIPAS and FTIR series are summarized in table 1 (15-22 km).

combined random errors of instruments as a function of altitude for H_2O vertical profiles obtained from MIPAS and MLS. For the tropical measurements, the combined estimated random error exceeds the standard deviation of the differences inferred from the observations. This indicates an overestimation of the retrieval uncertainties. For the other sites this is not the case although the spatial and temporal coincidence criteria were chosen similar. The result for the tropical site is particularly astonishing because for the combined error we used only the retrieval noise and ignore the estimates of other random error components. Thus, underestimation of the random uncertainty should be expected. However, the spatial and temporal criteria used in all the three atmospheric conditions are similar. Different rea-

Table 7.2 Averaged statistical means (M) and standard deviations (STD) of the relative differences $(2\frac{MIPAS-FTIR}{FTIR+MIPAS})$ [%] defined in altitude range of 15-22 km. R is correlation coefficient with in 15 to 22. The number of coincidences (N) within a spatiotemporal criteria of $\pm 2^\circ$ of latitude and $\pm$ 10° of longitude and time difference of $\pm$24hr. This is for MIPAS_CH4_224 and FTIR.

Site	Residual	R	Slope	intercept	$M \pm STD$	period	N
Addis Ababa 9.03° N	0.4	0.18	0.13	1.5	3.4± 9.4	Jun 2009-Feb 2011	29
Jungfraujoch 46.55° N	0.04	0.98	0.97	5.3	-2.8± 1.4	Jan 2009-Dec 2009	16
Ny-Ålesund 78.92° N	0.5	0.89	0.95	0.04	-2.4 ± 5.8	Mar 2009-Apr 2011	17

sons has reported for the overestimation of standard deviation of the absolute differences, as we have not taking all the sources of errors that contribute to the random uncertainties of the MIPAS measurements (i.e is the only error source considered noise), strong gradients of H_2O spatially and temporally in tropical atmospheric conditions and the overestimation of the standard deviation of mean absolute differences may also be existed due to the natural variability of the parameter (H_2O).

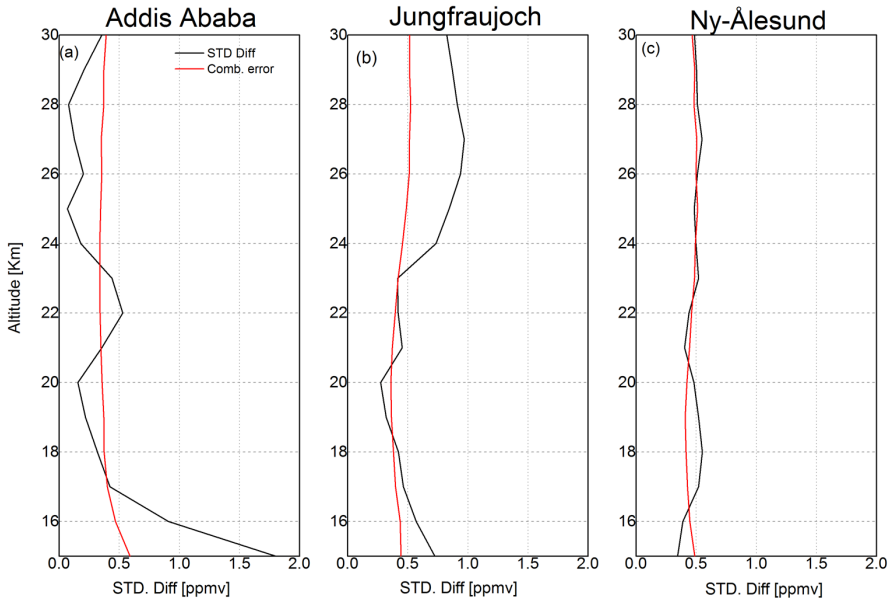

Fig. 7.4 The standard deviation of differences versus the combined error of the instruments MIPAS V5R_H2O_220 and MLS measurement for Addis Ababa, Jungfraujoch and Ny-Ålesund stations (left to right) on January 2010.

The bias between MIPAS and other data sources has been reported by different scholars,

such as the bias of MIPAS CH_4 and N_2O with caution in the tropical lower stratosphere e.g, [54]. In the lower stratosphere/upper troposphere (UT/LS) comparisons of ML2PP profiles and correlative measurements of individual CH_4 and N_2O profiles show oscillations in individual profiles caused by the processing algorithm and in the middle stratosphere, no significant bias is observed [27]. In the lower stratosphere (below about 25 to 30 km) MIPAS CH_4 is biased high with respect to satellite instruments, and the most likely estimate of this bias is 14 % [42]. The mean difference we obtained between MIPAS and FTIR over the tropical atmospheric conditions are in agreement with the deviations reported in Payan et al. [27].

7.4.1 Correlation plots of CH_4 and N_2O

Tracer-tracer correlation (i.e. CH_4-N_2O) measured by MIPAS has been used to show the variation of the uncertainty of MIPAS CH_4 as a function of latitude and altitude. The correlation coefficients of long lived trace gases were also used to show the latitudinal and altitudinal variation of uncertainties of an instrument. Figure 7.5 Show the correlation coefficients between MIPAS_CH4_220 and MIPAS_N2O_220, MIPAS_CH4_220 and MLS CH_4, MIPAS_CH4_224 and MIPAS_N2O_224 and MIPAS_CH4_224 and MLS CH_4. The correlation coefficients between MIPAS_CH4_220 and MIPAS_N2O_220 are only used to show the latitudinal variations of MIPAS_CH4_220 uncertainty. The larger the correlation of coefficient is the lesser the uncertainty and vice versa. We need only to show the uncertainty is different at different latitudinal bands. The correlation coefficient between MIPAS_CH4_220 and MIPAS_N2O_220 as a function of latitude and altitude are 0.30, 0.98 and 0.96 in the lower stratosphere over the tropics, mid and high latitudes respectively. Nevertheless, the correlation coefficient between MIPAS_CH4_224 and MIPAS_N2O_224 are 0.62, 0.80 and 0.66. Hence, the result indicates the reduction of uncertainty of MIPAS_CH4_224 as its correlation in the lower stratosphere exceeds that of MIPAS_CH4_220.

Correlation coefficients of CH_4 and N_2O values derived from MIPAS and MLS CH_4 are expected not to vary along the latitude. However, both correlation coefficients of MIPAS_CH4_220 and MIPAS_N2O_220 of MIPAS as well as MLS version 3.3 CH_4 with MIPAS_CH4_220 in a global scale with latitudinal bands of 15° and its vertical spacing of 1 km has been found to exhibit variation at the UT/LS. Thus, the correlation coefficients of below the modest 0.5 found over tropics at upper troposphere and lower stratosphere indicate the presence of large uncertainty of MIPAS_CH4_220 (see upper panel of Fig. 7.6).

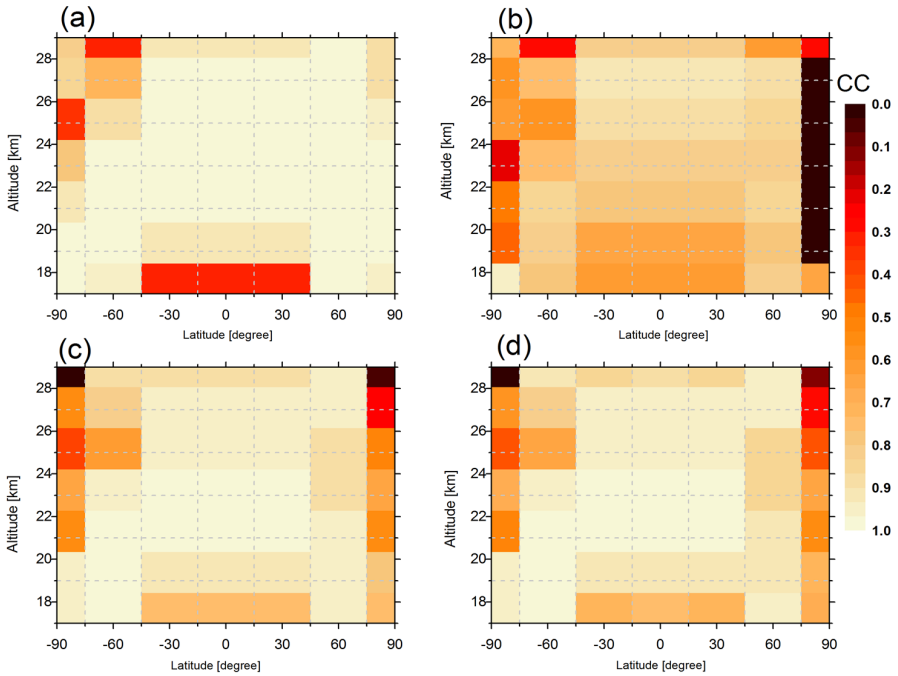

Fig. 7.5 Correlation coefficients between (a) MIPAS_CH4_220 and MIPAS_N2O_220 (b) MIPAS_CH4_220 and MLS CH_4 (c) MIPAS_CH4_224 and MIPAS_N2O_224 (d) MIPAS_CH4_224 and MLS CH_4 as a function of latitude and altitude for the period February 2010.

These results confirm those of the bias evaluation analysis using the standard deviation of the difference between MIPAS_CH4_220 and FTIR methane.

The influence of natural variability of water vapour on the uncertainty of MIPAS_CH4_220 and MIPAS_CH4_224 in the lower stratosphere of tropics with reduced effect on new version data. The contribution of water vapour variability to the large uncertainty of MIPAS_CH4_220 at lower stratosphere can be shown by the following assumption. Assume that water vapour variability in the lower stratosphere of the tropics has an effect on the amount of MIPAS CH_4 profile. The large uncertainty of methane derived from MIPAS instruments in the lower stratosphere of the tropics is due to water vapour variability and this has shown in Fig. 7.6 by taking into account the amount of water vapour variability that enhance the profile of methane in the tropics using the equation below. Hence, the true concentration of MIPAS CH_4 in the lower stratosphere is expressed as follows:

$$X_t = X_m - SD_{NV} \tag{7.5}$$

where X_t is the concentration amount after removing the effects of water vapour variability

on the vmr amount of CH_4 and N_2O, X_m is the amount of methane obtained from the measurement and SD_{NV} is the square root of estimated natural variability of H_2O variance at upper troposphere and lower stratosphere (see Fig. 7.6).
The latitudinal variation of uncertainty of MIPAS_CH4_220 has been related to the variability of water vapour. However, the latitudinal variation of the uncertainties of the new version data is reduced as water is jointly retrieved with methane. Figure 7.6 shows the reduction of latitudinal variations of uncertainty after Eq. (5) has been applied to the data sets. The correlation coefficient between MIPAS_CH4_220 and MIPAS_N2O_220 as a function of latitude and altitude after application of Eq. (5), high variation of correlation coefficient has been reduced as shown in Fig. 7.6. This indicates the effect of water vapour variability on the uncertainty of MIPAS_CH4_220 in the lower stratosphere of the tropics.

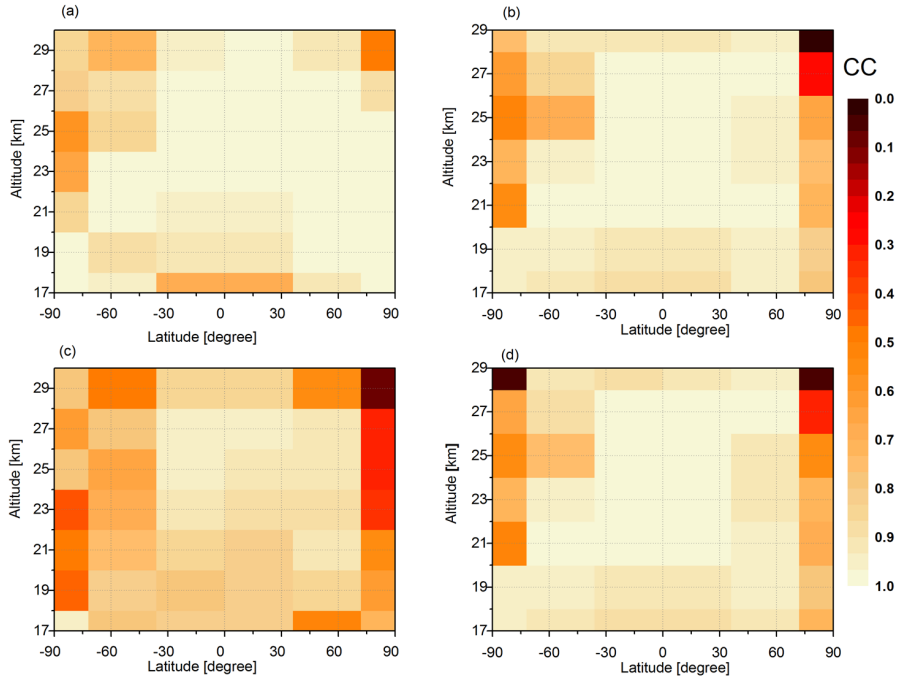

Fig. 7.6 Correlation coefficients between (a) MIPAS_CH4_220 and MIPAS_N2O_220 (b) MIPAS_CH4_220 and MLS CH4 (c) MIPAS_CH4_224 and MIPAS_N2O_224 (d) MIPAS_CH4_224 and MLS CH4 as a function of latitude and altitude for the period February 2010. After applying Eq. (5) to remove the effect of water vapour variability on the latitudinal variation of the correlation coefficient (CC).

7.4.2 H2O Variability Versus MIPAS CH4 Uncertainties

For atmospheric constituent measurements, the sample variance includes the natural variability of the measured quantities in addition to the variance of random error. Natural variability of water vapour over three atmospheric conditions can be derived from the data sets provided by at least two different techniques. Using Eq. 7.4, natural variability in terms of standard variation of water vapour over Addis Ababa was determined using January 2010 data set from MIPAS and MLS. For the same purpose we use collected MIPAS and FTIR (Addis Ababa) water vapour data sets measured between May 2009 and February 2011. The uncertainty of MIPAS methane over Addis Ababa is investigated using the two satellite measurements to determine the natural variability of water vapour as well as the uncertainty of MIPAS measurements of CH_4.

The random uncertainties of the measurements can be estimated from sets of pairs of collected data from MIPAS and FTIR or MIPAS and MLS as described in the methodology section. Figure 7.7 shows the estimated precisions of MIPAS instruments to measure CH_4 over three atmospheric conditions and it indicates that the mean altitude ranges between 15 and 27 km are 5.9 %, 4.8 %, 4.7 % for tropics (black solid line), mid (red solid line) and high (green solid line) latitudes respectively. This result is obtained using Eq. 7.4 for MIPAS and FTIR methane over the three atmospheric conditions and it also illustrates the standard uncertainty of MIPAS, which is larger in the tropics than in the mid and high latitude atmospheric conditions. However, the estimated uncertainties from MIPAS V5R_CH4_224 and FTIR methane for the three atmospheric conditions decreased as shown in the right panel of Fig. 7.7 with mean of the estimated error in the altitude ranges between 15 and 27 km are 2.4 %, 1.4 %, 5.1 % for tropics (black solid line), mid (red solid line) and high (green solid line) latitudes respectively.

Figure 7.8 shows the natural variability of MIPAS V5R_H2O_220 determined using the differential equation (Eq. 7.4) from the two instruments MIPAS V5R_H2O_220 and MLS (Ver3.3). The averaged standard natural variability of water in upper atmosphere (15-17 km) is 8.4 %, 5.4 % and 3.4 % for tropics, mid and high latitudes respectively.

The natural variability of H_2O using the data sets obtained from MIPAS is determined using the daily and monthly averaged values of the noise and sample variances for the altitude ranges of 15 to 22 km. The full error of the instrument is not taken in to account in this work, but we are attempting to use the main sources of the random error of the instrument along with the data set, since the noise is the dominant source of the random uncertainty of the instrument.

Figure 7.9 shows the natural variability of H_2O calculated by computing the variability of

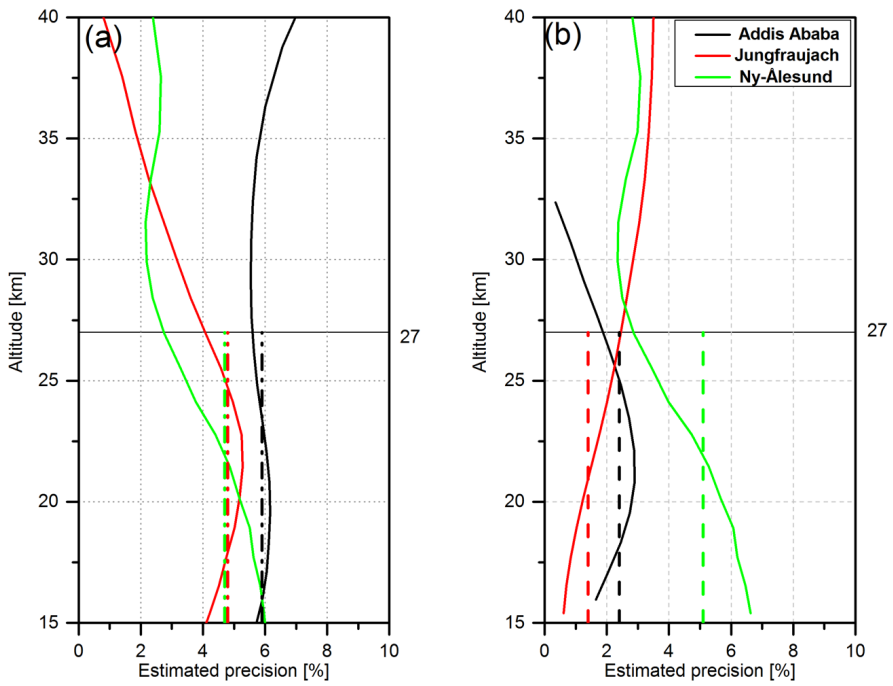

Fig. 7.7 Estimated random uncertainty of MIPAS_CH4_220 (left) and MIPAS_CH4_224 (right) from FTIR comparison at the three sites.

three years of data of MIPAS and the result confirms presence of the standard natural variability and standard MIPAS uncertainty of methane measurements over tropical, mid and high latitudes atmospheric conditions. Both the standard natural water vapour variability and standard MIPAS uncertainty in measuring methane are larger in tropical as compared to the values obtained for mid and high latitudes (right panel Fig. 7.9). The temporal variability of the water vapour followed by the natural variability of water vapour for the three conditions can be computed by subtracting the square of mean random uncertainty (noise) from the variances of the data set and the third panel represents the mean MIPAS noise or random uncertainty of the measurements for the three atmospheric conditions. We also explored the same results for seven consecutive days starting from Dec. 19, 2010 to Dec. 25, 2010. Figure 7.9 (left panel) represents the standard deviation of the water vapour of the three atmospheric conditions, which represents the natural variability of water vapour.

Table 7.4 shows the seasonal variations of both water variability and uncertainty in winter and spring at different layer of the atmosphere of the three sites. Both water variability and uncertainty of MIPAS CH_4 are high in tropics throughout the year. Mainly in the lower stratosphere (18-21 km) both the variability of water and the uncertainty of MIPAS are higher in tropics as compared to other latitude bands.

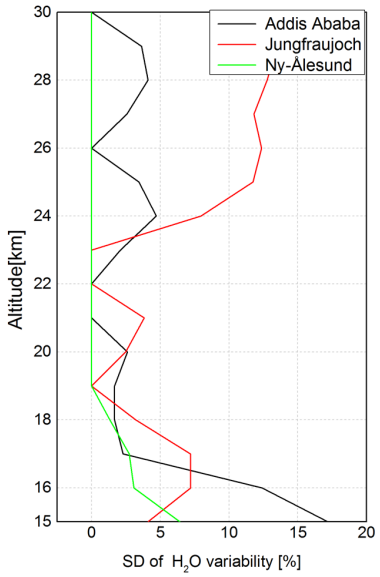

Fig. 7.8 The natural variability of H_2O over three measurement sites, computed from MIPAS and MLS.

7.5 The role of water variability on the uncertainty of MIPAS CH4 in tropics

In this part of the analysis the role of water vapour variability in the tropical tropospheric layer in the uncertainty of MIPAS methane is explored using correlation analysis. Temporal variability of water vapour in the upper troposphere and lower stratosphere (121-56 hpa) of tropics has been determined from MIPAS_H2O_220 for the time period of Jan, 2009 to Apr, 2012.

The role of LS water vapour variability on the TTL uncertainty of MIPAS methane can be investigated using monthly variability of water vapour over the tropical tropopause layer and comparing with the monthly random uncertainty of MIPAS methane. The color bar indicates the correlation coefficients between the two variables on temporal resolutions of a month and altitudinal spaces of 1 km in altitude ranges of upper troposphere and lower stratosphere of tropics using the three year (2009-2011) MIPAS CH_4 and H_2O.

We can explore the relationship between the random uncertainty of MIPAS methane and the natural variability of water vapour by employing linear regression analysis method. Figure 7.10 is a scatter plot of the standard natural variability of water vapour and the standard random uncertainty of MIPAS methane for the lower stratosphere over tropics using monthly

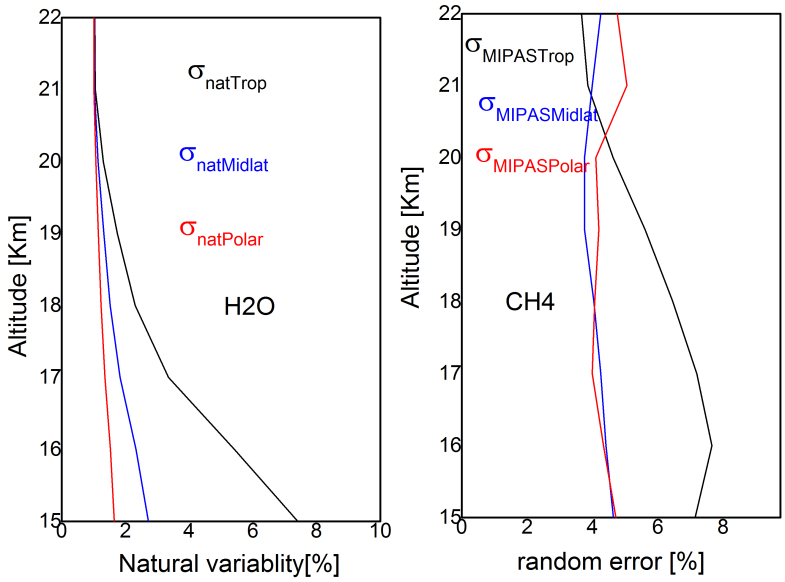

Fig. 7.9 The natural variability of H_2O (left) and the random uncertainty of MIPAS_CH4_220 (right). colored lines represent: black line for tropical, blue line for mid latitude and red line for polar using three years data sets of MIPAS, 2009-2011.

averaged values for time period of three years (Jan. 2009- Dec. 2011).

The large uncertainty of MIPAS observations of long lived species and the poor correlation between the tracer-tracer CH_4-N_2O in tropics might be correlated or coupled with water variability. The correlation of the monthly and seasonal standard natural variability of water vapour and standard uncertainty of MIPAS methane for tropics, over Addis Ababa at lower stratospheric layer (18-21 km) is 0.88.

The variability of water at the TTL is large which might have an association to the large uncertainty of MIPAS_CH4_220 for tropical atmospheric conditions, as the production of H_2O in the lower stratosphere is also through oxidation of methane in the upper troposphere and transport processes. The variability of H_2O in TTL is highly correlated to the temperature at the tropopause [25]. However, the correlation between MIPAS_CH4_224 uncertainty and water vapour variability was reduced as water vapour was jointly fitted with CH_4 (see left panel of Fig. 7.10). Similar results has been reported in methane and nitrous oxide obtained from MIPAS retrieved by ESA processor and assimilated by BASCOE and shows noisy results in tropical lower stratosphere [54].

Left panel of Fig. 7.10 shows the association between large uncertainty of MIPAS_CH4_220

Table 7.3 Standard uncertainties of MIPAS_CH4_220 (SD uncertainty (%)) and standard deviations of seasonal water vapour variability (H_2O var (%)) over Addis Ababa, Jungfraujoch and Ny-Ålesund.

layer	H_2O var (%)						SD uncertainty (%)					
	Winter			Summer			Winter			Summer		
	Addis	Jung	Ny	Addis	Jung	Ny	Addis	Jung	Ny	Addis	Jung	Ny
15-17 km	24.2	8.2	5.6	19.8	11	4.5	7.2	4.0	4.4	7.5	5.6	4.8
18-21 km	9.5	5.8	7.3	7.3	4.9	4.5	5.3	3.9	5.0	5.3	3.8	3.5
22-25 km	5.9	9.3	13.7	5.4	4.9	6.3	3.6	4.7	7.9	3.5	4.1	4.3

Table 7.4 Standard uncertainties of MIPAS_CH4_224 (SD uncertainty (%)) and standard deviations of seasonal water vapour variability (H_2O var (%)) over Addis Ababa (Addis), Jungfraujoch (Jung) and Ny-Ålesund (Ny).

layer	H_2O var (%)						SD uncertainty(%)					
	Winter			Summer			Winter			Summer		
	Addis	Jung	Ny	Addis	Jung	Ny	Addis	Jung	Ny	Addis	Jung	Ny
15-17 km	24.2	8.2	5.6	19.8	11	4.5	7.8	4.7	5.6	7.7	4.1	3.7
18-21 km	9.5	5.8	7.3	7.3	4.9	4.5	5.1	3.9	4.9	4.6	3.5	3.4
22-25 km	5.9	9.3	13.7	5.4	4.9	6.3	2.9	3.9	5.6	2.8	3.1	3.0

and water variability in altitude range between 18 and 21 km and the right panel is for MIPAS_CH4_224. In the tropics the impacts of water vapour on the new version data of MIPAS_CH4_224 has been reduced as their correlation coefficients in that altitude range is also low.

We conclude that the variability of water had an effect on the large uncertainty of MIPAS_CH4_220 in tropical atmospheric conditions. However, water vapour variability contribution on the uncertainty of MIPAS_CH4_224 has been reduced as explained in the bias evaluation section.

Table 7.5 Summary of correlation analysis of water vapour variability with random uncertainty of MIPAS_CH4_220 (first row) and MIPAS_CH4_224 (second row) from monthly averaged values in the lower stratosphere.

Residual	CC	R^2	intercept	slope	P value
0.01	0.88	0.78	0.002± 0.004	0.82± 0.04	< 0.001
0.07	0.95	0.72	0.8± 0.02	2.7± 0.3	< 0.001

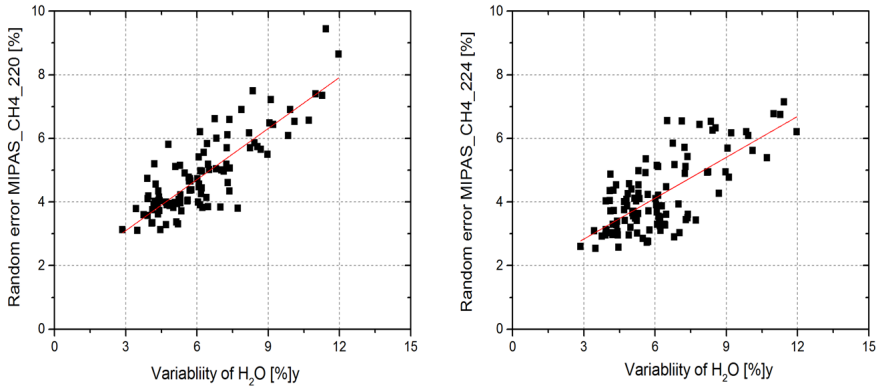

Fig. 7.10 The natural variability of H_2O and the random uncertainty of MIPAS_CH4_220 (right) and MIPAS_CH4_224 (left). Using a three years data set, 2009-2011 for altitude 18-21 km of tropics (Addis Ababa site)in the lower stratosphere.

7.6 Summary

In this chapter, we apply different methods to investigate the large uncertainty of MIPAS methane in the tropical upper troposphere and lower stratosphere as compared to the uncertainty at the same altitude level of mid and high latitudes. Similarly, the latitudinal variation of standard natural variability of water vapour has been determined using those techniques. Finally, we detected the natural variability of water vapour was a cause for high uncertainties on the MIPAS_CH4_220 measurements over tropics using the linear regression analysis. This has been reduced in the new data version MIPAS_CH4_224, where H_2O was jointly fitted with the target gas, CH_4.

Coincident methane measurements by the Michelson Interferometer for Passive Atmospheric Sounding (MIPAS_CH4_220, MIPAS_CH4_224), Microwave Limb Sounder (MLS) and ground-based FTIR are used to estimate random uncertainty of MIPAS_CH4_220 and MIPAS_CH4_224 through application of the bias evaluation, differential and correlation analy-

sis methods. The variation of random uncertainty as a function of latitude has been explored by taking three FTIR sites, Addis Ababa, Jungfraujoch and Ny-Ålesund represents tropics, mid and high latitude respectively.

The averaged relative differences between MIPAS_CH4_220 and ground-based FTIR in altitude ranges of 15-22 km are 12.3 %, 8.4 % and -1.2 % along with standard deviation of mean relative differences of 10.1 %, 5 % and 6.7 %. Whereas, from the comparison of the MIPAS_CH4_224 with FTIR, averaged bias and standard deviations of the difference in parenthesis are found to be 3.4 % (9.5 %), -2.6 % (1.4 %) and -2.7 % (5.9 %) for Addis Ababa, Jungfraujoch and Ny-Ålesund sites respectively. In both the comparisons, high bias is found in the upper troposphere and lower stratosphere (15-22 km) of tropics as compared to the same layers in mid and high latitudes, but it has been reduced in the new data version. Moreover, the differential method also estimated mean random uncertainty of MIPAS_CH4_220 in the altitude range of 15-27 km which are 5.9 %, 4.8 %, 4.7 % for Addis Ababa, Jungfraujoch and Ny-Ålesund respectively. For MIPAS_CH4_224, estimated mean random uncertainties are 2.4 %, 1.4 % and 5.1 %. From the comparison of MIPAS_H2O_220 with MLS in the three sites, standard deviation of the difference over the combined random uncertainty in the upper troposphere of the tropics are overestimated. This indicates the large natural variability of water vapour. From the differential method, we found that averaged natural variability of H2O in the altitude range of 15-17 km is 8.4 %, 5.4 % and 3.4 % in Addis Ababa, Jungfraujoch, and Ny-Ålesund respectively.

The correlation coefficient between MIPAS_CH4_220 and MIPAS_N2O_220 is 0.30, 0.98 and 0.96 in the lower stratosphere tropics, mid and high latitudes respectively. However, the correlation coefficient between MIPAS_CH4_224 and MIPAS_N2O_224 is 0.62, 0.80 and 0.66. The poor correlation between MIPAS_CH4_220 and MIPAS_N2O_220 in the lower stratosphere tropics indicates the large uncertainty of MIPAS_CH4_220 in the lower stratosphere of the tropics. Thus, all the above methods were applicable to estimate the random uncertainty of the measurements and showed a large uncertainty of MIPAS_CH4_220 with reduced in MIPAS_CH4_224 at lower stratosphere tropics. The cause of the large uncertainty of MIPAS_CH4_220 was the natural variability of water vapour as the correlation is 0.70 in the altitude range of 18-21 km. Whereas, the uncertainty of MIPAS_CH4_224 is reduced and its correlation to water vapour variability is 0.51. This indicates the contribution of water variability on the uncertainty of MIPAS_CH4_224 has been reduced as water vapour was jointly fitted with methane during the retrieval of MIPAS_CH4_224.

Chapter 8

Conclusions

In this PhD study, the detail retrieval strategy for two long-lived species over tropics, with focus on Addis Ababa site and the full error analysis of the ground-based observation have been discussed. The vertical profiles and partial column amounts of the target gases were determined in this project from the ground-based FTIR measurement located at Addis Ababa, Ethiopia. The vertical profiles derived from ground-based FTIR observations are also validated by the satellite based observations (MIPAS, MLS and AIRS) products. Finally, this study also addresses the impacts of water vapour variability on the large uncertainty of MIPAS_CH4_220 in the tropics. This uncertainty has been reduced in the new data version MIPAS_CH4_224, where H_2O was jointly fitted with the target gas, CH_4. The mean partial column of CH_4 and N_2O within the sensitivity ranges of the instrument, which is from the surface to around 27 km is determined as 2.85×10^{19} molecules $cm^{-2}\pm5.3$ % and 5.16×10^{18} molecules $cm^{-2}\pm6.95$ % respectively. The overall contribution of both statistical and systematic errors, i.e. a total error of CH_4 and N_2O from ground-based FTIR is 3.1 % and 3 %, respectively. Therefore, the ground-based FTIR at the Addis Ababa observatory is capable to monitor the vertical profiles of atmospheric gases.

We compared the atmospheric vertical profiles and partial columns of CH_4 and N_2O, measured with ground-based FTIR spectroscopy at the Addis Ababa University (9.01° N, 38.76° E, 2443 m a.s.l) in the years May 2009-February 2013 with MIPAS (version V5R_CH4_220, V5R_CH4_224, V5R_N2O_220 and V5R_N2O_224), the Microwave Limb Sounder on board of the Aura satellite (Aura/MLS) (MLS v3.3 of CH_4 and N_2O) and the Atmospheric Infrared Sounder (AIRS) (CH_4). Relative differences range in vertical profiles of CH_4 and N_2O from the measurements between MIPAS (version V5R_CH4_220, V5R_CH4_224, V5R_N2O_220 and V5R_N2O_224) and FTIR in altitude ranges of 15-27 km are -15 % to -3.8 %, -4.8 % to 4.6 %, 2 % to 10 %, -7 % to 15 %, respectively. Similarly, the mean

differences in partial column of CH_4 and N_2O within altitude ranges of 15 to 27 km are -11 %, -5.5 %, 2.39 % and 0.5 % respectively. Relative differences in vertical profiles of CH_4 and N_2O from the measurements between MLS v3.3 and FTIR in altitude ranges of 17-27 km are less than 9 % and 15 % respectively. Relative differences range in vertical profiles of CH_4 from the measurements between AIRS and FTIR in altitude ranges of 11-27 km is -4.8 % to 9 %. Therefore, the ground-based FTIR spectrometer can be recommended for CH_4 and N_2O satellite data (MIPAS, MLS and AIRS) validation.

In addition to the above findings, the large uncertainty of MIPAS_CH4_220 at the upper troposphere and lower stratosphere of tropics and its relation with water vapour variability are investigated. Furthermore, the reduction of uncertainty of MIPAS_CH4_224 has been explored. Likewise, the latitudinal variation of standard natural variability of water vapour and its relation to the latitudinal variation of uncertainty of MIPAS methane has been assessed.

Mean relative differences of $12.3\%, 8.4\%$ and -1.2% were obtained between MIPAS_CH4_220 and ground-based FTIR for the three sites in the altitude range 15-21 km. Whereas the mean relative differences between MIPAS and FTIR at 15-21 km altitude have been considerably reduced for data version MIPAS_CH4_224. They are now 3.4 %, -2.6 % and -2.7 % of tropical, mid latitudinal and polar site, respectively. Moreover, the average estimated uncertainties of MIPAS_CH4_220 were 5.9 %, 4.8 % and 4.7 % using the differential method in altitude ranges of 15 to 27 km in the tropics, mid and high latitudes, respectively. While the average estimated uncertainty of MIPAS_CH4_224 inferred by the differential analysis is low, 2.4 %, 1.4 % and 5.1 %. The correlation coefficient between MIPAS_CH4_220 and MIPAS_N2O_220 is 0.30, 0.98 and 0.96 in the lower stratosphere of the tropics, mid and high latitudes respectively. However, the correlation coefficient between MIPAS_CH4_224 and MIPAS_N2O_224 is 0.62, 0.80 and 0.66. Similarly, the inter comparison results of water vapour derived from MIPAS and MLS for the three latitude bands shows that the standard deviation of the mean difference are larger than the combined random errors in all the three conditions. Here, we detected the natural variability of water vapour was a cause for high uncertainties in the MIPAS_CH4_220 measurements over tropics using the correlation coefficient analysis. This causal has reduced in the new data version MIPAS_CH4_224 because water vapour has been fitted jointly with CH_4.

In short, the study has retrieved column abundances and profiles of two important greenhouse gases namely CH_4 and N_2O from solar absorption measurements taken at Addis Ababa, Ethiopia during a period that encompass May 2009 to March 2013. The fidelity of the data is assessed through comparison with data from MIPAS, MLS and AIRS satellites as well as full retrieval errors and their sources characterization. It is anticipated that

the use of the data in further scientific studies may provide some insight into processes that govern chemical transport and chemistry in the atmosphere as well as sources of green gases in this part of the globe.

8.1 Recommendations for Future Work

The recommendations for future work and main activities of ground based FTIR and satellite based observations of trace gases in tropics will be:

- The retrieval of methane and nitrous oxides from satellite observations required to take in to account the variability of water vapour in tropics.
- The retrieval of long-lived species in tropics from the satellite observations requires to consider the a priori of water vapour carefully applied on the target species where spectra signature is interfered.
- The retrieval of trace gases that have an absorption spectra overlapped with water vapour requires to consider the seasonal a priori profiles of target gases and interfering gases to minimize the impacts of temporal variability on the retrieved profile.
- maximizing the retrieval products of methane using only the small altitude ranges where the vertical gradients of temperature are constant as water vapour is mainly affected by temperature.
- Future activities will be focused on investigating the uncertainty of other satellite measurements of long-lived species in tropics.

References

[1] Neue, H. U., Gaunt, J. L., Wang, Z. P., BeckerHeidmann, P., and Quijano, C.: Carbon in tropical wetlands, Geoderma, 79, 163-185, 1997.

[2] Folkins, I., and Martin, R. V.: The vertical structure of tropical convection and its impact on the budgets of water vapor and ozone. J. Atmos. Sci. 62, 1560–1573, 2005.

[3] Boucher, O., Friedlingstein, P., Collins, B., and Shine, K. P.: The indirect global warming potential and global temperature change potential due to methane oxidation, Environ. Res. Lett., 4, 044007, doi:10.1088/1748-9326/4/4/044007, 2009.

[4] Michelsen, H. A., W. Irion, F., L. Manney, G., C. Toon, G., R. Gunson, G.: Features and trends in Atmospheric Trace Molecule Spectroscopy (ATMOS) version 3 stratospheric water vapor and methane measurements, J. Geophys. Res., 105(D^{18}), 22713–22724, 2000.

[5] Dlugokencky, E. J., Nisbet, E. G., Fisher, R., and Lowry, D.: Global atmospheric methane: budget, changes and dangers, Phil. Trans. R. Soc. A, 369, 2058–2072, doi:10.1098/rsta.2010.0341, 2011.

[6] Prather M .J., Holmes, C. D., and Hsu, J.: Reactive greenhouse gas scenarios: Systematic exploration of uncertainties and the role of atmospheric chemistry, Geophys. Res. Lett. 39, L09803, doi:10.1029/2012GL051440, 2012.

[7] Forster, P. M., Ramaswamy, V., Artaxo, P., Berntsen, T., Betts, R., Fahey, D. W., Haywood, J., Lean, J., Lowe, D. C., Myhre, G., Nganga, J., Prinn, R., Raga, G., Schulz, M., and Van Dorland, R.: Changes in Atmospheric Constituents and in Radiative Forcing, in: Climate Change 2007: The Physical Science Basis. Contribution of Working Group I to the Fourth Assessment Report of the Intergovernmental Panel on Climate Change, edited by: Solomon, S., Quin, D., Manning, M., Chen, Z., Marquis, M., Averyt, K. B.,

Tignor, M., and Miller, H. L., Cambridge University Press, Cambridge, United Kingdom and New York, NY, USA, 2007.

[8] Frankenberg, C., P. Bergamaschi, A. Butz, S. Houweling, J. F. Meirink, J. Notholt, A. K. Petersen, H. Schrijver, T. Warneke, and I. Aben, Tropical methane emissions: A revised view from SCIAMACHY onboard ENVISAT, Geophys. Res. Lett., 35, L15811, doi:10.1029/ 2008GL034300, 2008.

[9] Fueglistaler, S., Dessler, A. E., Dunkerton, T. J., Folkins, I., Fu, Q., and Mote, P. W.: Tropical tropopause layer, Rev. Geophys., 47, RG1004, doi:10.1029/2008RG000267, 2009.

[10] Petersen, A. K., Warneke, T., Frankenberg, C., Bergamaschi, P., Gerbig, C., Notholt, J., Buchwitz, M., Schneising, O., and Schrems, O.: First ground-based FTIR observations of methane in the inner tropics over several years, Atmos. Chem. Phys., doi:10.5194/acp-10-7231-2010, 2010.

[11] William J. Randel and Eric J. Jensen (2013); Physical processes in the tropical tropopause layer and their roles in a changing climate; REVIEW ARTICLE ; PUBLISHED ONLINE: 27 FEBRUARY 2013|DOI: 10.1038/NGEO1733; NATURE Geoscience.

[12] IPPC (Intergovernmental Panel on Climate Change): Third Assessment Report: Climate Change 2001: The Scientific Basis, Chapter 4, Cambridge University Press, UK, 2001.

[13] Solomon, S.: Stratopheric Ozone depletion: A review of Concepts and History, Rev. Geophys., 37, 275-315, 1999.

[14] Sussmann, R., Forster, F., Rettinger, M., and Bousquet, P.,: Renewed methane increase for five years (2007–2011) observed by solar FTIR spectrometry, Atmos. Chem. Phys., 12, 4885–4891, 2012.

[15] Ravishankara, A. R., J. S. Daniel, and R. W. Portmann, Nitrous oxide (N_2O): the dominant ozone-depleting substance emitted in the 21^{st} century, Science, DOI: 10.1126/science.1176985, 2009.

[16] Crevoisier, C., Nobileau, D., Armante, R., Chedin, A., and Scott, N. A., Pernin, J., Thonat, T., Schuck, T., Matsueda, H., Crepeau, L., Machida T., Sawa Y.: The 2007–2011

evolution of tropical methane in the mid-troposphere as seen from space by MetOp-A/IASI, Atmos. Chem.Phys., 12, 23731–2375, doi:10.5194/acpd-12-23731-2012, 2012.

[17] De Mazíère, M., Vigouroux, C., Bernath, P. F., Baron, P., Blumenstock, T., Boone, C., Brogniez, C., Catoire, V., Coffey, M., Duchatelet, P., Griffith, D., Hannigan, J., Kasai, Y., Kramer, I., Jones, N., Mahieu, E., Manney, G. L., Piccolo, C., Randall, C., Robert, C., Senten, C., Strong, K., Taylor, J., Tëtard, C., Walker, K. A., and Wood, S.: Validation of ACE-FTS v 2.2 methane profiles from the upper troposphere to the lower mesosphere, Atmos. Chem. Phys., 8, 2421–2435, 2008.

[18] WMO, Greenhouse Gas Bulletin, The State of Greenhouse Gases in the Atmosphere Based on Global Observations through 2009, No. 6: 24 November 2010.

[19] Meirink, J. F., Bergamaschi, P., and Krol, M. C.: Four-dimensional variational data assimilation for inverse modelling of atmospheric methane emissions: method and comparison with synthesis inversion, Atmos. Chem. Phys., 8, 6341–6353, doi:10.5194/acp-8-6341-2008, 2008b.

[20] Barthlott, S., Schneider, M., Hase, F., Blumenstock, T., kiel, M., Dubravica, D., Omaira, E., Sepûlveda, E., Mengistu Tsidu, G., Takele Kenea, S., Grutter, M., F. PlazaMedina, E., Stremme, W., Strong, K., Weaver, D., Palm, M., Warneke, T., Notholt, J., Mahieu, E., Servais, C., Jones, N., W. T., Griffith, D., Smale, D., and Robinson, J.: Tropospheric water vapour isotopologue data ($H_2^{16}O$, $H_2^{18}O$, and $HD^{16}O$) as obtained from NDACC/FTIR sola absorption spectra, Earth Syst. Sci. Data, 9, 15–29, doi:10.5194/essd-9-15, 2017.

[21] Mengistu Tsidu, G., Blumenstock, T., and Hase, F.: Observations of precipitable water vapour over complex topography of Ethiopia from ground-based GPS, FTIR, radiosonde and ERA-Interim reanalysis, Atmos. Meas. Tech., 8, 3277–3295, doi:10.5194/amt-8-3277-2015, 2015.

[22] Schneider, M., Gonzàlez, Y., Dyroff, C., Christner, E., Wiegele, A., Barthlott, S., García, O. E., Sepûlveda, E., Hase, F., Andrey, J., Blumenstock, T., Guirado, C., Ramos, R., and Rodríguez, S.: Empirical validation and proof of added value of MUSICA's tropospheric δ D remote sensing products, Atmos. Meas. Tech., 8, 483–503, doi:10.5194/amt-8-483-2015, 2015

[23] Schneider, M., Wiegele, A., Barthlott, S., Gonzàlez, Y., Christner, E., Dyroff, C., García, O. E., Hase, F., Blumenstock, T., Sepûlveda, E., Mengistu Tsidu, G., Takele

Kenea, S., Rodríguez, S., and Andrey, J.: Accomplishments of the MUSICA project to provide accurate, long-term, global and high-resolution observations of tropospheric [H_2O; δD] pairs; a review, Atmos. Meas. Tech., 9, 2845–2875, doi:10.5194/amt-9-2845-2016, 2016.

[24] Takele Kenea, S., Mengistu Tsidu, G., Blumenstock, T., Hase, F., von Clarmann, T., and Stiller, G. P.: Retrieval and satellite intercomparison of O_3 measurements from ground-based FTIR Spectrometer at Equatorial Station: Addis Ababa, Ethiopia, Atmos. Meas. Tech., 6, 95-509, doi:10.5194/amt-6-495-2013.

[25] Samuel Takele Kenea (2014); Determination of Atmospheric Water Vapour Isotopic Composition using Multi-Platform Instruments and Models over Ethiopia: Implications for Water Cycle; PhD thesis, Addis Ababa university.

[26] Fu, D., Walker, K. A., Mittermeier, R.,L., Strong, K., Sung, K., Fast, H., Bernath, P.,F., Boon, C.,D., Daffer, W., H., Fogal P., Kolonjari F., Loewen, P., Manney, G., L., Mikhailov, O., and Drummond, J.,R.,: Simultaneous trace gas measurements using two Fourier transform spectrometers at Eureka, Canada during spring 2006, and comparisons with the ACE-FTS, Atmos. Chem. Phys., 11, 5383–5405, 2011.

[27] Payan, S., CamyPeyret, C., Oelhaf, H., Wetzel, G., Maucher, G.,Keim, C., Pirre, M., Huret, N., Engel, A., Volk, M. C., Kuellmann, H., Kuttippurath, J., Cortesi, U., Bianchini, G., Mencaraglia, F., Raspollini, P., Redaelli, G., Vigouroux, C., De Mazíere,M., Mikuteit, S., Blumenstock, T., Velazco, V., Notholt, J.,Mahieu, E., Duchatelet, P., Smale, D., Wood, S., Jones, N., Piccolo, C., Payne, V., Bracher, A., Glatthor, N., Stiller, G., Grunow,K., Jeseck, P., Te, Y., and Butz, A.: Validation of version-4.61 methane and nitrous oxide observed by MIPAS, Atmos. Chem.Phys., 9, 413–442, doi:10.5194/acp-9-413-2009, 2009.

[28] Senten, C., De Maziere M., Dils B., Hermans C., Kruglanski M., Neefs E., Scolas F., Vandaele. C., Vanhaelewyn, A.G., Vigouroux C., Carleer M., F. Coheur P., Fally S., Barret B., L. Baray J., Delmas R., Leveau J.M., Metzger J., Mahieu E., Boone C.A., Walker K., F. Bernath P. and Strong, K.; Technical Note: New ground-based FTIR measurements at Ile de LaRíeunion: observations, error analysis, and comparisons with independent data; Atmos. Chem. Phys., 8, 3483–3508, 2008.

[29] Wunch, D., Taylor, J.R., Fu, D., Bernath, P., Drummond, J. R., Midwinter, C., Strong, K. and walker, K.A.: Simultaneous ground-based observations of O_3, HCl, N_2O, and

CH_4 over Toronto, Canada by three Fourier transform spectrometers with different resolutions, Atmos. Chem. Phys., 7, 1275–1292, 2007.

[30] Gavrilov, N. M., Makarova, M. V., Poberovskii, A. V. and Timofeyev, YU. M.; Comparisons of CH_4 ground based FTIR measurements near Saint Petersburg with GOSAT observations; Atmos. Meas. Tech., 7, 1003–1010, 2014.

[31] Rodgers, C. D.: Inverse Methods for Atmospheric Sounding: Theory and Practise, vol. 2 of Series on Atmospheric, Oceanic and Planetary Physics, World Scientific (publisher), 2000.

[32] Tikhonov, A.: On the regularization of ill-posed problems, Dokl. Acad. Nauk SSSR, 153, 49–52, 1963b.

[33] Sussmann, R., Borsdorff, T., Rettinger, M., Camy-Peyret, C., Demoulin, P., Duchatelet, P., Mahieu, E., and Servais, C.: Technical Note: Harmonized retrieval of column-integrated atmospheric water vapor from the FTIR network-first examples for long-term records and station trends, Atmos. Chem. Phys., 9, 8987–8999, doi:10.5194/acp-9-8987-2009, 2009.

[34] Borsdorff, T., Hasekamp, O, P, Wassmann, A, and Landgraf, J,: Insights into Tikhonov regularization: application to trace gas column retrieval and the efficient calculation of total column averaging kernels Atmos. Meas. Tech., 7, 523–535, doi:10.5194/amt-7-523-2014, 2014.

[35] Garcia, R. R., Marsh, D. R., Kinnison, D. E., Boville, B. A., and Sassi, F.: Simulation of secular trends in the middle atmosphere, 1950-2003, J. Geophys. Res., 112, D09301, doi:10.1029/2006JD007485, 2007.

[36] Hansen, C.: Analysis of discrete ill−posed problems by means of the L-curve, Soc. Indust. Appl. Math., 34, 561–580, 1992.

[37] Phillips, B. C.: A technique for the numerical solution of certain integral equations of the first kind, J. Ass. Comput. Mach., 9, 84–97, doi:10.1145/321105.321114, 1962.

[38] von Clarmann, T.: Validation of remotely sensed profiles of atmospheric state variables: strategies and terminology, Atmos. Chem. Phys., 6, 4311–4320, doi:10.5194/acp-6-4311-2006, 2006.

[39] Sofieva, V. F., Tamminen, J., Kyrölä, Laeng, E. A., Von Clarmann, T.,; Validation of GOMOS ozone precision estimates in the stratosphere. Atmos. Meas. Tech., 7, 2147–2158, doi:10.5194/amt-7-2147-2014, 2014.

[40] Toohey, M., and Strong. K. (2007), Estimating biases and error variances through the comparison of coincident satellite measurements,J. Geophys. Res., 112, D13306, doi:10.1029/2006JD008192.

[41] Rigby, M., Prinn, R. G., Fraser, P. J. Simmonds, P. G., Langenfelds, R. L., Huang, J., Cunnold, D. M., Steele, L. P., Krummel, P. B., Weiss, R. F., O'Doherty, S., Salameh, P. K., Wang, H. J., Harth, C. M., M ühle, J., and Porter, L. W.: Renewed growth of atmospheric methane, Geophys. Res. Lett., 35, L22805, doi:10.1029/2008GL036037, 2008.

[42] Engel, A., Bönisch, H., Schwarzenberger, T., Haase, H.P., Grunow, K., Abalichin, J., and Sala, S.: Long-term validation of ESA operational retrieval (version 6.0) of MIPAS Envisat vertical profiles of methane, nitrous oxide, CFC11, and CFC12 using balloon-borne observations and trajectory matching, Atmos. Meas. Tech., 4859, 1051–1062, doi:10.5194/amt-9-1051-2016, 2016.

[43] Fischer, H., Birk, M., Blom, C., Carli, B., Carlotti, M., von Clarmann, T., Delbouille, L., Dudhia, A., Ehhalt, D., Endemann, M., Flaud, J. M., Gessner, R., Kleinert, A., Koopman, R., Langen, J., LópezPuertas, M., Mosner, P., Nett, H., Oelhaf, H., Perron, G., Remedios, J., Ridolfi, M., Stiller, G., and Zander, R.: MIPAS: an instrument for atmospheric and climate research, Atmos. Chem. Phys., 8, 2151–2188, doi:10.5194/acp-8-2151-2008, 2008.

[44] Vogelmann, H., Sussmann, R., Trickl, T., and Reichert, A.: Spatio temporal variability of water vapor investigated using lidar and FTIR vertical soundings above the Zugspitze, Atmos. Chem. Phys., 15, 3135–3148, doi: 10.5194/acp-15-3135-2015, 2015.

[45] Nassar, R., Bernath, P. F., Boone, C. D., Manney, G. L., McLeod, S. D., Rinsland, C. P., Skelton, R., and Walker, K. A.: Stratospheric abundances of water and methane based on ACE-FTS measurements, Geophys. Res. Lett., 32, L15S04, doi:10.1029/2005GL022383, 2005.

[46] von Clarmann, T., Glatthor, N., Grabowski, U., Höpfner, M., Kellmann, S., Kiefer, M., Linden, A., Mengistu Tsidu, G., Milz, M., Steck, T., Stiller, G. P., Wang, D. Y.,

Fischer, H., Funke, B., Gil-López, S., and López-Puertas, M.: Retrieval of temperature and tangent altitude pointing from limb emission spectra recorded from space by the Michelson Interferometer for Passive Atmospheric Sounding (MIPAS), J. Geophys. Res., 108, 4736, doi:10.1029/2003JD003602, 2003b.

[47] Milz, M., von Clarmann, T., Fischer, H., Glatthor, N., Grabowski, U., Höpfner, M., Kellmann, S., Kiefer, M., Linden, A., Mengistu Tsidu, G., Steck, T. and Stiller, G.P., (2005); Water vapor distributions measured with the Michelson Interferometer for Passive Atmospheric Sounding on board Envisat (MIPAS/Envisat),J. Geophys. Res., 110, D24307, doi:10.1029/2005JD005973.

[48] Plieninger, J., laeng, A., Lossow, S., von Clarmann, T., Stiller, G. P., Kellmann, S., Linden, A., Kiefer, M., Walker, K.A., Noel, S., Hervig, M.E., McHugh, M., Lambert, A., Urban, J., Elkins, J.W., and Mrtagh, D.: Validation of revised methane and nitrous oxide profiles from MIPASENVISAT, Atmos. Meas. Tech., 9, 765779, doi:10.5194/amt-9-765-2016,2016.

[49] Schneider, M., Hase, F., and Blumenstock. T.: Water vapour profiles by ground-based FTIR spectroscopy: study for an optimised retrieval and its validation, Atmos. Chem. Phys., 6,811–830, 2006.

[50] Wang, J., Zhang, L., Dai, A., Hove, T. V., and Baelen, J. V.: A near-global, 2 hourly data set of atmospheric precipitable water from ground-based GPS measurements, J. Geophys. Res., 112, D11107, doi:10.1029/2006JD007529, 2007.

[51] WMO (2000), stratospheric processes and their Role in climate (SPARC) assessment of upper tropospheric and stratospheric water vapour. SPARC Rep. 2, WACRP-113, WMO/TD-1043, Geneva.

[52] Plumb, R. A.: Tracer interrelationships in the stratosphere, Rev. Geophys., 45, n/a–n/a, 540 doi:10.1029/2005RG000179, doi:10.1029/2005RG000179, 2007.

[53] Laeng, A., Plieninger, J., von Clarmann, T., Stiller, G. , Eckert, E., Glatthor, N., Grabowski, Haenel, N., Kiefer, M., Kellmann, S., Linden, A., Lossow, S., Deaver, L., Engel, A., Harvig, M., Levin, I., McHugh, M., Noel, G., and Walker, K.: Validation of MIPAS IMK/IAA methane profiles, Atmos. Meas. Tech., 8, 5251–5261, doi:10.5194/amt-8-5251-2015, 2015.

[54] Errera, Q., Ceccherini, S., Christophe, Y., Chabrillat, S., Hegglin, M. I., Lambert, A., Ménard, R., Raspollini, P., Skachko, S., van Weele, M., and Walker, K. A.: Harmonization and Diagnostics of MIPAS ESA CH_4 and N_2O Profiles Using Data Assimilation; Atmos. Meas. Tech.,9,5895-5909, doi:10.5194/amt-9-5895-2016, 2016.

[55] Dlugokencky, E.J., L.P. Steele, P.M. Lang, and K.A. Masarie, The growth rate and atmospheric methane burden, Nature, 393, 447-450, 1998.

[56] IPCC, 2001: Climate change 2001: impacts, adaptation and vulnerability, Contribution of Working Group II to the Third Assessment Report of the Intergovernmental Panel on Climate Change, edited by J. J. McCarthy, O. F. Canziani, N. A. Leary, D. J. Dokken and K. S. White (eds). Cambridge University Press, Cambridge, UK, and New York, USA, 2001. ISBN 0-521-01500-6.

[57] Volk, C. M., J. W. Elkins, D. W. Fahey, G. S. Dutton, J. M. Gilligan, M. Loewenstein, J. R. Podolske, K. R. Chan, and M. R. Gunson, Evaluation of source gas lifetimes from stratospheric observations, J. Geophys. Res., 102, 25,543–25,564, 1997.

[58] Stanford, J. and Ziemke, J.: CH_4 and N_2O photochemical lifetimes in the upper stratosphere: In situ estimates using SAMS data. [Stratospheric And Mesospheric Sounder]. Geophysical Research Letters - GEOPHYS RES LETT. 18. 677-680, 1991.

[59] Ricaud, P., Attiè, J.-L., Teyssèdre, H., El Amraoui, L., Peuch, V. -H., Matricardi, M., and Schluessel, P.: Equatorial total column of nitrous oxide as measured by IASI on MetOp-A: implications for transport processes, Atmos. Chem. Phys., 9, 3947–3956, https://doi.org/10.5194/acp-9-3947-2009, 2009.

[60] Strahan, S. E., M. Loewenstein, and J. R. Podolske, Climatology and small scale structure of lower stratospheric N_2O based on in situ observations, J. Geophys. Res., 104, 2195– 2208, 1999.

[61] Portmann, R. W., and S. Solomon (2007), Indirect radiative forcing of the ozone layer during the 21^{st} century, Geophys. Res. Lett., 34, L02813, doi:10.1029/ 2006GL028252.

[62] Collins, W. J., Sitch, S., and Boucher, O.: How vegetation impacts affect climate metrics for ozone precursors, J. Geophys. Res., 115, D23308, doi:10.1029/2010JD014187, 2010.

[63] Livesey, N. J., Filipak, M. J., Froidevaux, L., Read, W. G., Lambert, A., Santee, M. L., Jiang, J. H., Pumphrey, H. C., Waters, J. W., Cofield, R. E., Cuddy, D. T., Daffer,

W. H., Drouin, B. J., Fuller, R. A., Jarnot, R. F., Jiang, Y. B., Knosp, B. W., Li, Q. B., Perun, V. S., Schwartz, M. J., Snyder, W. V., Stek, P. C., Thurstans, R. P., Wagner, P. A., Avery, M., Browell, E. V., Cammas, J. P., Christensen, L. E., Diskin, G. S., Gao, R. S., Jost, H.J., Loewenstein, M., Lopez, J. D., Nedelec, P., Osterman, G. B., Sachse, G. W., and Webster, C. R.: Validation of Aura Microwave Limb Sounder O_3 and CO observations in the upper troposphere and lower stratosphere, J. Geophys. Res., 113, D15S02, doi:10.1029/2007JD008805, 2008.

[64] Laeng, A., Hubert, D., Verhoelst, T., von Clarmann, T., Dinelli, B. M., Dudhia, A., Raspollini, P., Stiller, G., Grabowski, U., Keppens, A., Kiefer, M., Sofieva, V., Froidevaux, L., Walker, K. A., Lambert, J. C., and Zehner, C.: The Ozone Climate Change Initiative: Comparison of four Level 2 Processors for the Michelson Interferometer for Passive Atmospheric Sounding (MIPAS), Remote Sens. Environ., submitted, 2014.

[65] Banwell, C. N., and McCash, E. M.: Fundamentals of Molecular Spectroscopy, 4^{th} ed., McGrawHill Book Company, Toronto, 1994.

[66] Backus G.E. and Gilbert J.F.,: (1970), Uniquenessin the inversion of inaccurate gross Earth data, Trans. R. Soc. Lon, Ser. A, 266, 123-192.

[67] Holton, J. R. and Gettelman, A.: Horizontal transport and the dehydration of the stratosphere, Geophys. Res. Lett., 28, 27992802, 2001.

[68] Rodgers, C. D.: Inverse methods for Atmospheric sounding: Theory and practice, World scientific, Singapore. 2004.

[69] Payne vivienne H.(2005); Retrieval of Water Vapour and Methane From the MIPAS satellite instruments; PhD thesis, university of Oxford.

[70] Hase, F., Hannigan, J. W., Coffey, M. T., Goldman, A., Hopfner, M., Jones, N. B., Rinsland, C. P., and Wood, S.W.: Intercomparison of retrieval codes used for the analysis of high-resolution, ground-based FTIR measurements, J. Quant. Spectrosc. Radiat. Transfer, 87, 25−52, 2004.

[71] Celarier, E.A., E.J. Brinksma, J.F. Gleason, J.P. Veefkind, A. Cede, J.R. Herman, D. Ionov, F. Goutail, J.P. Pommereau, J.C. Lambert, M. van Roozendael, G. Pinardi, F. Wittrock, A. Schönhardt, A. Richter, O.W. Ibrahim, T. Wagner, B. Bojkov, G. Mount, E. Spinei, C.M. Chen, T.J. Pongetti, S.P. Sander, E.J. Bucsela, M.O. Wenig, D.P.J. Swart, H.

Volten, M. Kroon and P.F. Levelt, Validation of Ozone Monitoring Instrument nitrogen dioxide columns,J. Geophys. Res., 113, D15S15, doi:10.1029/2007JD008908, 2008.

[72] Cortesi, U., C. Lambert, J., DeClercq, C., Bianchini, G., Blumenstock, T., Bracher, A., Castelli, E., Catoire, V., V. Chance, K., De Maziére, M., Demoulin, P., GodinBeekmann, S., Jones, N., Jucks, K., Keim, C., Kerzenmacher, T., Kuellmann, H., Kuttippurath, J., Iarlori, M., Y. Liu, G., Liu, Y., S. McDermid, I., J. Meijer, Y., Mencaraglia, F., Mikuteit, S., Oelhaf, H., Piccolo, C., Pirre, M., Raspollini, P., Ravegnani, E., J. Reburn, W., Redaelli, G., J. Remedios, J., Sembhi, H., Smale, D., Steck, T., Taddei, A., Varotsos, C., Vigouroux, C., Waterfall, A., Wetzel, G. and Wood, S., Geophysical validation of MIPAS-ENVISAT operational ozone data, Atmos. Chem. Phys., 7, 4807–4867, 2007.

[73] von Clarmann, T., H*ö*pfner, M., Kellmann, S., Linden, A., Chauhan, S., Funke, B., Grabowski, U., Glatthor, N., Kiefer, M., Schieferdecker, T., Stiller, G. P., and Versick, S.: Retrieval of temperature, H_2O, O_3, HNO_3, CH_4, N_2O, $ClONO_2$ and ClO from MIPAS reduced resolution nominal mode limb emission measurements, Atmos. Meas. Tech., 2, 159–175, doi:10.5194/amt-2-159-2009, 2009

[74] Schoeberl, M. R., Douglass, A. R., Hilsenrath, E., Bhartia, P. K., Beer, R., Waters, J. W., Gunson, M. R., Froidevaux, L., Gille, J. C., Barnett, J. J., Levelt, P. F., and DeCola, P.: Overview of the EOS Aura mission, IEEE Trans. Geosci. Remote Sens., 44, 1066–1074, 2006.

[75] Waters, J. W., Froidevaux, L., Harwood, R. S., Jarnot, R. F., Pickett, H. M., Read, W. G., Siegel, P. H., Cofield, R. E., Filipiak, M. J., Flower, D. A., Holden, J. R., Lau, G. K., Livesey, N. J., Manney, G. L., Pumphrey, H. C., Santee, M. L., Wu, D. L., Cuddy, D. T., Lay, R. R., Loo, M. S., Perun, V. S., Schwartz, M. J., Stek, P. C., Thurstans, R. P., Boyles, M. A., Chandra, K. M., Chavez, M. C., Chen, G.S., Chudasama, B. V., Dodge, R., Fuller, R. A., Girard, M. A., Jiang, J. H., Jiang, Y., Knosp, B. W., LaBelle, R. C., Lam, J. C., Lee, K. A., Miller, D., Oswald, J. E., Patel, N. C., Pukala, D. M., Quintero, O., Scaff, D. M., Snyder, W. V., Tope, M. C., Wagner, P. A., and Walch, M. J.: The Earth Observing System Microwave Limb Sounder (EOS MLS) on the Aura satellite, IEEE T. Geosci. Remote, 44, 1075–1092, doi:10.1109/tgrs.2006.873771, 2006.

[76] Barnes, J. E., Kaplan, T., Vömel, H., and Read, W. G.: NASA/Aura/Microwave Limb Sounder water vapor validation at Mauna Loa Observatory by Raman lidar, J. Geophys. Res., 113, D15S03, doi:10.1029/2007JD008842, 2008.

[77] Livesey, N. J., Filipak, M. J., Froidevaux, L., Read, W. G., Lambert, A., Santee, M. L., Jiang, J. H., Pumphrey, H. C., Waters, J. W., Cofield, R. E., Cuddy, D. T., Daffer, W. H., Drouin, B. J., Fuller, R. A., Jarnot, R. F., Jiang, Y. B., Knosp, B. W., Li, Q. B., Perun, V. S., Schwartz, M. J., Snyder, W. V., Stek, P. C., Thurstans, R. P., Wagner, P. A., Avery, M., Browell, E. V., Cammas, J.P., Christensen, L. E., Diskin, G. S., Gao, R. S., Jost, H.J., Loewenstein, M., Lopez, J. D., Nedelec, P., Osterman, G. B., Sachse, G. W., and Webster, C. R.: Validation of Aura Microwave Limb Sounder O3 and CO observations in the upper troposphere and lower stratosphere, J. Geophys. Res., 113, D15S02, doi:10.1029/2007JD008805, 2008.

[78] Lambert, A., Read, W. G., Livesey, N. J., Santee, M. L., Manney, G. L., Froidevaux, L., Wu, D. L., Schwartz, M. J., Pumphrey, H. C., Jimenez, C., Nedoluha, G. E., Cofield, R. E., Cuddy, D. T., Daffer, W. H., Drouin, B. J., Fuller, R. A., Jarnot, R. F., Knosp, B. W., Pickett, H. M., Perun, V. S., Snyder, W. V., Stek, P. C., Thurstans, R. P., Wagner, P. A., Waters, J. W., Jucks, K. W., Toon, G. C., Stachnik, R. A., Bernath, P. F., Boone, C. D., Walker, K. A., Urban, J., Murtagh, D., Elkins, J. W., and Atlas, E.: Validation of the Aura Microwave Limb Sounder middle atmosphere water vapor and nitrous oxide measurements, J. Geophys. Res.: Atmospheres, 112, D24S36, doi:10.1029/2007JD008724, 2007.

[79] Livesey, N. J., Read, W. G., Froidevaux, L., Lambert, A., Manney, G. L., Pumphrey, H. C., Santee, M. L., Schwartz, M. J., Wang, S., Cofield, R. E., Cuddy, D. T., Fuller, R. A., Jarnot, R. F., Jiang, J. H., Knosp, B. W., Stek, P. C., Wagner, P. A., and Wu, D. L.: Earth Observing System (EOS) Aura Microwave Limb Sounder (MLS) Version 3.3 Level 2 data quality and description document, Tech. Rep. D-33509, JPL, 2011.

[80] Minschwaner, K., and Manney,: Derived Methane in the Stratosphere and Lower Mesosphere from Aura Microwave Limb Sounder Measurements of Nitrous Oxide, Water Vapor, and Carbon Monoxide, J. Atmos. Chem., 2015.

[81] Chahine, M., Pagano, T., Aumann, H., Atlas, R., Barnet, C., Chen, L., Divakarla, M., Fetzer, E., Goldberg, M., Gautier, C., Granger,S., Irion, F. W., Kakar, R., Kalnay, E., Lambrigtsen, B., Lee, S., Marshall, J. L., McMillan, W., McMillin, L., Olsen, E. T., Revercomb, H., Rosenkranz, P., Smith, W., Staelin, D., Strow, L., Susskind, J., Tobin, D., and Wolf, W.: The Atmospheric Infrared Sounder (AIRS): improving weather forecasting and providing new insights into climate, B. Am. Meteorol. Soc., 87, 891–894, doi:10.1175/BAMS-87-7-891, 2006.

[82] Xiong, X.Z. C. Barnet, E. Maddy, C. Sweeney, X.P. Liu, L.H. Zhou and M. Goldberg, 2008, Characterization and validation of methane products from the Atmospheric Infrared Sounder (AIRS),J. Geophys. Res. Biogeosci. 113, doi:1410.1029/2007jg000500.

[83] Xiong, X., E. S. Maddy, C. Barnet, A. Gambacorta, P. K. Patra, F. Sun, and M. Goldberg: Retrieval of nitrous oxide from Atmospheric Infrared Sounder: Characterization and validation, J. Geophys. Res. Atmos., 119, 9107–9122, doi:10.1002/2013JD021406, 2014.

[84] Rothmann L. S., D. Jacquemart, A. Barbe, D. C. Benner, M. Birk, L. R. Brown, M. R. Carleer, C. Chackerian, K. Chance, L. H. Coudert, V. Dana, V. M. Devi, J. M. Flaud, R. R. Gamache, A. Goldman, J. M. Hartmann, K. W. Jucks, A. G. Maki, J. Y. Mandin, S. T. Massie, J. Orphal, A. Perrin, C. P. Rinsland, M. A. H. Smith, J. Tennyson, R. N. Tolchenov, R. A. Toth, A. J. Vander, P. Varanasi, G. Wagner: The HITRAN 2004 molecular spectroscopic database. J. Quant. Spectrosc. Rad. Trans. 96, 139-204, 2005.

[85] Rothmann L. S., I. E. Gordon, Y. Babikov, A. Barbe, D. C. Benner, P. F. Bernath,M. Birk, L. Bizzocchi, V. Boudon, L. R. Brown, A. Campargue, K. Chance, L. H. Coudert, V. M. Devi, B. J. Drouin, A. Fayt, J.M. Flaud, R. R. Gamache, J. Harrison, J.M. Hartmann, C. Hill, J. T. Hodges, D. Jacquemart, A. Jolly, J. Lamouroux, R. J. LeRoy, G. Li, D. Long, C. J. Mackie, S. T. Massie, S. Mikhailenko,H.S. P. Müller, O. V. Naumenko, A. Nikitin, J. Orphal, V. I. Perevalov, A., Perrin, E. R., Polovtseva, C. Richard, M. A. H. Smith, E. Starikova, K. Sung, S. A. Tashkun, J. Tennyson, G. C. Toon, V. G. Tyuterev and G. Wagner, 2013. The HITRAN 2012 molecular spectroscopic database. J. Quant. Spectrosc. Rad. Trans. 130, 4-50, doi:10.1016/j. jqsrt.2013.07.002

[86] Mengistu Tsidu, G.: Determination of optimized microwindows for analysis of absorption spectra from ground-based FTIR spectrometer, MSc thesis, Addis Ababa University, Addis Ababa, Ethiopia, 1998.

[87] Meier, A., Toon, G. C., Rinsland, C. P., Goldman, A., and Hase, F.: Spectroscopic Atlas of Atmospheric Microwindows in the middle Infra-Red, IRF Technical Report 048, ISSN 0284-1738 (Institutet for Rymdfysik, Kiruna, Sweden), Appendix E, 2004.

[88] Rinsland, C.P., Boone, C., Nassar, R., Walker, K., Bernath, P., Mahieu, E., Zander, R., J.C. McConnell, J. C., and Chiou, L.: Trends of HF, HCl, CCl_2F_2, CCl_3F, $CHClF_2$ (HCFC-22), and SF_6 in the lower stratosphere from Atmospheric Chemistry Experiment (ACE) and Atmospheric Trace Molecule Spectroscopy (ATMOS) measurements near

30° N latitude, Published in GEOPHYSICAL RESEARCH LETTERS, VOL. 32, 22 June 2005.

[89] Sussmann, R. and Borsdorff, T.: Technical Note: Interference errors in infrared remote sounding of the atmosphere, Atmos. Chem. Phys., 7, 3537–3557, 2007.

[90] Dils, B., De Mazière, M., Müller, J.F., Blumenstock, T., Buchwitz, M., de Beek, R., Demoulin, P., Duchatelet, P., Fast, H., Frankenberg, C., Gloudemans, A., Griffith, D., Jones, N., Kerzenmacher,T. , Kramer, I., Mahieu, E., Mellqvist, J., Mittermeier, R.L., Notholt, J., Rinsland, C.P., Schrijver, H., Smale, D., Strandberg, A., Straume, A.G., Stremme, W., Strong, K., Sussmann, R., Taylor, J., van den Broek, M., Velazco, V., Wagner, T., Warneke, T., Wiacek, A., and Wood, S., Comparisons between SCIAMACHY and ground-based FTIR data for total columns of CO, CH_4,CO_2 and N_2O, Atmos. Chem. Phys., 6, 1953–1976, 2006.

[91] Sussmann, R., Forster, F., Rettinger, M., and Jones, N.: Strategy for high-accuracy-and-precision retrieval of atmospheric methane from the mid-infrared FTIR network, Atmos. Meas. Tech., 4, 1943–1964, doi:10.5194/amt-4-1943-2011, 2011.

[92] Rodgers, C. D., and Connor, B. J.: Intercomparison of remote sounding instruments,J. Geophys. Res., 108(D3), 4116, doi:10.1029/2002JD002299, 2003.

[93] Plieninger, J., von Clarmann, T., Stiller, G. P., Grabowski, U., Glatthor, N., Kellmann, S., Linden, A., Haenel, F., Kiefer, M., Hpfner, M., Laeng, A., and Lossow, S.: Methane and nitrous oxide retrievals from MIPAS-ENVISAT, Atmos. Meas. Tech., 8, 46574670, doi:10.5194/amt-8-4657-2015, 2015.

[94] Fioletov, V. E., D. W. Tarasick, and I. Petropavlovskikh, Estimating ozone variability and instrument uncertainties from SBUV(/2), ozonesonde, Umkehr, and SAGE II measurements: Short-term variations, J. Geophys. Res., 111, D02305, doi:10.1029/2005JD006340, 2006.

[95] Stiller, G. P., Kiefer, M., Eckert, E., von Clarmann, T., Kellmann, S., GarcíaComas, M., Funke, B., Leblanc, T., Fetzer, E., Froidevaux, L., Gomez, M., Hall, E., Hurst, D., Jordan, A., Kämpfer, N., Lambert, A., McDermid, I. S., McGee, T., Miloshevich, L., Nedoluha, G., Read, W., Schneider, M., Schwartz, M., Straub, C., Toon, G., Twigg, L. W., Walker, K., and Whiteman, D. N.: Validation of MIPAS IMK/IAA temperature, water vapor, and ozone profiles with MOHAVE-2009 campaign measurements, Atmos. Meas. Tech., 5, 289–320, doi:10.5194/amt-5-289-2012, 2012.